

**Aromatic Functionalized Rosette Nanotubes**

by

Zhaoyi Qin

A thesis submitted in partial fulfillment of the requirements for the degree of

Master of Science

Department of Chemistry  
University of Alberta

© Zhaoyi Qin, 2014

## Abstract

Rosette Nanotubes (RNTs) are a class of self-assembled organic nanomaterials generated through the spontaneous hierarchical organization of guanine-cytosine (G<sup>^</sup>C) bases with a built-in self-assembling ability. Driven by non-covalent intermolecular forces in solution, G<sup>^</sup>C bases self-assemble into six-membered macrocycles termed rosettes, which then undergo a second level of organization to stack into RNTs. RNTs have been widely utilized in drug delivery and tissue engineering. However, the use of RNTs in other research fields such as electronics remains unexplored. Due to the ease of chemical functionalization and the highly ordered nanostructure of RNT, it is an excellent scaffold to construct ordered matrix of organic electronic materials, which is essential for the performance of organic electronic devices. This thesis introduces a new method to prepare aromatic functionalized G<sup>^</sup>C bases and investigate their unique self-assembly process and physical properties for the potential applications of RNTs in organic electronics.

The first chapter reviews examples of self-assembled organic nanomaterials in the literature, with detailed descriptions of designs, significant properties, and applications.

This chapter also presents various RNT systems developed by our group. The second

chapter introduces a new method to functionalize RNTs with small aromatic groups as the initial steps to utilize RNTs for electronic applications. The self-assembly of aromatic functionalized G<sup>A</sup>C bases prepared via a new synthetic pathway is explored and the resulting RNTs are characterized. The third chapter describes the synthesis and self-assembly of oligothiophene functionalized G<sup>A</sup>C bases for organic electronics and discusses the unique structural and electronic properties of the resulting RNTs. The thesis concludes with a discussion of the prospects for utilizing RNTs in organic electronic devices.

## Acknowledgments

Foremost, I would like to thank my supervisor, Professor Hicham Fenniri, for his support, for his guidance, and for believing in me throughout graduate school. I would like to thank Professors Dennis Hall and Jonathan Veinot for taking the time to serve on my committee.

I am deeply indebted to all the present and past members of the Fenniri group whom I have been privileged to work with. I am particularly thankful to Dr. Rachel Beingessner and Dr. Venkatakrishnan Parthasarathy for all of their help with organic synthesis. I owe an enormous debt of Dr. Jae-Young Cho for performing TEM and AFM in this thesis and many thanks to his help with SEM. Dr. Zhimin Yan provided much assistance with NMR spectroscopy. I am very grateful to Liang Shuai, Dr. Weizheng Shen, Kumashi Sharma, and Uyen Ho with whom I worked closely and for all the stimulating discussions we had. I also appreciate your friendship over the years. Many thanks to Dr. Mounir El Bakkari, Dr. Alaaeddin Alsbaiee, Dr. Usha Hermraz, Dr. Christophe Danumah, Dr. Takeshi Yamazaki, Rahul Agrawal, and Mohammad Hassan for their assistance throughout the years.

I am thankful to the support services and research facilities at the National Institute for Nanotechnology and University of Alberta. I am thankful to Dr. Mike Xia, Dr. Kai Cui from NINT, and personnel from the NMR Lab, Spectral Services Lab, Mass Spectrometry Lab, machine shop, storeroom, glass shop and shipping from the Department of Chemistry.

I would like to thank my parents and friends for your blessing, encouragement, and sacrifices you made for me. My parents made all of this possible and supported me through the good times and the bad. Many thanks to my friends, Minhao Zeng, Meijing Wang, and Xiangyu Chen, for keeping me sane all these years.

## Table of Content

	Page
<b>Chapter 1. Self-assembled organic nanomaterials</b>	
1.1. Introduction.....	1
1.2. Nucleic acid systems.....	3
1.3. Peptide systems.....	7
1.4. $\pi$ -Conjugated systems.....	12
1.5. RNT as a specific example.....	14
1.6. Conclusion.....	20
1.7. References.....	22
<b>Chapter 2. Synthesis and characterization of aromatic functionalized G<sup>+</sup>C bases</b>	
2.1. Introduction.....	29
2.2. Deprotection procedures of the G <sup>+</sup> C bases.....	32
2.3. NMR studies of the G <sup>+</sup> C bases.....	34
2.3.1. Choice of deuterated NMR solvents.....	34
2.3.2. NMR characterization in <i>d</i> -TFA and <i>d</i> -TFA: <i>d</i> <sub>6</sub> -DMSO (2:5).....	35
2.4. Self-assembly studies of the G <sup>+</sup> C bases.....	47

2.4.1. Nanotube formation in MeOH .....	47
2.4.2. Nanotube formation in other solvents.....	50
2.5. Conclusion .....	53
2.6. Experimental Section.....	54
2.6.1. General procedures .....	54
2.6.2. Synthesis and characterization data of target molecules.....	57
2.7. References.....	67

### **Chapter 3. Synthesis and self-assembly of oligothiophene–G<sup>AC</sup> base hybrids**

3.1. Introduction.....	71
3.2. Synthesis of oligothiophene functionalized G <sup>AC</sup> bases .....	73
3.3. Self-assembly.....	81
3.3.1. Effect of solvent and aging .....	81
3.3.2. Effect of temperature variation .....	85
3.3.3. Diameter measurements.....	90
3.4. Conclusion .....	92
3.5. Experimental Section.....	94
3.5.1. General procedures .....	94
3.5.2. Synthesis of target molecules.....	97

3.6. References ..... 113

**Chapter 4. Summary of this thesis work and outlook**

4.1. Summary of this thesis work ..... 117

4.2. Outlook ..... 119

4.3. References ..... 123

**Bibliography ..... 125**

## List of Figures

	Page
<b>Figure 1.1:</b> Proposed structure for the binary self-assembly of <b>1</b> and <b>2</b> (T:A = 1:1) .....	4
<b>Figure 1.2:</b> AFM images for the binary self-assembly of <b>1</b> and <b>2</b> (T:A = 1:1) (A, B) and possible elongation mechanism for the helical stacks (C) .....	5
<b>Figure 1.3:</b> Representation of a single strand DNA (ssDNA) templated self-assembly of chromophores (black strand, ssDNA; blue bar, chromophores; red bar, hydrogen bonding unit) and molecular structures of dT40, NT, and OPVT.....	6
<b>Figure 1.4:</b> The 20 amino acids at physiological pH 7.4, grouped according to their side chains.....	8
<b>Figure 1.5:</b> Chemical structure of the peptide amphiphile (PA) (A), molecular model of PA (B), and schematic representation of the self-assembly of PAs into a nanofiber (C).....	9
<b>Figure 1.6:</b> STM images of OPV-GAGAG at liquid-solid interface (A–C), a schematic representation of the hydrogen bonding between OPV-GAGAG molecules (D), and a molecular model of OPV-GAGAG superimposed with a zoom of the STM image (E) .....	11

<b>Figure 1.7:</b> Molecular structure of the amphiphilic HBC (A), TEM image of the nanotube (B, C), and a molecular model representing the self-assembled graphitic nanotube (D) .....	13
<b>Figure 1.8:</b> Molecular structure of L-module <b>1</b> (A), molecular model of the rosette resulting from <b>1</b> (B),* and the molecular model of the RNT. *The thin yellow lines show the hydrogen bond network. ....	14
<b>Figure 1.9:</b> Molecular structure of twin G <sup>^</sup> C base <b>1</b> (A), self-assembled double rosette (B), self-assembled RNT obtained from rosette stacking (C), negatively stained TEM image (D, scale bar = 50 nm) and TM-AFM image of the RNTs (E).....	16
<b>Figure 1.10:</b> RNTs with nucleated Au NPs (gold spheres) (A, B), a close-up view of the nucleation site (C), TM-AFM image (D) and TEM image (E) of Au NP coated RNTs.....	17
<b>Figure 1.11:</b> Molecular structure of G <sup>^</sup> C base <b>1</b> (A), self-assembled rosette (B) and RNT (C)*, schematic representation of RNTs' self-organization into monolayer and then lamellar prolate nanospheroids (D), solvent-promoted transition between RNT and nanospheroids (E), TM-AFM images of RNTs (F) and nanospheroids (G). *One module is removed from each rosette along the RNT wall to unveil the inner channel (red). ....	18

<b>Figure 1.12:</b> Aromatic functionalized G <sup>Λ</sup> C bases.....	20
<b>Figure 2.1:</b> G <sup>Λ</sup> C aldehyde as a main precursor for RNTs.....	29
<b>Figure 2.2:</b> G <sup>Λ</sup> C iodide as a novel precursor for RNTs.....	30
<b>Figure 2.3:</b> A proposed mechanism for the keto-enol tautomerization of <b>2.2a</b> in <i>d</i> -TFA.....	34
<b>Figure 2.4:</b> 1D <sup>1</sup> H (A) and <sup>13</sup> C (B) and 2D COSY (C), HSQC (D) and HMBC (E) NMR spectra of <b>2.2a</b> in <i>d</i> -TFA.....	38
<b>Figure 2.5:</b> A resonance structure of <b>2.2a</b> for the shielding of C <sub>3</sub> .....	39
<b>Figure 2.6:</b> 1D <sup>1</sup> H (A) and <sup>13</sup> C (B) and 2D COSY (C), HSQC (D) and HMBC (E) NMR spectra of <b>2.2a</b> in <i>d</i> -TFA: <i>d</i> <sub>6</sub> -DMSO (2:5).....	41
<b>Figure 2.7:</b> Broad doublet was found for the G <sup>Λ</sup> C bases <b>2.2a</b> at 25 °C (A) which became sharp at 50 °C (B). The solvent was <i>d</i> -TFA: <i>d</i> <sub>6</sub> -DMSO (2:5).....	42
<b>Figure 2.8:</b> A proposed mechanism for the doublet broadening of <b>2.2a</b> .....	43
<b>Figure 2.9:</b> 1D <sup>1</sup> H NMR spectra of <b>2.2c</b> in <i>d</i> -TFA (A) and in <i>d</i> -TFA: <i>d</i> <sub>6</sub> -DMSO (2:5) (B).....	44
<b>Figure 2.10:</b> 1D <sup>1</sup> H NMR spectra of <b>2.2b</b> in <i>d</i> -TFA at 25 °C, 50 °C and 65 °C.....	46

<b>Figure 2.11:</b> SEM images of <b>2.2a</b> (A), <b>2.2b</b> (B), <b>2.2c</b> (C), <b>2.2d</b> (D) and <b>2.2e</b> (E) in Methanol (0.01 mg/mL). Scale bar = 300 nm.....	48
<b>Figure 2.12:</b> UV-vis spectra of <b>2.2a–e</b> in MeOH.....	49
<b>Figure 2.13:</b> SEM images of <b>2.2a</b> in DMSO (0.01 mg/mL) at 0 h (A), 1 h (B) and 2 d (C). Scale bar = 300 nm. ....	50
<b>Figure 2.14:</b> TEM (A, scale bar = 100 nm) and AFM (B) images of <b>2.2a</b> (0.01 mg/mL) in DMSO, aged for 1 h.....	51
<b>Figure 2.15:</b> SEM images of <b>2.2d</b> in MeCN (A), DMF (B) and DMSO (C) at 0 h. Scale bar 300 nm.....	52
<b>Figure 3.1:</b> Oligothiophene-G <sup>^</sup> C base hybrids.....	73
<b>Figure 3.2:</b> Synthesis of G <sup>^</sup> C iodide .....	74
<b>Figure 3.3:</b> Synthesis of terthiophenylboronic ester BpinH <sub>2</sub> T <sub>3</sub> .....	75
<b>Figure 3.4:</b> Synthesis of sexithiophenylboronic ester BpinH <sub>4</sub> T <sub>6</sub> .....	79
<b>Figure 3.5:</b> Suzuki-Miyaura coupling and deprotection reaction .....	80
<b>Figure 3.6:</b> Time-dependent SEM images of GCH <sub>2</sub> T <sub>3</sub> HCl in DCM (A–C) and CB (D–F) at 0.01 mg/mL. Scale bar = 300 nm.....	82

<b>Figure 3.7:</b> Time-dependent SEM images of GCH4T6HCl in DCM (A–C), 1,2-DCE (D–F), and CB (G–I) at 0.01 mg/mL. Scale bar = 300 nm.....	84
<b>Figure 3.8:</b> Variable temperature UV-vis spectra with increasing temperature (A) and decreasing temperature (B) and the corresponding SEM images of GCH2T3HCl (C–G) in CB (0.01 mg/mL, $1.4 \times 10^{-5}$ M). Scale bar = 300 nm.....	87
<b>Figure 3.9:</b> Variable temperature UV-vis spectra with increasing temperature (A) and decreasing temperature (B) and the corresponding SEM images of GCH4T6HCl (C–G) in 1,2-DCE (0.01 mg/mL, $8.8 \times 10^{-6}$ M). Scale bar = 300 nm.....	89
<b>Figure 3.10:</b> TEM (A, scale bar = 50 nm) and AFM (B) images of GCH2T3HCl.....	91
<b>Figure 3.11:</b> TEM (A, scale bar = 150 nm) and AFM (B) images of GCH4T6HCl.....	92

## List of Tables

	Page
<b>Table 2.1:</b> General scheme for the synthesis of the novel G <sup>AC</sup> bases 2.2a–i .....	32
<b>Table 3.1:</b> Borylation attempts of BrH <sub>2</sub> T <sub>3</sub> to generate BpinH <sub>2</sub> T <sub>3</sub> .....	77

## List of Abbreviations

1D	One-dimensional
2D	Two-dimensional
AFM	Atomic force microscopy
aq	Aqueous
BnOH	Benzyl alcohol
Boc <sub>2</sub> O	Di-tert-butylidicarbonate
Bu <sub>4</sub> NI	Tetra-n-butylammounium iodide
bs	Broad singlet
C	Celsius
CB	Chlorobenzene
CD	Circular dichroism
COSY	Correlation spectroscopy
d	Day or Doublet (only used for NMR data)
<i>d</i>	Deuterated
DCE	Dichloroethane
DCM	Dichrolomethane
DMAP	4-N,N-dimethylaminopyridine

DMF	N,N-dimethylformamide
DMSO	Dimethyl sulphoxide
DNA	Deoxyribonucleic acid
ESI-MS	Electrospray ionization mass spectrometry
Et <sub>3</sub> N	Triethylamine
Et <sub>2</sub> O	Diethyl ether
EtOAc	Ethyl acetate
G^C	Guanine-cytosine
h	Hour
HCl	Hydrogen chloride
HMBC	Heteronuclear multiple bond correlation
HSQC	Heteronuclear single quantum coherence
HPLC	High performance liquid chromatography
IC <sub>6</sub> H <sub>4</sub> NH <sub>2</sub>	4-Iodoaniline
K <sub>2</sub> CO <sub>3</sub>	Potassium carbonate
KF	Potassium fluoride
KHCO <sub>3</sub>	Potassium bicarbonate
KOAc	Potassium acetate
m	Multiplet

MeCN	Acetonitrile
MeNH <sub>2</sub>	Methylamine
MeOH	Methanol
min	Minute
mp	Melting point
MS	Mass spectrometry
NaH	Sodium hydride
Na <sub>2</sub> SO <sub>4</sub>	Sodium sulfate
NH <sub>3</sub>	Ammonia
NH <sub>2</sub> OH·HCl	Hydroxylamine hydrochloride
nm	Nanometers
NMR	NMR Nuclear magnetic resonance
Pd(PPh <sub>3</sub> ) <sub>4</sub>	Tetrakis(triphenylphosphine)palladium(0)
PhMe	Toluene
ppm	Parts per million
R <sub>f</sub>	Retention factor
RNTs	Rosette nanotubes
rt	Room temperature
s	Second or Singlet (only used for NMR data)

SEM	Scanning electron microscopy
STEM	Scanning transmission electron microscopy
TEM	Transmission electron microscopy
TFA	Trifluoroacetic acid
TFAA	Trifluoroacetic anhydride
THF	Tetrahydrofuran
TM-AFM	Tapping mode atomic force microscopy
UV-vis	Ultraviolet-visible
VT	Variable temperature

## Chapter 1

### Self-assembled organic nanomaterials

#### 1.1. Introduction

Molecular self-assembly describes the spontaneous organization of discrete molecules into stable and ordered structures driven by noncovalent intermolecular forces such as hydrogen bonding, hydrophobic affinity, and  $\pi$ - $\pi$  stacking. In nature, molecular self-assembly is found ubiquitous in the formation of numerous sophisticated biological architectures, for instance, DNA double helix<sup>1</sup> and proteins<sup>2</sup> with nanoscale dimensions of 1 to 100 nm. The development of self-assembly as a “bottom up” strategy to construct artificial nanostructures was pioneered by Whitesides and co-workers<sup>3,6</sup> in the 1990s. This approach originated from the earlier studies of supramolecular chemistry, which earned Cram, Pederson, and Lehn the 1987 Nobel Prize in Chemistry.<sup>4</sup> They discovered recognition and selective binding between molecules and cryptand cages (Lehn)<sup>5</sup> and between ions and crown ethers (Cram<sup>6</sup> and Pederson<sup>7</sup>) directed by noncovalent intermolecular interactions. Understanding those interactions allows the rational design of more complex self-assembled nanostructures, which largely depend on the build-in interaction patterns of the building blocks.<sup>8</sup> Moreover, because the intermolecular interactions that drive the self-assembly of the nanostructures are weak forces compared

to covalent bonds, the formation and strength of the interactions can be manipulated by external conditions (*e.g.*, temperature, solvent, pH, *etc.*).<sup>9</sup>

Nowadays, self-assembly has been recognized as a powerful “bottom-up” strategy and is still one of the few practical methods to produce a vast array of elaborate nanostructures.<sup>8,10</sup> Self-assembled organic nanomaterials have received much attention due to their wide range of applications from chemical catalysis through biomaterials to electronics. Many of the applications utilize biological self-assembly systems, such as DNA, peptide, and dendron rodcoil, driven by noncolvant weak interactions (*e.g.*, hydrogen bonding, hydrophobic affinity,  $\pi$ - $\pi$  stacking *etc.*).<sup>11</sup> The  $\pi$ -Conjugated systems constitute a unique case because the anisotropic  $\pi$ - $\pi$  stacking is the only intermolecular driving force.<sup>12</sup>

As the amount of literature<sup>11,12,13</sup> in the field of self-assembled organic nanomaterials is tremendous and it is impossible to exhaustively review the relevant literature, this chapter will only describe the systems that have been most widely used and are most pertinent to my work. They are nucleic acid (Section 1.2), peptide (Section 1.3), and  $\pi$ -conjugated systems (Section 1.4). The rosette nanotube (RNT), which is developed by our group, and on which my work relies, will be discussed as a specific example in Section 1.5. In all

these four sections, only recent and representative examples chosen from relevant literature will be described.

## **1.2. Nucleic acid systems**

The molecular recognition ability of DNA enables coding, transmitting, and expressing genetic information in all living things. The chemical foundation of this recognition system is provided by the specific bonding of DNA nitrogenous base pairs, the highly precise adenine (A) – thymidine (T) and guanine (G) – cytosine (C) hydrogen bonding interactions. The pioneering work by Seeman in the early 1990s demonstrates that various unusual DNA architectures with programmed nanostructures can be constructed through the pairings of designed bases.<sup>1,14</sup> Since then, attempts have been made to explore the programmed artificial DNAs for material purposes. Much of the attention has been focused on developing so-called DNA hybrid materials by combining DNA motifs, including its smaller constituents nucleosides and nucleotides, with many functional molecules.<sup>15</sup> Thanks to the synergistic behavior of both components, these new classes of materials overcome the shortcomings inherent to one component alone and can be designed to meet specific needs by modifying the properties of each component.<sup>16</sup>

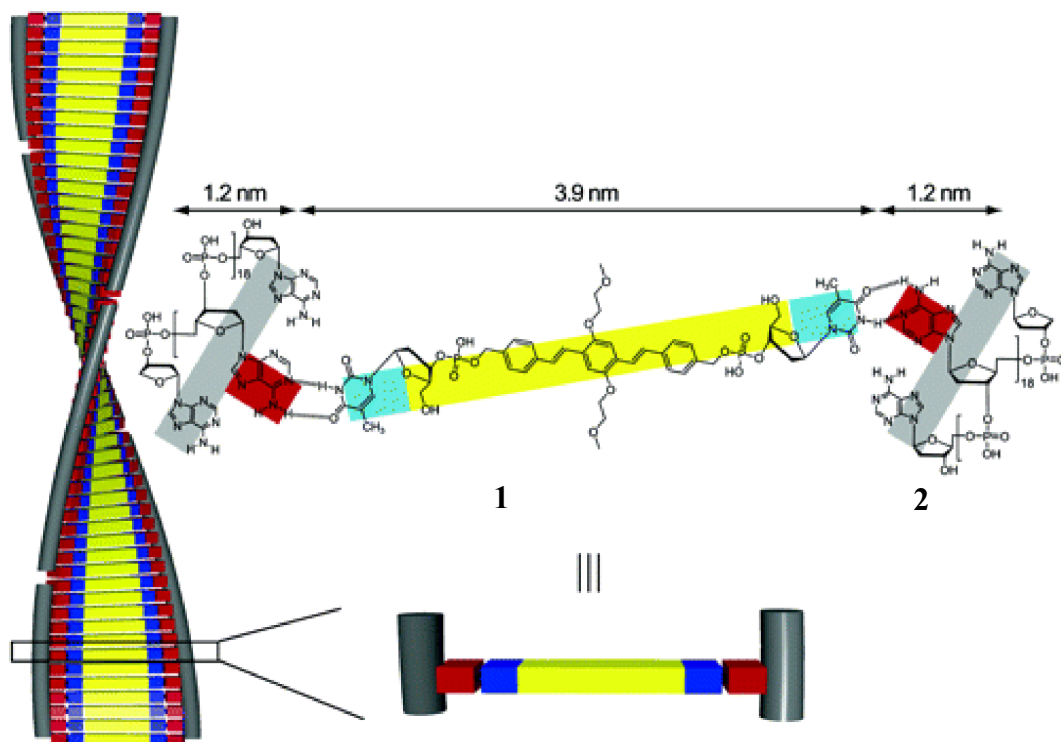


**Figure 1.1:** Proposed structure for the binary self-assembly of **1** and **2** (T:A = 1:1).

Reproduced with permission.<sup>17</sup> Copyright 2006 American Chemical Society.

For example, in 2006, Meijer *et al.*<sup>17</sup> synthesized a bola-shape hybrid molecule **1** combining an oligo(*p*-phenylenevinylene) (OPV) core with two thymidine moieties at its both ends (Figure 1.1). The thymidine moieties provide strong hydrophilicity, chirality, and molecular recognition ability to the self-assembling unit, *i.e.*, the hybrid molecule **1**. Its complementary self-assembly partner is the 20-meric oligoadenine sequence **2**. It is used as the template to sandwich the OPV chromophores between two strands of oligoadenine to form supramolecular helical stacks. The driving force of this self-assembly process is mainly the hydrogen bonding between thymidine and adenine

moieties.

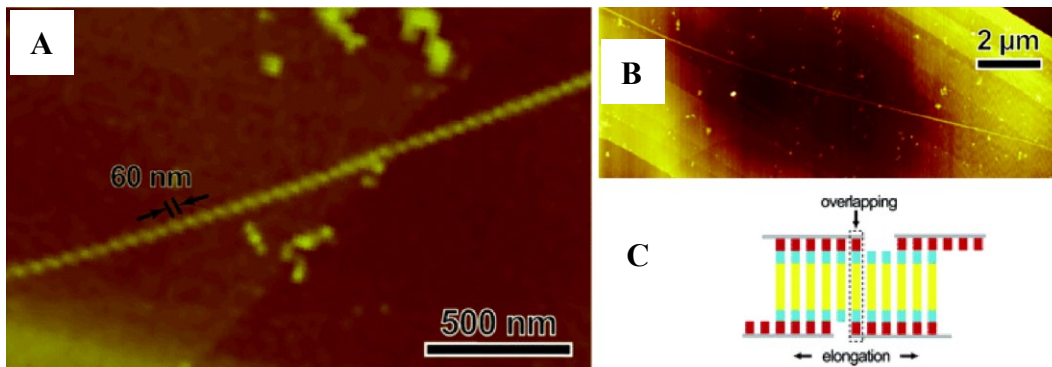


**Figure 1.2:** AFM images for the binary self-assembly of **1** and **2** (T:A = 1:1) (A, B) and possible elongation mechanism for the helical stacks (C). Reproduced with permission.<sup>17</sup>

Copyright 2006 American Chemical Society.

The authors investigated the self-assembly behavior of the two components **1** and **2** in a 1:1 thymine (T)/adenine (A) stoichiometry with atomic force microscopy (AFM). The AFM images clearly show the formation of elongated and right-handed helical stacks with a length of 15 μm and a helical pitch of 60 nm (Figure 1.2A, B). The elongation of the helical structures is attributed to the partial overlapping of **2** at the end of the binary assemblies (Figure 1.2C). Moreover, the measured thickness of the helical stacks (6.4 nm) is compatible with the sum of the molecular width of **1** (3.9 nm) and two strands of **2** (two times 1.2 nm) calculated by molecular modeling.

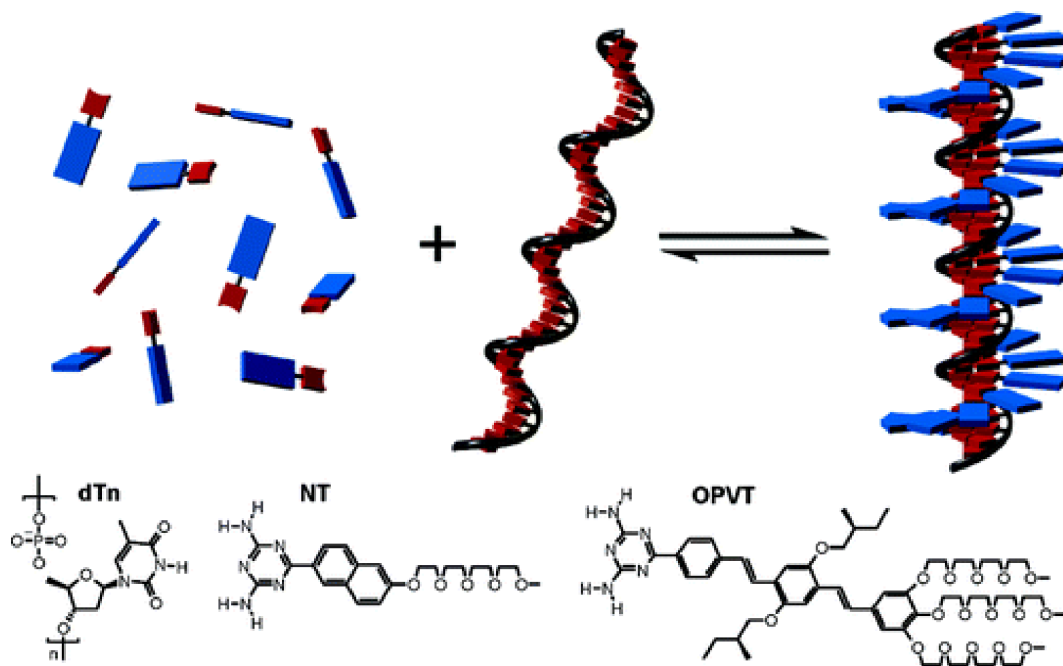


**Figure 1.3:** Representation of a single strand DNA (ssDNA) templated self-assembly of chromophores (black strand, ssDNA; blue bar, chromophores; red bar, hydrogen bonding unit) and molecular structures of dT40, NT, and OPVT. Reproduced with permission.<sup>18</sup>

Copyright 2007 American Chemical Society.

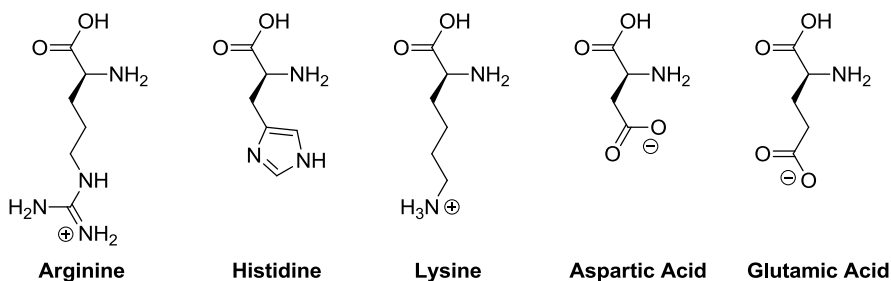
The group of Meijer and Schenning<sup>18</sup> reported a single strand DNA (ssDNA) templated self-assembly of chromophores, giving a new type of DNA hybrid for the construction of organized self-assembled nanostructures (Figure 1.3). In this hybrid architecture, a single 40-meric oligothymine chain (dT40) is used as the template to organize adenine-modified naphthalenes (NT) and oligo(*p*-phenylenevinylene) (OPVT) into supramolecular stacks through hydrogen bonding between thymine and adenine. Remarkably, after NT is added to dT40, a positive Cotton effect is present at the wavelength where the achiral NT

absorbs. This finding shows the binding of NT to dT40 and the chirality expressed in the supramolecular organization of NTs by the ssDNA template dT40. Another chromophore, OPVT is arranged in a right-handed helical structure upon binding to the same template dT40, indicated by the positive Cotton effect at higher wavelength and the negative Cotton effect at lower wavelengths.

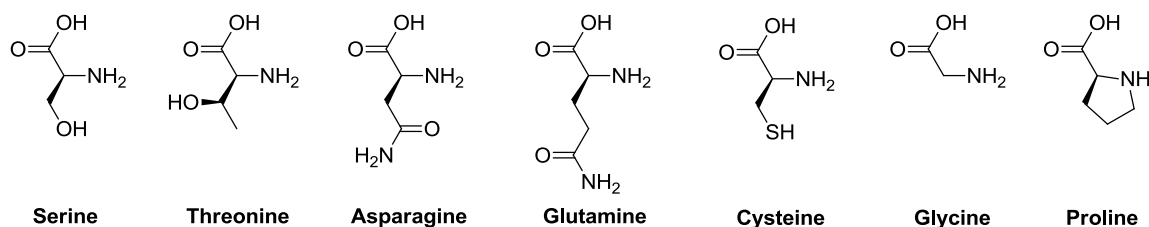
### **1.3. Peptide systems**

Amino acids are amphiprotic organic molecules composed of amine and carboxylic acid and bear side groups specific to each amino acid (Figure 1.4). In nature, peptides and proteins are constructed of amino acids. The self-assembly of complementary peptides into secondary structures (*e.g.*,  $\alpha$ -helix and  $\beta$ -sheet) and subsequent tertiary structures for proteins is driven by the dominating hydrogen bonding<sup>19</sup> and weak interactions such as the hydrophobic effect<sup>20</sup> and  $\pi$ - $\pi$  stacking.<sup>21</sup> Electrostatic forces also play an important role as the charged residues are exposed to the outer surface of a protein to favor their interactions with water.<sup>19d,22</sup> The self-assembled proteins are therefore stimuli-responsive to changes in external environments such as pH, ionic strength, and temperature variations.<sup>23</sup>

### A. Aminoacids with Electrically Charged Side Chains



### B. Aminoacids with Polar Uncharged Side Chains



### C. Aminoacids with Nonpolar Side Chains

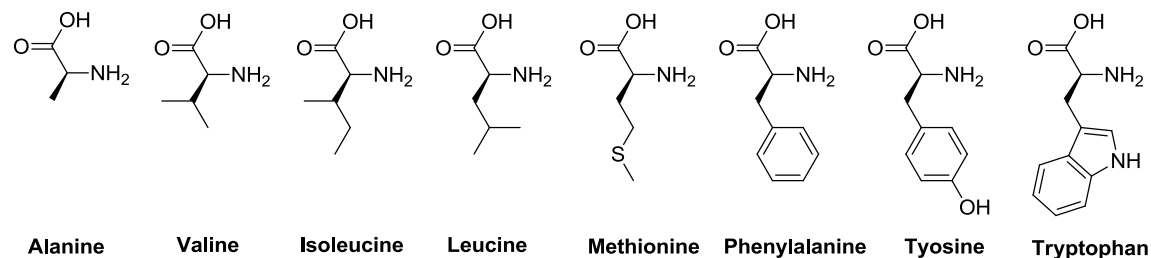


**Figure 1.4:** The 20 amino acids at physiological pH 7.4, grouped according to their side chains

Inspired by nature, artificial peptides with self-assembling behaviors have been developed to construct a vast array of functional nanostructures including nanotubes, nanofibers, nanobelts, and nanovesicles.<sup>24</sup> Among the various designs of peptides for supramolecular nanostructures, peptide amphiphiles stand for a novel approach.<sup>19d,25</sup> These peptides usually comprise a hydrophilic head of polar peptide sequence and a hydrophobic tail that can be an aliphatic chain or a nonpolar peptide sequence. The

peptide amphiphiles system has found its applications in a wide range of bionanomaterials such as biosensors and tissue engineering.<sup>26</sup>

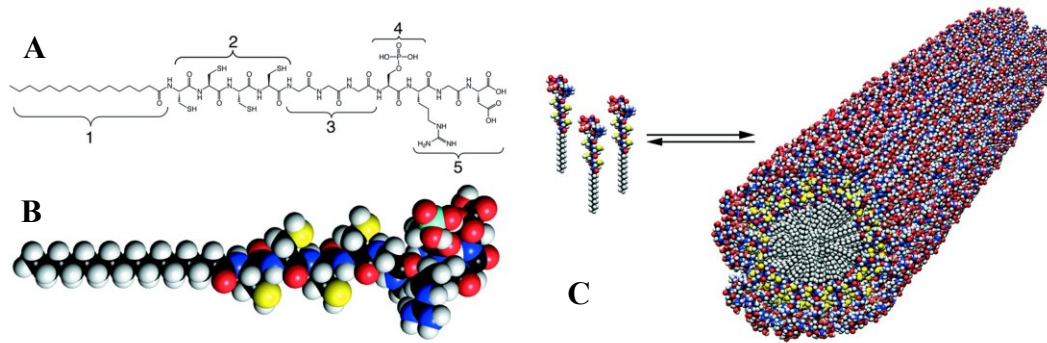


**Figure 1.5:** Chemical structure of the peptide amphiphile (PA) (A), molecular model of PA (B), and schematic representation of the self-assembly of PAs into a nanofiber (C).

Reproduced with permission.<sup>25a</sup> Copyright 2001 AAAS.

The work of the Stupp group<sup>25a</sup> more than a decade ago presented the use of a peptide amphiphiles (PA) to prepare 1D nanostructures in water through self-assembly (Figure 1.5). The self-assembling PA molecule is based on a long alkyl tail with hydrophobic character (Region 1, Figure 1.5A) and a hydrophilic peptide sequence head (Region 2–5, Figure 1.5A). Hydrophobic affinity of the alkyl tails and hydrogen bonding between the peptide heads directs the self-assembly of the PAs into nanofibers of high aspect ratio with a diameter of  $\sim 7.6$  nm and up to micrometers long, revealed by transmission electron microscopy (TEM). In addition, four consecutive cysteine amino acids (Region 2) incorporated into the sequence can form cross-linking disulfide bonds upon oxidation for

covalent capture of the self-assembled structure and to make the nanofiber robust. Region 3 of Figure 1.5A is a flexible linker composed of three glycine residues. The single phosphorylated serine residue incorporated in Region 4 allows the self-assembled nanofiber with cross-linking to strongly interact with calcium ions and directs mineralization of hydroxyapatite (HA). Region 5 is the recognition sequence of Arg-Gly-Asp (RGD) that plays an important role in cellular attachment. The resulting mineralized nanofiber with the crystallographic c axis of HA aligned with the long axis of the fiber is identical to the hierarchical organization of bone at the lowest level.

More recently, another category of work involving the combination of peptide amphiphiles and  $\pi$ -conjugated oligomers have also attracted much attention.<sup>27</sup> In these studies,  $\pi$ -conjugated oligomers are orientated and packed in highly ordered nanostructures directed by the peptide sequence. Such systems are designed to control the morphology of semiconducting materials at the nanoscale level and improve their electronic performance<sup>28</sup> and construct nanowires.<sup>29</sup>

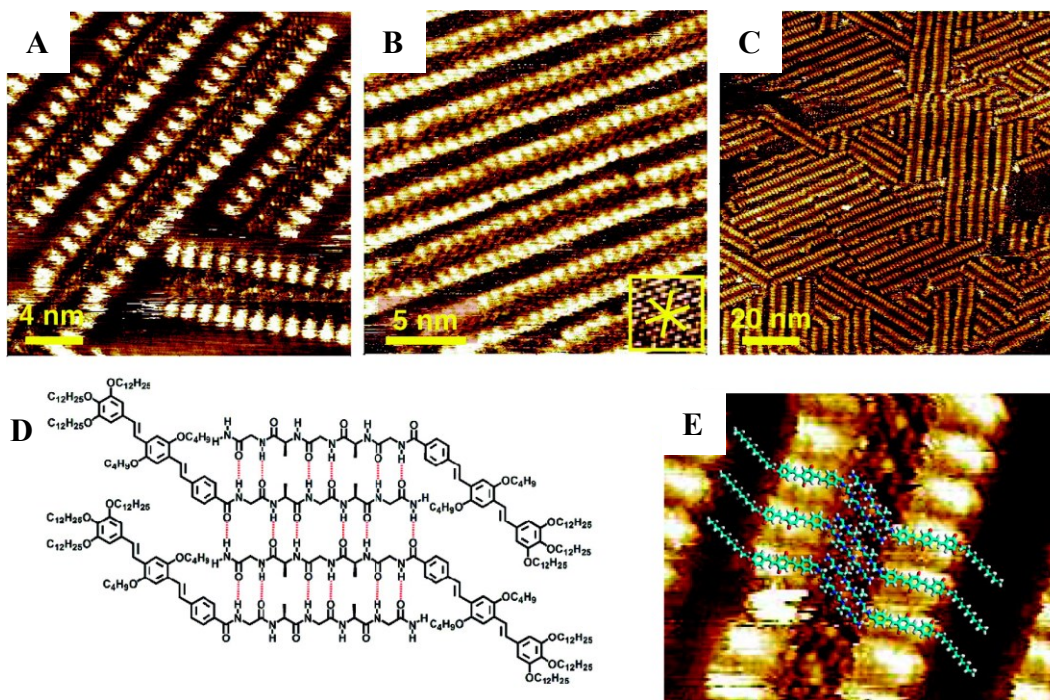


**Figure 1.6:** STM images of OPV-GAGAG at liquid-solid interface (A–C), a schematic representation of the hydrogen bonding between OPV-GAGAG molecules (D), and a molecular model of OPV-GAGAG superimposed with a zoom of the STM image (E). Reproduced with permission.<sup>30</sup> Copyright 2008 American Chemical Society.

For example, in 2008, Schenning and co-workers<sup>30</sup> synthesized a hybrid peptide amphiphile composed of an oligo(*p*-phenylenevinylene) (OPV) and a silk-inspired gly-ala-gly-ala-gly (GAGAG) peptide sequence with a propensity to form a  $\beta$ -sheet secondary structure (Figure 1.6). The self-assembly of the OPV-GAGAG conjugate at liquid-solid interface was investigated by scanning tunneling microscopy (STM). The STM images reveal the formation of very regular one-dimensional bilayers and each of them contains three rows (Figure 1.6A–C). The bright rows are related to the OPVs

(highest tunneling efficiency) while the darker rod in between corresponds to the peptide moieties. The measurements of the bilayers by STM show that the width of a bilayer is 5.1 nm, the distance between different OPV units is 1.2 nm, and the angle between the OPV and the peptide  $\sim 157^\circ$ . A molecular model of an antiparallel  $\beta$ -sheet arrangement fits the measurement very well (Figure 1.6D, E). In this conformation, the OPV-GAGAG molecules are aligned antiparallel next to each other and six hydrogen bonds are formed between each peptide backbone to hold the  $\beta$ -sheet structure.

#### **1.4. $\pi$ -Conjugated systems**

Over the past decade, many self-assembled 1D nanostructures have been developed based on  $\pi$ -conjugated semiconducting organic molecules such as hexabenzocoronene<sup>31</sup> and porphyrins<sup>32</sup> with disk-shaped aromatics. Owing to the planar molecular framework and highly delocalized  $\pi$ -systems of these organic semiconductors, their self-assembly is dominated by strong  $\pi$ - $\pi$  stacking with large anisotropy and consequently leads to the formation of 1D nanostructures.<sup>29b,33</sup> Thus, the formation of such nanostructures can be controlled by varying the self-assembly conditions including concentration, solvent, and temperature.<sup>34</sup> Moreover such nanostructures, using organic semiconductors as the self-assembling building blocks, often reveal the extraordinary electronic properties provided by the extended  $\pi$ -systems, and, as a result, have potential applications in

organic electronic devices.<sup>35</sup>

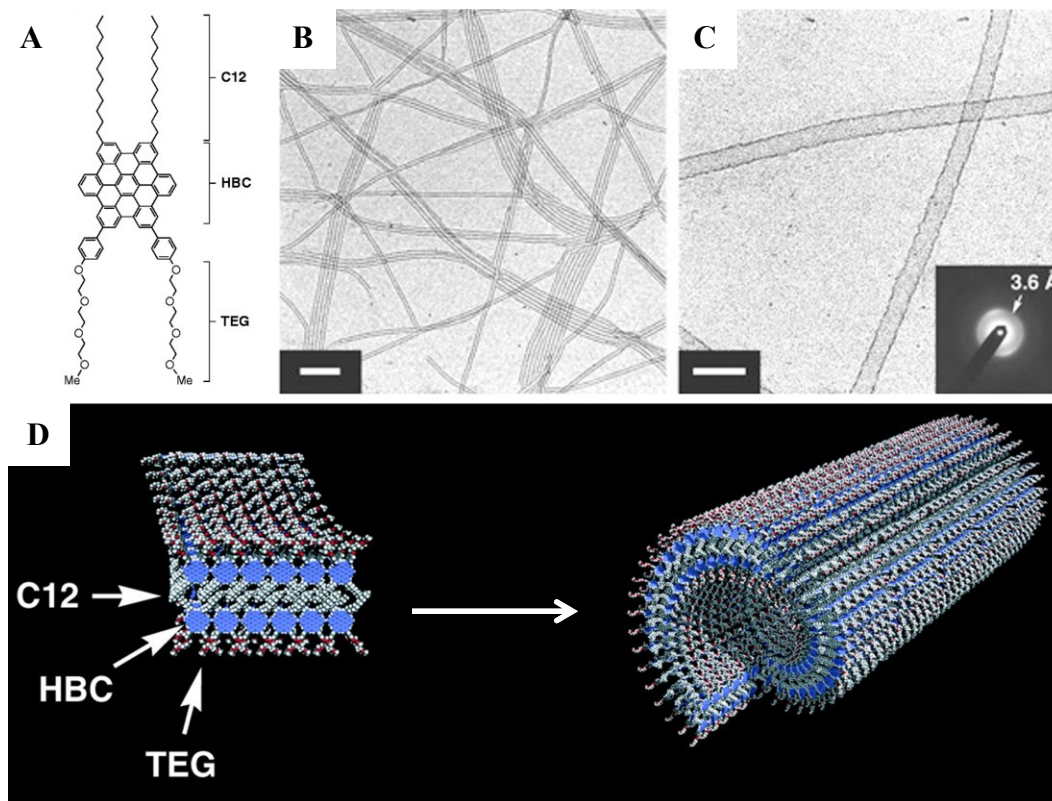


**Figure 1.7:** Molecular structure of the amphiphilic HBC (A), TEM image of the nanotube (B, C), and a molecular model representing the self-assembled graphitic nanotube (D). Reproduced with permission.<sup>36</sup> Copyright 2004 AAAS.

For example, the group of Fukushima and Aida<sup>36</sup> discovered an amphiphilic hexabenzocoronene (HBC) with two triethylene glycol chains (TEG) on one side and two dodecyl chains (C12) on the other that self-assembles into a nanotubular structure with an open-ended hollow (Figure 1.7). The 10- $\mu\text{m}$ -long nanotube reveals a high aspect ratio with a uniform external diameter of 20 nm measured by TEM. The wall composed of a

helical bilayer of  $\pi$ -stacked graphene molecules is estimated to be 3 nm and an internal tube diameter is therefore 14 nm. From the I-V profile, the resistivity of the nanotube is determined as 2.5 M $\Omega$ . It suggests that the electrical conductivity of this graphitic nanotube is comparable to an inorganic semiconducting nanotube of gallium nitride with a resistivity of  $\sim 10$  M $\Omega$ .

### 1.5. RNT as a specific example

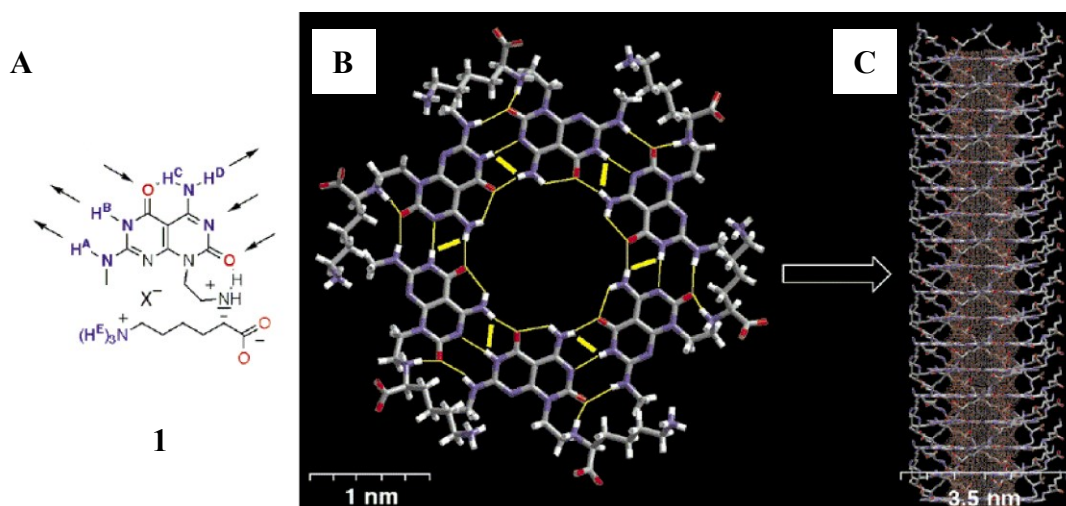


**Figure 1.8:** Molecular structure of L-module **1** (A), molecular model of the rosette resulting from **1** (B),\* and the molecular model of the RNT. \*The thin yellow lines show the hydrogen bond network. Reproduced with permission.<sup>37</sup> Copyright 2001 American Chemical Society.

About a decade ago, Fenniri et al. reported a new class of self-assembled organic nanomaterials called rosette nanotubes (RNTs) (Figure 1.8).<sup>37</sup> They are constructed

through the hierarchical self-assembly of the heteroaromatic bicyclic base G<sup>^</sup>C under physiological conditions. The G<sup>^</sup>C base is a hydrophobic hybrid molecule combining two complementary DNA bases, the Watson-Crick donor-donor-acceptor of guanine (G) and acceptor-acceptor-donor of cytosine (C). Such hydrogen bonding arrays direct the self-assembly of G<sup>^</sup>C bases to produce a six-membered supermacrocycle, termed a rosette. The resulting rosette is stabilized by 18 hydrogen bonds. Driven by hydrophobic affinity and  $\pi$ - $\pi$  stacking, the rosettes undergo a second level of organization to form a well-defined 1D tubular nanostructure in water. We name the self-assembled nanomaterials with this kind of architecture rosette nanotubes (RNTs). The inner diameter of RNT is defined by the distance separating the hydrogen bonding arrays within a G<sup>^</sup>C base and the outer diameter mainly depends on the functional groups on the periphery of the structure.<sup>38</sup> Since then, owing to its ease of chemical modification and compatibility with biological systems, RNTs have found applications in many biomedical research fields, such as drug delivery and tissue engineering.<sup>39</sup>

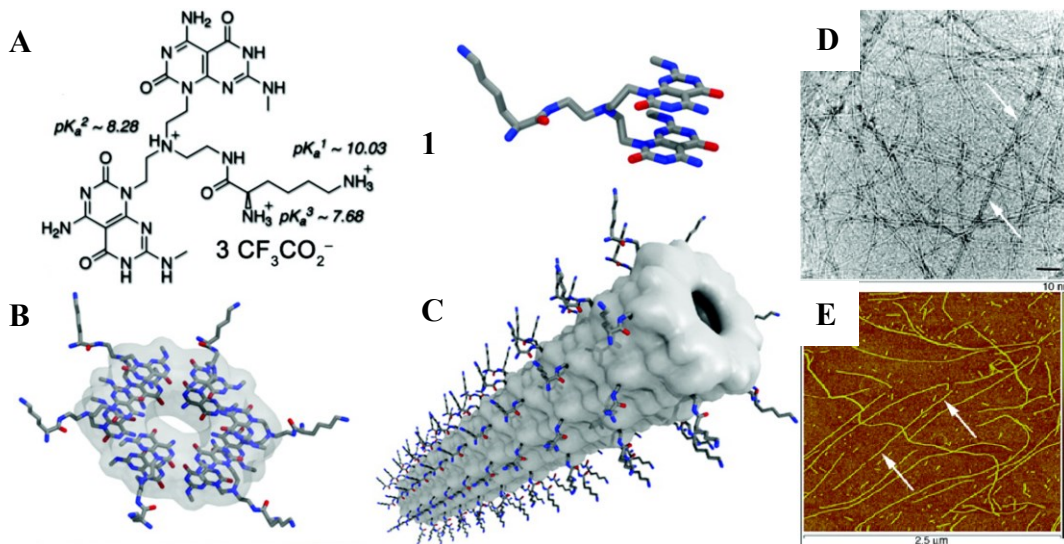


**Figure 1.9:** Molecular structure of twin G<sup>^</sup>C base **1** (A), self-assembled double rosette (B), self-assembled RNT obtained from rosette stacking (C), negatively stained TEM image (D, scale bar = 50 nm) and TM-AFM image of the RNTs (E). Reproduced with permission.<sup>40,41</sup> Copyright 2005 and 2010 American Chemical Society.

At the same time, our group has also been focusing on tuning the stability of the RNT architectures. For example, the twin G<sup>^</sup>C variant is designed to lower the charge density, lower steric repulsion of functional groups, and gain more hydrogen bonds per self-assembling unit.<sup>40</sup> In water, twin G<sup>^</sup>C bases **1** (Figure 1.9A, B) functionalized with positively charged lysine side chains self-assemble into double rosettes (Figure 1.9B), maintained by 36 hydrogen bonds per each. Then the double rosettes self-assemble into helical stacks, resulting in RNTs (Figure 1.9C). TEM (Figure 1.9D) measures a diameter of  $4.0 \pm 0.3$  nm and TM-AFM (Figure 1.9E) features a diameter of 3.3 nm. These values are comparable to the calculated average diameter of 3.8 nm.

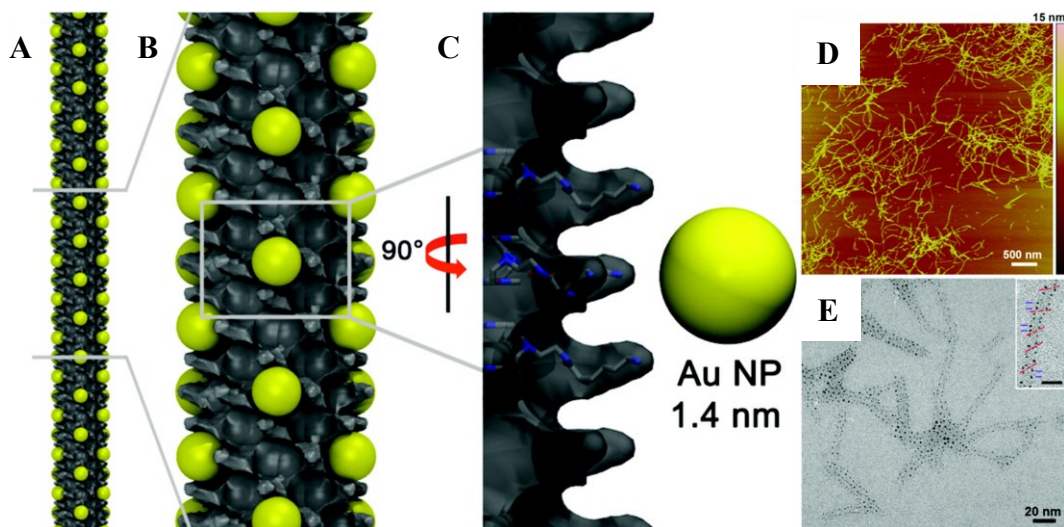


**Figure 1.10:** RNTs with nucleated Au NPs (gold spheres) (A, B), a close-up view of the nucleation site (C), TM-AFM image (D) and TEM image (E) of Au NP coated RNTs. Reproduced with permission.<sup>41</sup> Copyright 2010 American Chemical Society.

The self-assembled RNTs of twin G $\wedge$ C bases **1** as shown in Figure 1.9 were used as a template to form Au nanoparticles (NPs) with a narrow size distribution (Figure 1.10A–C).<sup>41</sup> The growth of the Au NPs on the RNTs is reasoned as follows. The positively charged lysine side chains on the RNTs coordinate to the negatively charged tetrachloroaurate ( $\text{AuCl}_4^-$ ). Then  $\text{AuCl}_4^-$  is reduced by hydrazine ( $\text{N}_2\text{H}_4$ ) and each lysine site acts as a nucleation point for the formation of Au NPs. In the experiment, a solution of **1** in water (50  $\mu\text{M}$ ) was mixed with  $\text{HAuCl}_4$  at molar ratio of 1:20 [**1**]/[ $\text{HAuCl}_4$ ] and the [ $\text{HAuCl}_4$ ]/[ $\text{N}_2\text{H}_4 \cdot \text{H}_2\text{O}$ ] molar ratio was kept at 10:1. It yielded Au NPs with a mean diameter of  $1.4 \pm 0.2$  nm and an average interparticle distance of  $3.8 \pm 0.8$  nm. While a

solution of **1** in water at 1 mM with the same  $[1]/[HAuCl_4]$  and  $[HAuCl_4]/[N_2H_4 \cdot H_2O]$  ratios gave the mean NP diameter of  $1.5 \pm 0.1$  nm with an interparticle distance of  $3.5 \pm 0.4$  nm. TM-AFM image (Figure 1.10D) of the Au NPs incorporated RNTs features a height of  $\sim 4.6$  nm greater than that of the RNTs without Au NPs (3.3 nm). The TEM image in Figure 1.10E shows the morphogenesis of the Au NPs appearing as small dots on the RNT surface.

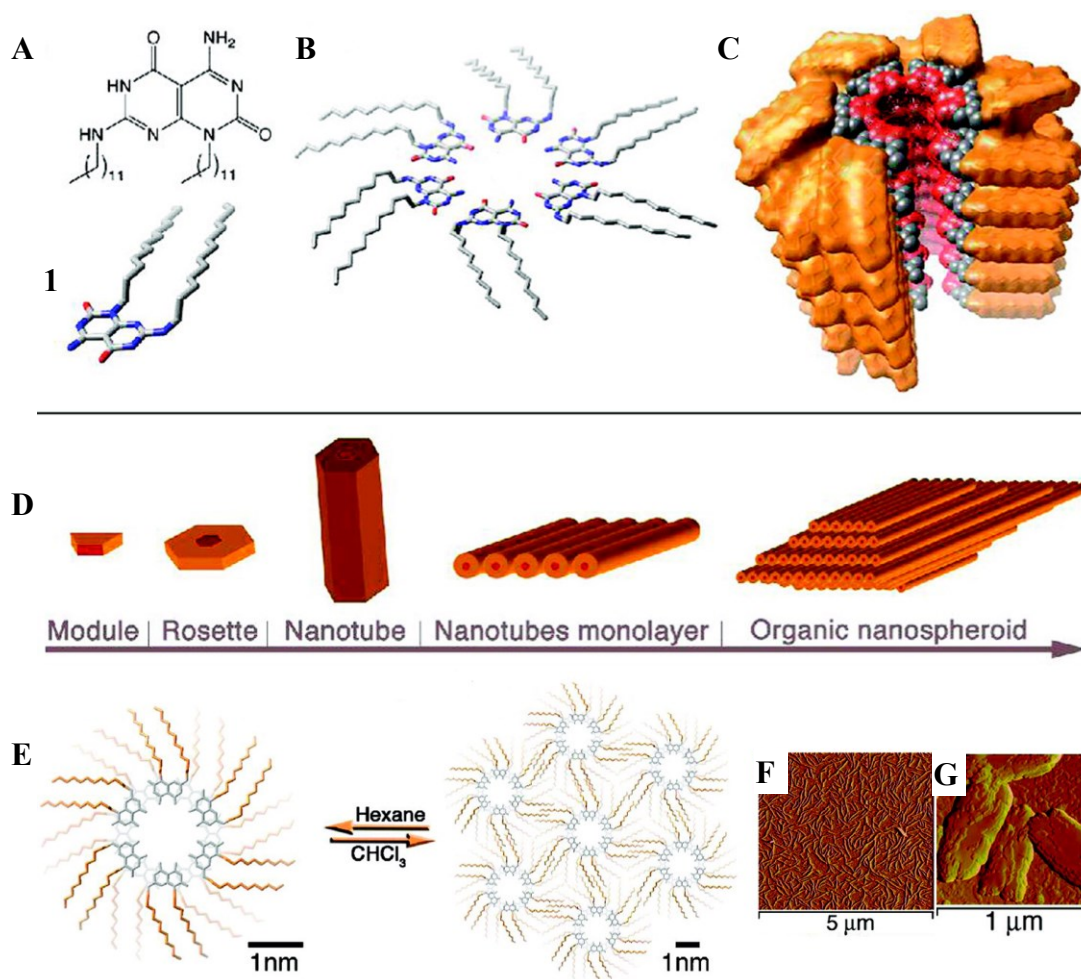


**Figure 1.11:** Molecular structure of G<sup>C</sup> base **1** (A), self-assembled rosette (B) and RNT

(C)\*, schematic representation of RNTs' self-organization into monolayer and then lamellar prolate nanospheroids (D), solvent-promoted transition between RNT and nanospheroids (E), TM-AFM images of RNTs (F) and nanospheroids (G). \*One module is removed from each rosette along the RNT wall to unveil the inner channel (red). Reproduced with permission.<sup>42</sup> Copyright 2008 American Chemical Society.

In another example, a G<sup>+</sup>C base bearing two C<sub>12</sub> alkyl chains **1** was discovered to self-assemble into RNTs in hexane, a nonpolar solvent (Figure 1.11A–C, F).<sup>42</sup> In this solvent, the solvation of the alkyl chains is favorable but the base is not due to its polar nature. The self-assembly of **1** into RNTs is driven by polar and stacking interactions between the bases rather than hydrophobic affinity, one of the driven forces for the previously shown water-soluble hydrophilic RNTs. Furthermore, nonpolar hexane is anticipated to strengthen the intermolecular hydrogen bonding to stabilize rosettes. In another nonpolar solvent, chloroform, the formation of RNTs is driven by similar intermolecular interactions. But the solvation free energy of the RNTs in chloroform is lower than that in hexane, so the solute–solute interactions (i.e. interchain van der Waals) are favorable relative to the solute–solvent interactions. It results in subsequent self-organization of the RNTs into lamellar prolate nanospheroids to minimize the solute–solvent interactions and maximize the favorable solute–solute interactions (Figure 1.11D, E, G).

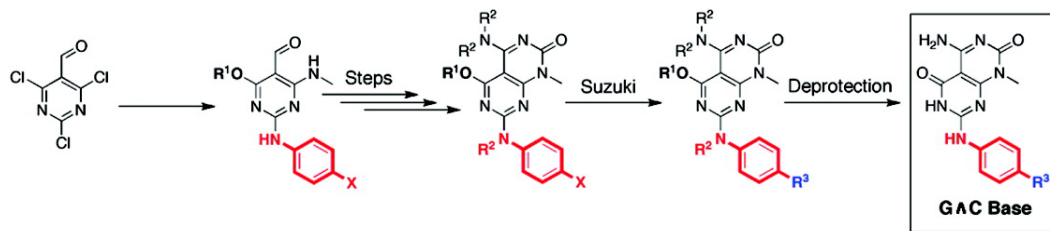


**Figure 1.12:** Aromatic functionalized GAC bases. Reproduced with permission.<sup>43</sup>

Copyright 2008 American Chemical Society.

An iodophenyl functionalized GAC base is also developed and further derivatized using a Suzuki-Miyaura coupling reaction<sup>43</sup> (Figure 1.12, see Chapter 2 and 3 for more details).

My work is to investigate the self-assembly of these new types of GAC bases and functionalize the iodophenyl GAC base with oligothiophenes (Figure 3.x, Chapter 3) for organic electronic applications.

## 1.6. Conclusion

Great progress has been made in self-assembled organic nanomaterials in the past decades. Many of these nanomaterials are inspired by biological self-assembly systems, such as DNA and proteins. They are based on diverse noncovalent molecular interactions like hydrogen bonding,  $\pi$ - $\pi$  stacking, electrostatic forces, hydrophobic forces etc.  $\pi$ - $\pi$  stacking can work solely to direct the self-assembly of  $\pi$ -conjugated nanostructures. These nanomaterials have found their applications in various fields, from artificial cells

and tissues to nanoelectronics.

RNTs, a type of self-assembled organic nanomaterials developed by our group, are based on the self-assembly of heterobicyclic G<sup>A</sup>C base. It is a self-complementary hybrid molecule composed of guanine and cytosine with their respective hydrogen bonding arrays. The G<sup>A</sup>C base is designed to easily allow chemical functionalization, making RNTs suitable for biomedical research as well as templating metal-NPs growth. However, the use of RNTs in organic electronics is nearly unexplored. So my work presented in this thesis focuses on addressing this issue. The second chapter introduces a new method to functionalize RNTs with small aromatic groups as the initial steps to utilize RNTs for electronic applications. The third chapter describes the synthesis of oligothiophene functionalized G<sup>A</sup>C bases and the investigation of the self-assembly of them under various conditions. Those molecules have potential applications in organic electronic devices.

## 1.7. References

1. Seeman, N. C. *Angew. Chem., Int. Ed.* **1998**, *37*, 3220-3238.
2. (a) Gazit, E. *Chem. Soc. Rev.* **2007**, *36*, 1263-1269. (b) Zhao, X.; Pan, F.; Xu, H.; Yaseen, M.; Shan, H.; Hauser, C. A. E.; Zhang, S.; Lu, J. R. *Chem. Soc. Rev.* **2010**, *39*, 3480-3498.
3. (a) Seto, C. T.; Whitesides, G. M. *J. Am. Chem. Soc.* **1993**, *115*, 905-916. (b) Mathias, J. P.; Simanek, E. E.; Seto, C. T.; Whitesides, G. *Angew. Chem., Int. Ed.* **1993**, *32*, 1766-1769.
4. [http://www.nobelprize.org/nobel\\_prizes/chemistry/laureates/1987/](http://www.nobelprize.org/nobel_prizes/chemistry/laureates/1987/) (accessed July 7, 2014).
5. (a) Berl, V.; Huc, I.; Khoury, R. G.; Krische, M. J.; Lehn, J. M. *Nature*, **2000**, *407*, 720-723. (b) Ramstrom, O.; Bunyapaiboonsri, T.; Lohmann, S.; Lehn, J. M. *Biochim. Biophys. Acta.* **2002**, *1572*, 178-186.
6. (a) Cram, D. J. *Science* **1988**, *240*, 760-767. (b) Cram, D. J. *Nature* **1992**, *356*, 29-36.
7. Pederson, C. J. *J. Am. Chem. Soc.* **1967**, *89*, 7017-7036.
8. Whitesides, G. M.; Mathias, J. P.; Seto, C. T. *Science* **1991**, *254*, 1312-1319.
9. Ikkala, O.; Brinke, G. *Chem. Commun.* **2004**, *19*, 2131-2137.

10. (a) Lehn, J. M. *Angew. Chem., Int. Ed.* **1988**, *27*, 89-112. (b) Lehn, J. M. *Angew. Chem., Int. Ed.* **1990**, *29*, 1304-1319. (c) Lehn, J. M. *Science* **2002**, *295*, 2400-2403. (d) Whitesides, G. M.; Grzybowski, B. *Science* **2002**, *295*, 2418-2421.
11. (a) Stupp, S. I.; Palmer, L. C. *Chem. Mater.* **2014**, *26*, 507-518. (b) Moulin, E.; Cid, J. J.; Giuseppone, N. *Adv. Mater.* **2013**, *25*, 477-487.
12. Kim, F. S.; Ren, G.; Jenekhe S. A. *Chem. Mater.* **2011**, *23*, 682-732.
13. (a) Bong, D. T.; Clark, T. D.; Granja, J. R.; Ghadiri, M. R. *Angew. Chem. Int. Ed.* **2001**, *40*, 988-1011. (b) Bonifazi, D.; Maggini, L. *Chem. Soc. Rev.* **2012**, *41*, 211-241.
14. (a) Chen, J. H.; Seeman, N. C. *Nature*, **1991**, *350*, 631-633. (b) Seeman, N. C. *Nature*, **2003**, *421*, 427-431.
15. Alemdaroglu, F.; Herrmann, A. *Org. Biomol. Chem.* **2007**, *5*, 1311-1320.
16. (a) Storhoff, J. J.; Mirkin, C. A. *Chem. Rev.* **1999**, *99*, 1849-1862. (b) Kwak, M.; Herrmann, A. *Chem. Soc. Rev.* **2011**, *40*, 5745-5755.
17. Iwaura, R.; Hoeben, F. J. M.; Masuda, M.; Schenning, A. P. H. J.; Meijer E. W.; Shimizu, T. *J. Am. Chem. Soc.* **2006**, *128*, 13298-13304.
18. Janssen, P. G. A.; Vandenbergh, J.; van Dongen, J. L. J.; Meijer, E. W.; Schenning, A. P. H. J. *J. Am. Chem. Soc.* **2007**, *129*, 6078-6079.
19. (a) Ghadiri, M. R.; Granja, J. R.; Milligan, R. A.; McRee, D. E.; Khazanovich, N.

- Nature* **1993**, *366*, 324-327. (b) Hartgerink, J. D.; Granja, J. R.; Milligan, R. A.; Ghadiri, M. R. *J. Am. Chem. Soc.* **1996**, *118*, 43-50. (c) Ranganathan, D.; Lakshmi, C.; Karle, I. L. *J. Am. Chem. Soc.* **1999**, *121*, 6103-6107. (d) Paramonov, S. E.; Jun, H. W.; Hartgerink, J. D. *J. Am. Chem. Soc.* **2006**, *128*, 7291-7298.
20. (a) Santoso, S.; Hwang, W.; Hartman, H.; Zhang, S. *Nano Lett.* **2002**, *2*, 687-691. (b) von Maltzahn, G.; Vauthey, S.; Santoso, S.; Zhang, S. *Langmuir* **2003**, *19*, 4332-4337. (c) Khoe, U.; Yang, Y.; Zhang, S. *Macromol. Biosci.* **2008**, *8*, 1060-1067. (d) Khoe, U.; Yang, Y.; Zhang, S. *Langmuir* **2009**, *25*, 4111-4114.
21. (a) Toledano, S.; Williams, R. J.; Jayawarna, V.; Ulijn, R. V. *J. Am. Chem. Soc.* **2006**, *128*, 1070-1071. (b) Laromaine, A.; Koh, L.; Murugesan, M.; Ulijn, R. V.; Stevens, M. M. *J. Am. Chem. Soc.* **2007**, *129*, 4156-4157. (c) Ulijn, R. V.; Smith, A. M. *Chem. Soc. Rev.* **2008**, *37*, 664-675. (d) Das, A. K.; Collins, R.; Ulijn, R. V. *Small* **2008**, *4*, 279-287. (e) Cousins, B. G.; Das, A. K.; Sharma, R.; Li, Y.; McNamara, J. P.; Hillier, I. H.; Kinloch, I. A.; Ulijn, R. V. *Small*, **2009**, *5*, 587-590.
22. Stendahl, J. C.; Rao, M. S.; Guler, M. O.; Stupp, S. I. *Adv. Funct. Mater.* **2006**, *16*, 499-508.
23. Jun, H. W.; Paramonov, S. E.; Dong, H.; Forraz, N.; McGuckin, C.; Hartgerink, J. D. *J. Biomater. Sci. Polym. Ed.* **2008**, *19*, 665-676.

24. Childers, W. S.; Ni, R.; Mehta, A. K.; Lynn, D. G. *Curr. Opin. Chem. Biol.* **2009**, *13*, 652-659.
25. (a) Hartgerink, J. D.; Beniash, E.; Stupp, S. I. *Science* **2001**, *294*, 1684-1688. (b) Silva, G. A.; Czeisler, C.; Niece, K. L.; Beniash, E.; Harrington, D. A.; Kessler, J. A.; Stupp, S. I. *Science* **2004**, *303*, 1352-1355. (c) Behanna, H. A.; Donners, J. J. J. M.; Gordon, A. C.; Stupp, S. I. *J. Am. Chem. Soc.* **2005**, *127*, 1193-1200.
26. Lowik, D. W. P. M.; van Hest, J. C. M. *Chem. Soc. Rev.* **2004**, *33*, 234-245.
27. (a) Jatsch, A.; Schillinger, E. K.; Schmid, S.; Bäuerle, P. *J. Mater. Chem.* **2010**, *20*, 3563-3578. (b) Kim, H. S.; Parquette, J. R. *Nanoscale* **2012**, *4*, 6940-6947.
28. Nilsson, K. P. R.; Rydberg, J.; Baltzer, L.; Inganäs, O. *Proc. Natl. Acad. Sci. U.S.A.* **2003**, *100*, 10170-10174.
29. (a) Hoeben, F. J. M.; Jonkheijm, P.; Meijer, E. W.; Schenning, A. P. H. J. *Chem. Rev.* **2005**, *105*, 1491-1546. (b) Schenning, A. P. H. J.; Meijer, E. W. *Chem. Commun.* **2005**, *26*, 3245-3258. (c) Grimsdale, A. C.; Müllen, K. *Angew. Chem., Int. Ed.* **2005**, *44*, 5592-5629. (e) Wu, J.; Pisula, W.; Müllen, K. *Chem. Rev.* **2007**, *107*, 718-747.
30. Matmour, R.; De Cat, I.; George, S. J.; Adriaens, Wencke.; Leclere, P.; Bomans, P. H. H.; Sommerdijk, N. A. J. M.; Gielen, J. C.; Christianen, P. C. M.; Heldens, J. T.;

- van Hest, J. C. M.; Lowik, D. W. P. M.; De Feyter, S.; Meijer, E. W.; Schenning, A. P. H. J. *J. Am. Chem. Soc.* **2008**, *130*, 14576-14583.
31. Wu, J.; Pisula, W.; Müllen, K. *Chem. Rev.* **2007**, *107*, 718-747.
32. (a) Wang, Z.; Medforth, C. J.; Shelnut, J. A. *J. Am. Chem. Soc.* **2004**, *126*, 15954-15955. (b) Schwab, A. D.; Smith, D. E.; Rich, C. S.; Young, E. R.; Smith, W. F.; de Paula, J. C. *J. Phys. Chem. B* **2003**, *107*, 11339-11345. (c) Schwab, A. D.; Smith, D. E.; Bond-Watts, B.; Johnston, D. E.; Hone, J.; Johnson, A. T.; de Paula, J. C.; Smith, W. F. *Nano Lett.* **2004**, *4*, 1261-1265. (d) Rotomskis, R.; Augulis, R.; Snitka, V.; Valiokas, R.; Liedberg, B. *J. Phys. Chem. B* **2004**, *108*, 2833-2838. (e) Wang, Z.; Medforth, C. J.; Shelnut, J. A. *J. Am. Chem. Soc.* **2004**, *126*, 16720-16721.
33. Lehn, J. M. *Supramolecular Chemistry: Concepts and Perspectives*; John Wiley & Sons: Hoboken, NJ, 1995.
34. (a) Muthukumar, M.; Ober, C. K.; Thomas, E. L. *Science* **1997**, *277*, 1225-1232. (b) Halperin, A.; Tirrell, M.; Lodge, T. *Adv. Polym. Sci.* **1992**, *100*, 31-71.
35. Kim, F. S.; Ren, G.; Jenekhe, S. A. *Chem. Mater.* **2011**, *23*, 682-732.
36. Hill, J. P.; Jin, W.; Kosaka, A.; Fukushima, T.; Ichihara, H.; Shimomura, T.; Ito, K.; Hashizume, T.; Ishii, N.; Aida, T. *Science* **2004**, *304*, 1481-1483.
37. Fenniri, H.; Mathivanan, P.; Vidale, K. L.; Sherman, D. M.; Hallenga, K.; Wood, K.

- V.; Stowell, J. G. *J. Am. Chem. Soc.* **2001**, *123*, 3854-3855.
38. Fenniri, H.; Deng, B. L.; Ribbe, A. E.; Hallenga, K.; Jacob, J.; Thiyagarajan, P. *Proc. Natl. Acad. Sci. U.S.A.* **2002**, *99*, 6487-6492.
39. (a) Chen, Y.; Bilgen, B.; Pareta, R. A.; Myles, A. J.; Fenniri, H.; Ciombor, D. M.; Aaron, R. K.; Webster, T. J. *Tissue Eng.* **2010**, *16*, 1233-1243. (b) Le, M. H. A.; Suri, S. S.; Rakotondradany, F.; Fenniri, H.; Singh, B. *Vet. Res.* **2010**, *41*, 75-86. (c) Zhang, L.; Hemeraz, U. D.; Fenniri, H.; Webster, T. J. *J. Biomed. Mater. Res. A* **2010**, *95A*, 550-563. (d) Meng, X.; Stout, D. A.; Sun, L.; Beingsner, R. L.; Fenniri, H.; Webster, T. J. *J. Biomed. Mater. Res. A* **2010**, *101A*, 1095-1102. (e) Song, S.; Chen, Y.; Yan, Z.; Fenniri, H.; Webster, T. J. *Int. J. Nanomed.* **2011**, *6*, 101-107. (f) Chen, Y.; Song, S.; Yan, Z.; Fenniri, H.; Webster, T. J. *Int. J. Nanomed.* **2011**, *6*, 1035-1044. (g) Suri, S. S.; Mills, S.; Aulakh, G. K.; Rakotondradany, F.; Fenniri, H.; Singh, B. *Int. J. Nanomed.* **2011**, *6*, 3113-3123.
40. Moralez, J. G.; Raez, J.; Yamazaki, T.; Motkuri, R. K.; Kovalenko, A.; Fenniri, H. *J. Am. Chem. Soc.* **2005**, *127*, 8307-8309.
41. Chhabra, R.; Moralez, J. G.; Raez, J.; Yamazaki, T.; Cho, J. Y.; Myles, A. J.; Kovalenko, A.; Fenniri, H. *J. Am. Chem. Soc.* **2010**, *132*, 32-33.
42. Tikhomirov, G.; Yamazaki, T.; Kovalenko, A.; Fenniri, H. *Langmuir* **2008**, *24*, 4447-4450.

43. Beingsner, R. L.; Deng, B. L.; Fanwick, P. E.; Fenniri, H. *J. Org. Chem.* **2008**, *73*, 931-939.

## Chapter 2

### Synthesis and characterization of aromatic functionalized G $\wedge$ C bases

#### 2.1. Introduction

G $\wedge$ C aldehyde (Figure 2.1), first reported by Dr. Fenniri *et al.* in 2001,<sup>1a</sup> is the main precursor for rosette nanotubes (RNTs). Due to the ease of chemical functionalization of G $\wedge$ C aldehyde through the reductive amination reaction,<sup>1</sup> our group has successfully developed a variety of RNTs, which express unique chemical groups on their outer surface, for applications in tissue engineering and drug delivery.<sup>2</sup>

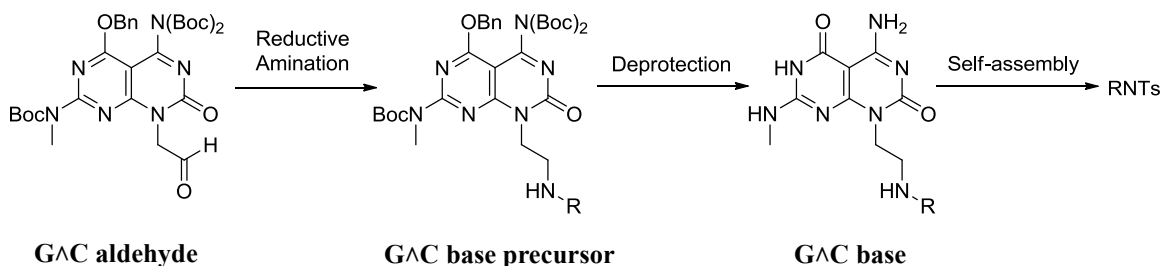


**Figure 2.1:** G $\wedge$ C aldehyde as a main precursor for RNTs

In 2008, Beingessner, Deng *et al.* reported a novel precursor termed G $\wedge$ C iodide that can be readily functionalized with aromatic groups using the Suzuki-Miyaura coupling reaction (Figure 2.2).<sup>3</sup> Their findings provide a promising method to develop aromatic functionalized RNTs as the initial attempts to utilize RNTs in electronic applications. The advantages of this method can be summarized as follows. First, Suzuki-Miyaura coupling

has the advantages of availability of common boronic acids (boronic esters and organotrifluoroborate salts may be used instead), mild reaction conditions, and easy preparation.<sup>4</sup> Second, unlike the synthesis of G $\wedge$ C aldehyde, in which further modification is required to create the active site (oxidation of the olefin to aldehyde under Lemieux-Johnson conditions), the active site of G $\wedge$ C iodide for the cross-coupling is introduced directly by highly regioselective S<sub>N</sub>Ar reaction under phase transfer catalysis (PTC) conditions. PTC has proved to be a powerful tool in organic synthesis due to its advantages of mild and environmentally acceptable reaction conditions, simple operation, scalable production and low cost.<sup>5</sup>

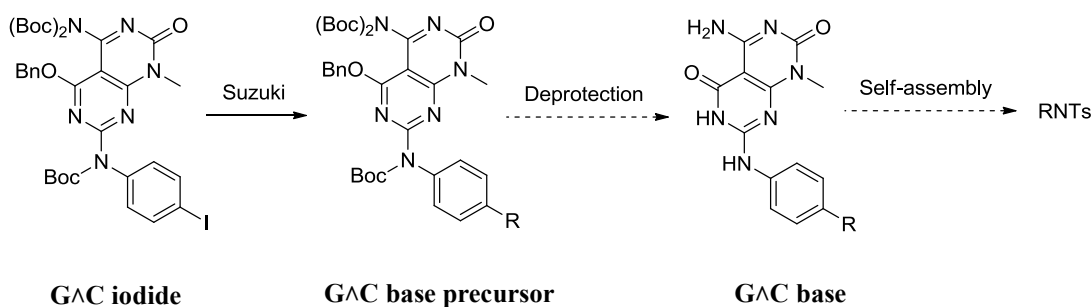
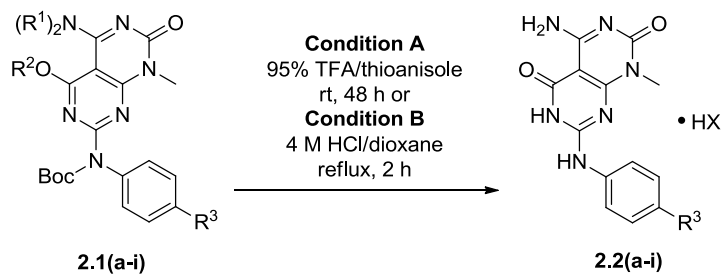


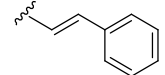
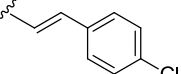
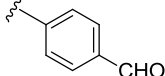
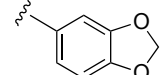
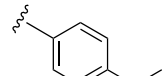
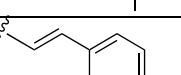
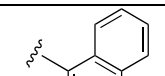
**Figure 2.2:** G $\wedge$ C iodide as a novel precursor for RNTs

However, their work was not completed. There were two key steps that needed to be done (Figure 2.2). First, we needed to fully characterize the G $\wedge$ C bases by NMR to confirm their structures and purity<sup>6</sup>. In their work, only one G $\wedge$ C base precursor was deprotected and only <sup>1</sup>H NMR was obtained for the resulting G $\wedge$ C base.<sup>3</sup> The inability to

acquire  $^{13}\text{C}$  NMR spectra was attributed to the poor solubility of this class of compounds.<sup>3</sup> Second, we needed to obtain the evidence that these new G<sup>A</sup>C bases could self-assemble into RNTs. The most direct evidence for the formation of RNTs can be provided by visual characterization techniques (e.g. scanning electron microscopy, transmission electron microscopy, and atomic force microscopy).<sup>7</sup> My work, which is presented in the following sections, addresses the above problems.

## 2.2. Deprotection procedures of the G $\wedge$ C bases



Entry	R <sup>1</sup>	R <sup>2</sup>	R <sup>3</sup>	Condition	Yield (%)
1	H	Bn		A	<b>2.2a</b> , 92%
2	H	TMSE		A	<b>2.2b</b> , 67%
3	Boc	Bn		B	<b>2.2c</b> , 52%
4	Boc	Bn		B	<b>2.2d</b> , 78%
5	Boc	Bn		B	<b>2.2e</b> , 80%
6	Boc	Bn		B	<b>2.2f</b>
7	Boc	Bn		B	<b>2.2g</b>
8	Boc	Bn		B	<b>2.2h</b>
9	Boc	Bn		B	<b>2.2i</b>

X<sup>-</sup> = CF<sub>3</sub>COO<sup>-</sup> for entries 1-2 and Cl<sup>-</sup> for entries 3–9

**Table 2.1:** General scheme for the synthesis of the novel G $\wedge$ C bases **2.2a–i**

Nine functionalized G $\wedge$ C bases **2.2a–i** were synthesized from their respective precursors

**2.1a–i** (Table 2.1) made by Deng *et al.* as described in the reference.<sup>3</sup> Entries 1–2 were functionalized with halogens. Entries 3–9 were functionalized with aromatic groups. Bn and Boc groups of **2.1a** were removed in 95% TFA/thioanisole at room temperature. This deprotection method has been widely reported by our group.<sup>1a–g,3</sup> The deprotection of **2.1a** followed by washing with Et<sub>2</sub>O gave the self-assembling G^C base **2.2a** as a TFA salt in 92% yield. In a similar procedure, the precursor **2.1b** with 2-trimethylsilyl ethyl (TMSE) and Boc protecting groups was converted to the G^C base **2.2b** as a TFA salt in 84% yield. For the deprotection of **2.1c–e**, alternative conditions were applied (4 M HCl/dioxane). This method has also been used by our group in recent years.<sup>1e,8</sup> The G^C base **2.2c** was obtained as the HCl salt in 52% yield after deprotection in 4 M HCl/dioxane at reflux and washing with Et<sub>2</sub>O. A similar procedure gave **2.2d** and **2.2e** as HCl salts in 78% and 80% yield respectively. Compounds **2.2f–i** were obtained using the same method as **2.1c–e**. Compounds **2.2a–e** were characterized by NMR, high-resolution mass spectroscopy, and elemental analysis. Compounds **2.2f–i** were only characterized by high-resolution mass spectroscopy. NMR and combustion data of them will be acquired in future work.

## 2.3. NMR studies of the G<sup>AC</sup> bases

### 2.3.1. Choice of deuterated NMR solvents

In general, poor solubility of the G<sup>AC</sup> bases **2.2a–e** as organic salt, limited the choice of deuterated solvents for NMR characterization. In particular, **2.2a** could not be dissolved in a wide range of either nonpolar or polar solvents (cyclohexane, toluene, benzene, chlorobenzene, dioxane, tetrahydrofuran, dichloromethane, acetone, methanol, nitromethane, dimethylformamide, dimethyl sulfoxide and water) except in TFA (more than ca. 10 g/L). In *d*-TFA, an acid-catalyzed keto-enol tautomerization of **2.2a** (Figure 2.3) broadens the resonances and doubles the number of expected resonances in both <sup>1</sup>H NMR and <sup>13</sup>C NMR spectra, which complicates peak assignments. The keto form is the minor tautomer and the enol form is the major tautomer (Figure 2.3).

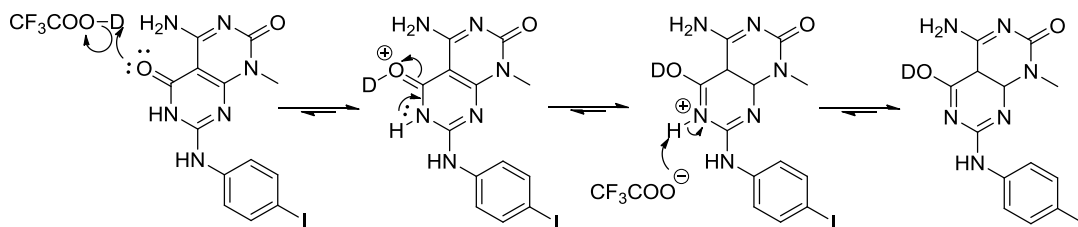


**Figure 2.3:** A proposed mechanism for the keto-enol tautomerization of **2.2a** in *d*-TFA

Later on, **2.2a** was found to be also soluble in a mixture of TFA and DMSO (ca. 6 g/L in TFA:DMSO, 2:5). The <sup>1</sup>H NMR and <sup>13</sup>C NMR spectra of **2.2a** in *d*-TFA:*d*<sub>6</sub>-DMSO (2:5) are much sharper and clearer than in pure *d*-TFA. The structure of **2.2b** is similar to **2.2a**

and the only difference is their halophenyl groups (iodophenyl for **2.2a** and bromophenyl for **2.2b**). Not surprisingly, they showed identical solubility and characteristics in NMR studies.

Compounds **2.2c–e** functionalized with aromatic groups were not soluble in organic solvents with a wide range of polarity from cyclohexane to dimethyl sulfoxide (same as **2.2a/b**). Furthermore, the solubility of **2.2c/d** (ca. 2 g/L) in TFA is much lower relative to **2.2a/b** but they dissolve better (ca. 6 g/L) in TFA:DMSO (2:5). Compound **2.2e** is soluble in both TFA (more than ca. 10 g/L) and TFA:DMSO (2:5) (more than ca. 6 g/L) probably due to its benzaldehyde group of high polarity. In the  $^1\text{H}$  NMR characterization of **2.2c**, both pure *d*-TFA and *d*-TFA:*d*<sub>6</sub>-DMSO (2:5) were used. Like **2.2a/b**, resonances are sharper and simplified for the latter. *d*-TFA:*d*<sub>6</sub>-DMSO (2:5) was chosen for **2.2d/e**, because this mixture of solvent was found to be the best for NMR characterization of this class of G $\wedge$ C bases.

### **2.3.2. NMR characterization in *d*-TFA and *d*-TFA:*d*<sub>6</sub>-DMSO (2:5)**

The  $^1\text{H}$  NMR spectrum of **2.2a** in *d*-TFA (Figure 2.4A) shows two sets of resonances for the aromatic and methyl protons with a population ratio of 2:1 resulted from the keto-enol tautomerization (see Section 2.3.1 and Figure 2.3). The two doublets ( $^3J = 5.9$  Hz) at 7.99

ppm and 7.14 ppm are assigned to the two groups of aromatic protons in the minor tautomer (keto). The COSY spectrum (Figure 2.4C) indicates the coupling interactions between them. The doublet ( $^3J = 7.6$  Hz) at 7.87 ppm and the doublet ( $^3J = 8.2$  Hz) at 7.34 ppm are related to the two coupled groups of aromatic protons in the major tautomer (enol). Resonances C<sub>9</sub>H and C<sub>11</sub>H are more deshielded than C<sub>8</sub>H and C<sub>12</sub>H due to the electron-donating amine and electron-withdrawing iodine group.<sup>6</sup> The two singlets at 3.75 ppm and 3.67 ppm are related to the methyl protons C<sub>6</sub>H of the minor and major tautomers respectively. The 2D HSQC spectrum (Figure 2.4D) shows one-bond heteronuclear correlations between the protons and carbons, e.g. the proton at 7.99 ppm is attached to the carbon at 143.0 ppm, and allows the assignment of the carbon resonances at 143.0 ppm (C<sub>9, 11</sub>, minor tautomer) 141.0 ppm (C<sub>9, 11</sub>, major tautomer), 130.2 ppm (C<sub>8, 12</sub>, minor tautomer), 127.2 ppm (C<sub>8, 12</sub>, major tautomer), 31.9 ppm (C<sub>6</sub>, major tautomer) and 31.7 ppm (C<sub>6</sub>, minor tautomer). The 2D HMBC spectrum (Figure 2.4E) shows two long-range correlations between C<sub>6</sub>H and two carbons. One covered by the solvent peak at about 163.4 ppm and the other at 152.1 ppm indicate C<sub>2</sub> and C<sub>13</sub>. C<sub>9, 11</sub>H at 7.87 ppm and C<sub>8, 12</sub>H at 7.34 ppm are correlated to the carbons at 136.1 ppm (C<sub>10</sub>) and 93.9 ppm (C<sub>7</sub>) over multiple bonds respectively. The most downfield resonance at 166.1 ppm (Figure 2.4B) indicates the most electron deficient amide carbon C<sub>4</sub>. The resonances at 158.2 ppm and 155.6 ppm correspond to the heteroaromatic carbons C<sub>1</sub> and C<sub>5</sub>. The

resonance at 86.2 ppm is assigned to the shielded heteroaromatic carbon C<sub>3</sub> that bears a negative charge when the lone pair on the amine is donated to C<sub>2</sub> in a resonance structure (Figure 2.5). The assignments of carbons on the heterobicycle are consistent with that of recently reported G<sup>+</sup>C derivatives.<sup>1,3</sup> The resonances at 133.0 ppm and 98.0 ppm might correspond to carbons C<sub>10</sub> and C<sub>7</sub> of the minor tautomer (keto).

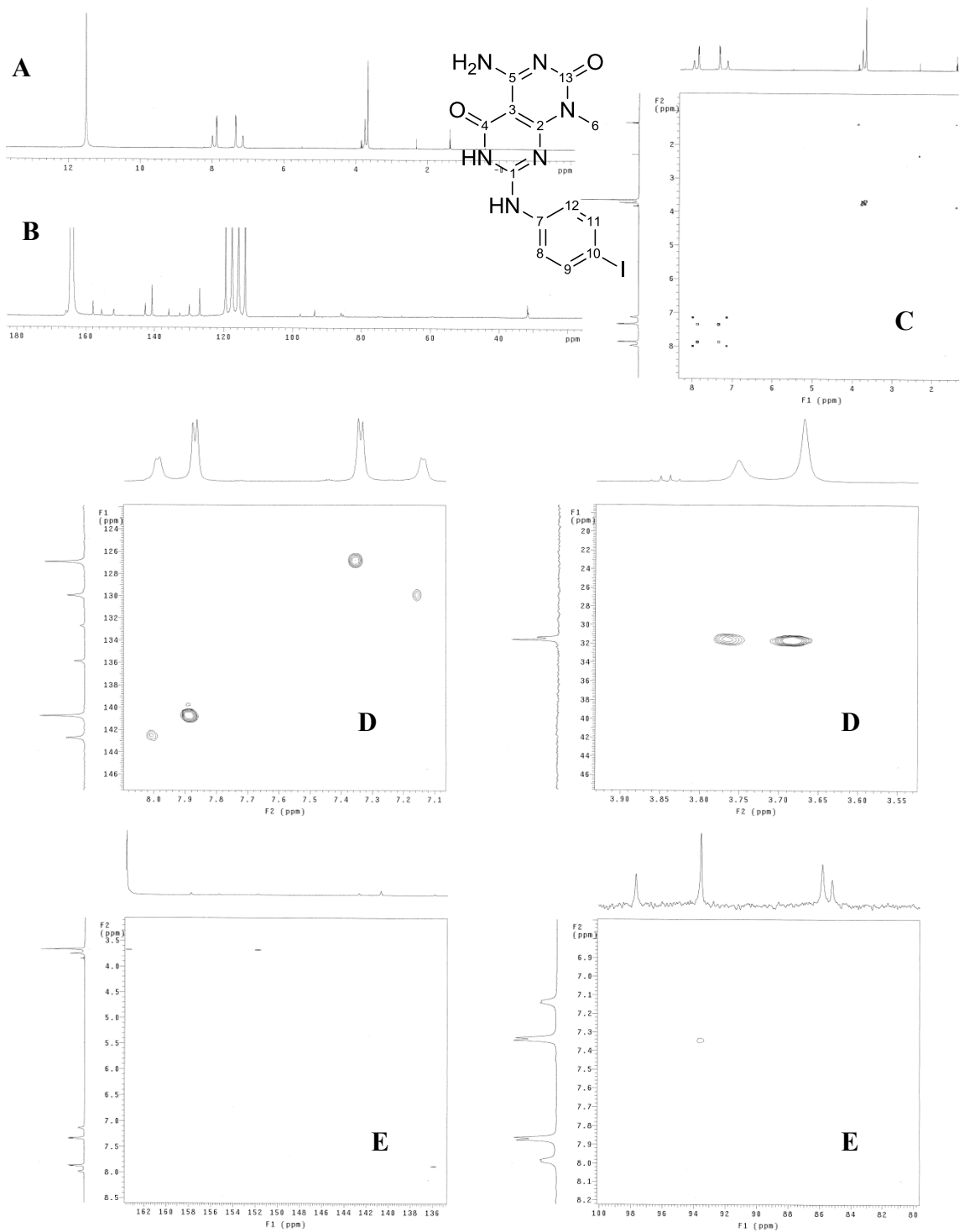


**Figure 2.4:** 1D  $^1\text{H}$  (A) and  $^{13}\text{C}$  (B) and 2D COSY (C), HSQC (D) and HMBC (E) NMR spectra of **2.2a** in *d*-TFA

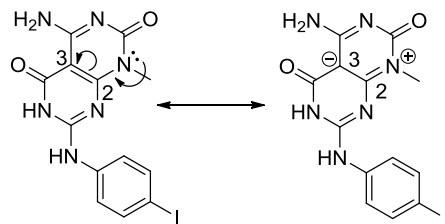


**Figure 2.5:** A resonance structure of **2.2a** for the shielding of C<sub>3</sub>

Relative to the NMR spectra of **2.2a** in *d*-TFA, sharper and simplified resonances are found in *d*-TFA:*d*<sub>6</sub>-DMSO (2:5) in general (Figure 2.6). The doublet ( $^3J = 8.8$  Hz) at 7.75 ppm corresponds to the more deshielded aromatic protons C<sub>9,11</sub>H and the doublet ( $^3J = 8.2$  Hz) at 7.39 ppm corresponds to C<sub>8,12</sub>H. The COSY spectrum (Figure 2.6C) shows the coupling interactions between them. The singlet at 3.35 ppm corresponds to the methyl protons C<sub>6</sub>H. The 2D HSQC spectrum (Figure 2.6D) shows that C<sub>9,11</sub>H are attached to the carbon at 138.1 ppm and this carbon is assigned to C<sub>9,11</sub>. In a similar way, the carbon resonances at 124.8 ppm and 29.6 ppm are assigned to C<sub>8,12</sub> and C<sub>6</sub> respectively. The 2D HMBC spectrum (Figure 2.6E) shows two long-range correlations between C<sub>6</sub>H and two carbons (161.0 ppm and 148.3 ppm) that correspond to C<sub>2</sub> and C<sub>13</sub>. C<sub>9,11</sub>H at 7.75 ppm are correlated to the carbons at 138.1 ppm (C<sub>9</sub>–C<sub>11</sub>H and C<sub>11</sub>–C<sub>9</sub>H) and 136.5 ppm (C<sub>10</sub>) over multiple bonds. The most downfield resonance at 161.4 ppm (Figure 2.6B) corresponds to the most electron deficient amide carbon C<sub>4</sub>. The resonances at 156.0 ppm and 153.8 ppm correspond to the heteroaromatic carbons C<sub>1</sub> and C<sub>5</sub>. The resonance at 84.1 ppm was assigned to the shielded heteroaromatic carbon C<sub>3</sub>. The assignments of

carbons on the heterobicycle are consistent with that of recently reported GAC derivatives.<sup>1,3</sup> The last unassigned carbon resonance at 90.1 ppm corresponds to the shielded aromatic carbon C<sub>7</sub>.

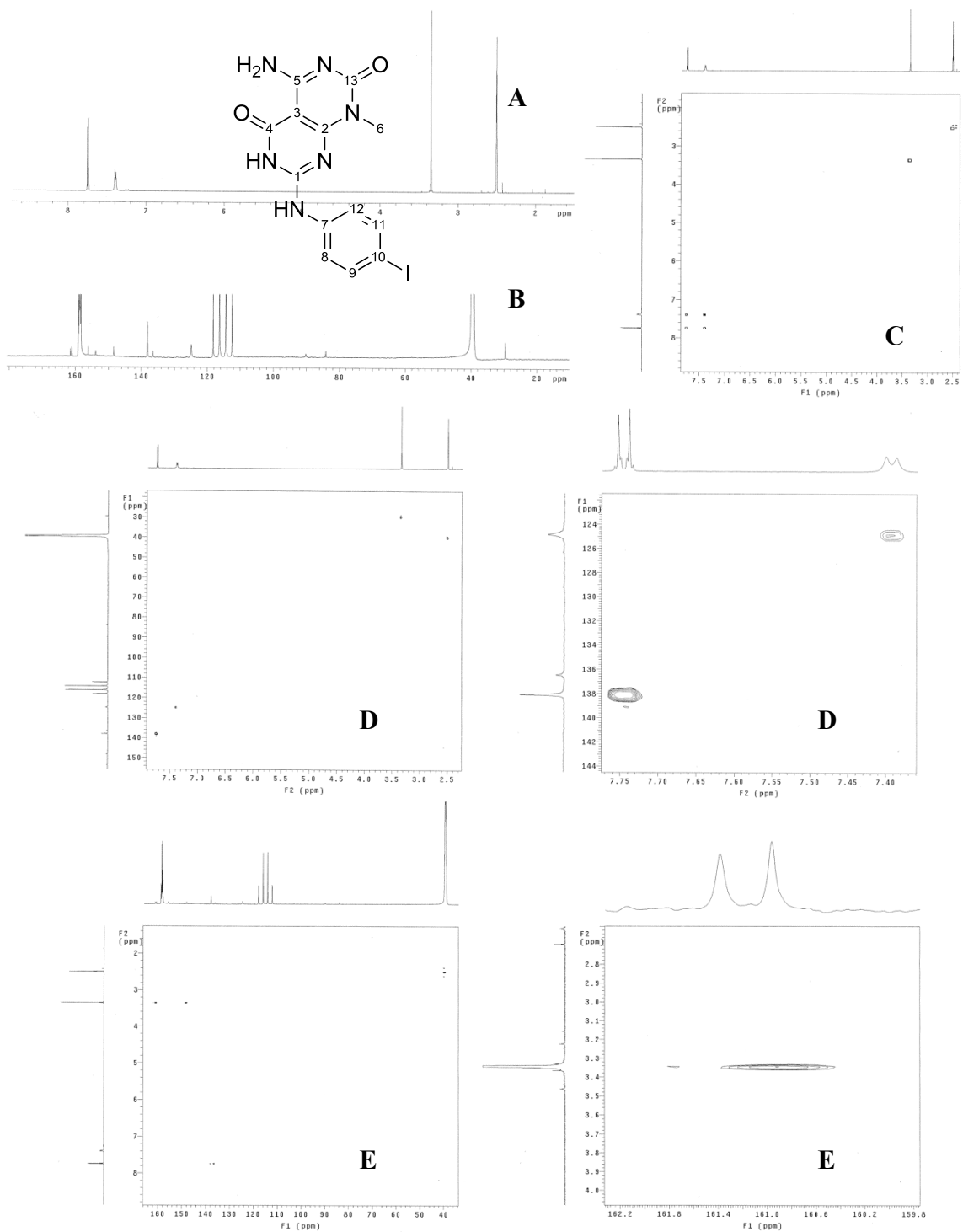


**Figure 2.6:** 1D  $^1\text{H}$  (A) and  $^{13}\text{C}$  (B) and 2D COSY (C), HSQC (D) and HMBC (E) NMR spectra of **2.2a** in  $d\text{-TFA}:d_6\text{-DMSO}$  (2:5)

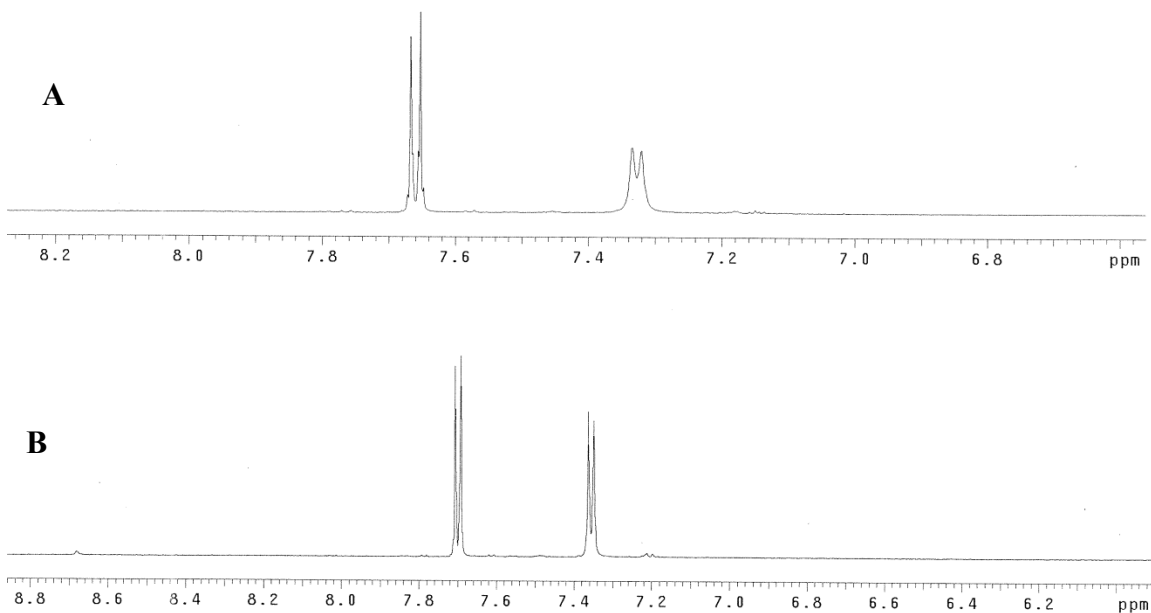


**Figure 2.7:** Broad doublet was found for the GAC bases **2.2a** at 25 °C (A) which became sharp at 50 °C (B). The solvent was *d*-TFA:*d*<sub>6</sub>-DMSO (2:5).

For the GAC base **2.2a**, a broad doublet was observed in the <sup>1</sup>H NMR spectrum when *d*-TFA:*d*<sub>6</sub>-DMSO (2:5) was used as the solvent at 25 °C (Figure 2.7A). The broad doublet (<sup>3</sup>*J* = 8.2 Hz, 2H) is representing C<sub>8,12</sub>H and is found at 7.35 ppm. C<sub>8,12</sub>H protons are coupled to C<sub>9,11</sub>H protons indicated by the doublet (<sup>3</sup>*J* = 8.8 Hz, 2H) at 7.70 ppm. Small shoulders were discovered around the doublet of C<sub>9,11</sub>H probably due to the second order effects because C<sub>9,11</sub>H protons are magnetic inequivalent. The 0.05 ppm difference in the chemical shifts shown in Figure 2.6A and Figure 2.7A results from a slight variation in the composition of the binary solvent system. At 50 °C, the doublet for C<sub>8,12</sub>H became sharper (Figure 2.7B). The chemical shift remained the same but the J-coupling constant

of the resonance  $C_{8,12}H$  increased to 8.8 Hz, which confirmed the coupling interactions between  $C_{8,12}H$  and  $C_{9,11}H$ . The small shoulders around the resonance  $C_{9,11}H$  disappeared. Resonance structures (Figure 2.8) were proposed to explain these results. The resonance structures restricted the rotation of the bond between the aniline nitrogen and  $C_7$ .<sup>9</sup> It resulted in slightly different chemical environment of  $C_8H$  and  $C_{12}H$  and broadened the doublet. As the temperature increases, the N- $C_7$  bond rotation became faster, which equalized  $C_8H$  and  $C_{12}H$  in chemical environment and sharpened the doublet. The small shoulders around the  $C_{9,11}H$  doublet 25 °C might also be attributed to the rotamers because those shoulders disappeared at 50 °C where the bond rotation became faster.

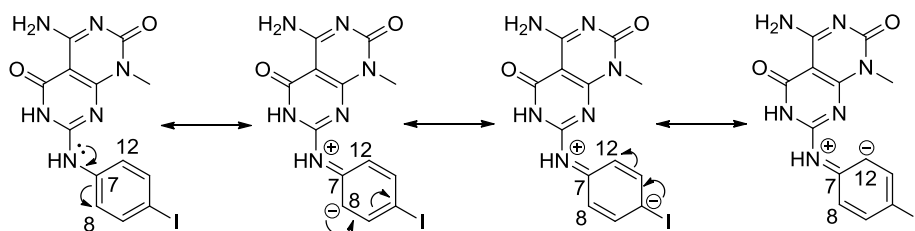


**Figure 2.8:** A proposed mechanism for the doublet broadening of **2.2a**

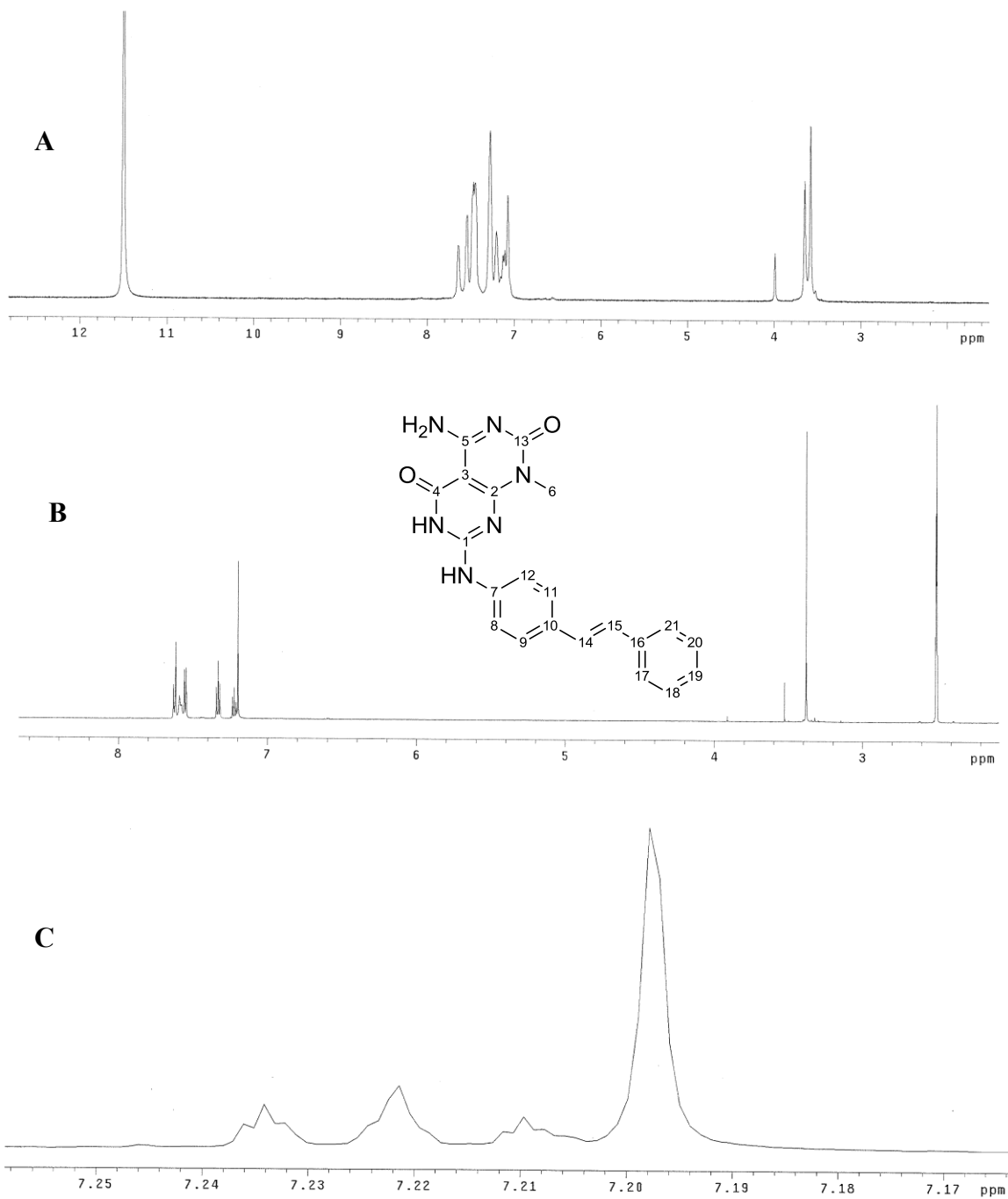


**Figure 2.9:** 1D  $^1\text{H}$  NMR spectra of **2.2c** in *d*-TFA (A) and in *d*-TFA:*d*<sub>6</sub>-DMSO (2:5) (B).

Expanded aromatic region of  $^1\text{H}$  NMR spectra of **2.2c** in *d*-TFA:*d*<sub>6</sub>-DMSO (2:5) (C).

**2.2c** was chosen as a model to demonstrate the general NMR characteristics of the

functionalized G<sup>Λ</sup>C bases **2.2c–e**. In *d*-TFA, the spectrum (Figure 2.9A) shows a group of multiplets at 7.65 – 7.07 ppm corresponding to the aromatic and alkenyl protons. The two singlets at 3.65 ppm and 3.58 ppm correspond to the methyl protons (C<sub>6</sub>H) of the minor and major tautomers respectively. The singlet at 3.99 ppm corresponds to the solvent residue dioxane from the deprotection step. In *d*-TFA:*d*<sub>6</sub>-DMSO (2:5), better-defined resonances for aromatic, alkenyl and methyl protons are displayed (Figure 2.9B). The doublet at 7.62 ppm (<sup>3</sup>*J* = 8.8 Hz, 2H) is assigned to the aromatic aniline protons (C<sub>9,11</sub>H) close to the olefin. The broad doublet at 7.58 ppm (<sup>3</sup>*J* = 8.2 Hz, 2H) corresponds to the aromatic aniline protons (C<sub>8,12</sub>H) adjacent to the secondary amine. Resonances C<sub>17,21</sub>H are related to the doublet at 7.55 ppm (<sup>3</sup>*J* = 7.6 Hz, 2H). The doublet of doublet at 7.32 ppm (<sup>3</sup>*J* = 7.6 Hz, 2H) is correlated to C<sub>18,20</sub>H. The multiplet (1H) at 7.22 ppm corresponds to the terminal aromatic proton C<sub>19</sub>H. The two singlets at 3.52 ppm and 3.38 ppm correspond to the minor solvent residue dioxane and the methyl protons C<sub>6</sub>H, respectively. The broad singlet (2H) at 7.20 ppm (Figure 2.9C) might correspond to the olefin protons C<sub>14</sub>H and C<sub>15</sub>H but further NOESY should be carried out to confirm its assignment.

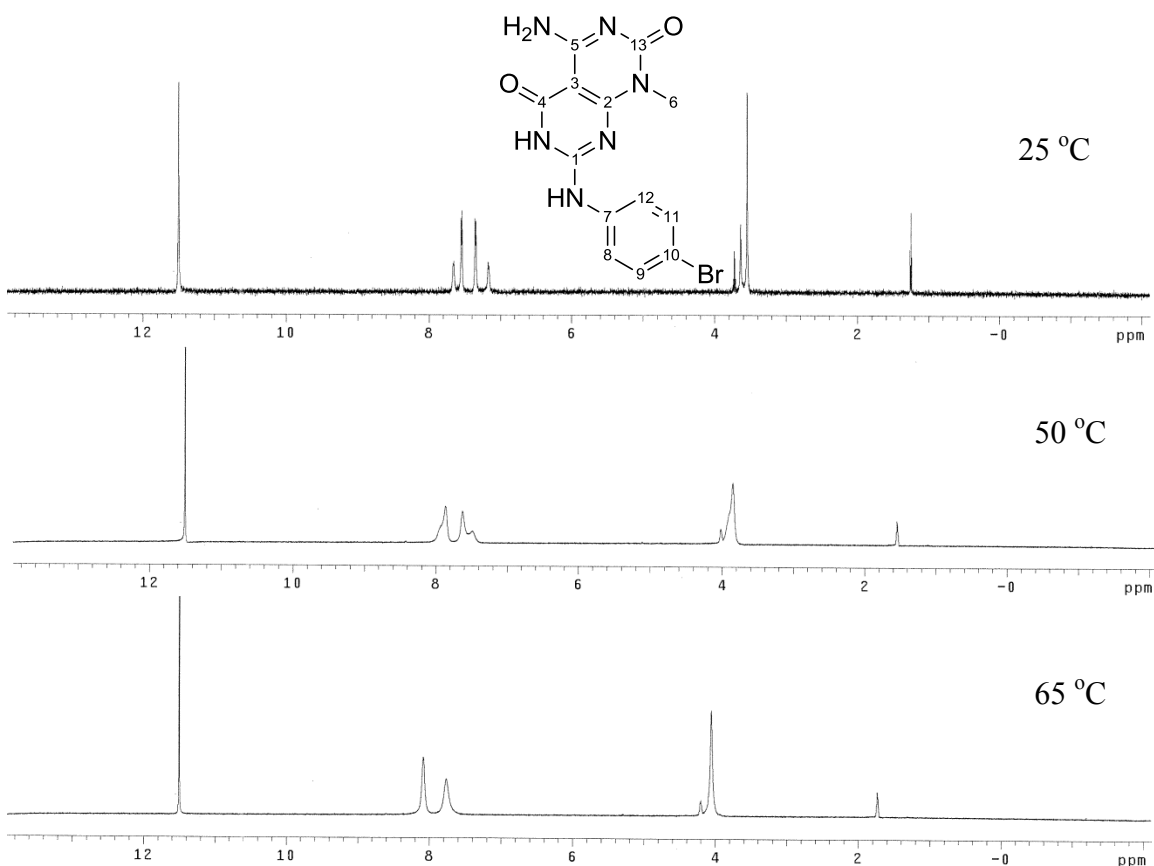


**Figure 2.10:** 1D  $^1\text{H}$  NMR spectra of **2.2b** in *d*-TFA at 25 °C, 50 °C and 65 °C

Similar keto-enol tautomerization discussed previously for **2.2a** was also observed for **2.2b** (25 °C, Figure 2.10). To investigate temperature effects on the tautomerization of **2.2b** in *d*-TFA,  $^1\text{H}$  NMR spectra at 25 °C, 50 °C and 65 °C were recorded (Figure 2.10). At 25 °C, the spectrum shows two broad singlets at 7.65 ppm and 7.17 ppm corresponding to the aromatic protons of the minor tautomer (keto). The two doublets with the same  $J$  coupling constant ( $^3J = 8.2$  Hz) at 7.55 ppm and 7.35 ppm correspond to the aromatic protons of the major tautomer (enol). The two singlets at 3.64 ppm and 3.55 ppm are related to the methyl protons of the minor and major tautomers respectively. The

integration of each resonances shows that the population ratio of the two tautomers is 2:1. As the temperature increased to 50 °C, resonances of the two tautomers became deshielded, moved closer to each other and began to merge. The broad singlet at 7.86 ppm and the partially merged resonance (7.62 ppm) with a small shoulder (7.49 ppm) correspond to the aromatic protons. The broad singlet at 3.84 ppm corresponds to the methyl protons. At 65 °C, the spectrum shows completely merged and sharper resonances that are further deshielded furthermore. The resonances at 8.08 ppm and 7.76 ppm were assigned to the aromatic protons and the resonance at 4.05 ppm was correlated to the methyl protons. In general, the two sets of resonances for the aromatic and methyl protons merged as the temperature increased, which indicated that the two tautomers were interconverting in rapidly as the temperature increased.<sup>10</sup>

## **2.4. Self-assembly studies of the G<sup>+</sup>C bases**

### **2.4.1. Nanotube formation in MeOH**

Stock solutions of **2.2a–e** were prepared in a similar way, at a very low concentration (0.01 mg/mL) due to their poor solubility. MeOH was chosen as the solvent in our initial attempts because it is a polar protic organic solvent and has been used to obtain RNTs in multiple cases.<sup>1d,f,11</sup> After the compound was added to MeOH, it was sonicated for 2 min to break down the solid. An initial heating of the stock solution (known to promote RNT

formation<sup>1b</sup>) did not help in this case because it led to immediate aggregation and precipitation of the compound. The stock solutions were allowed to age for 1 day (**2.2a/d**) or 2 days (**2.2b/c/e**). The SEM samples were prepared by depositing small aliquots (10  $\mu$ L) on carbon coated TEM grids for 15 s before the excess was removed by blotting with filter paper at the edge of the grid. The samples were then dried under vacuum prior to imaging.

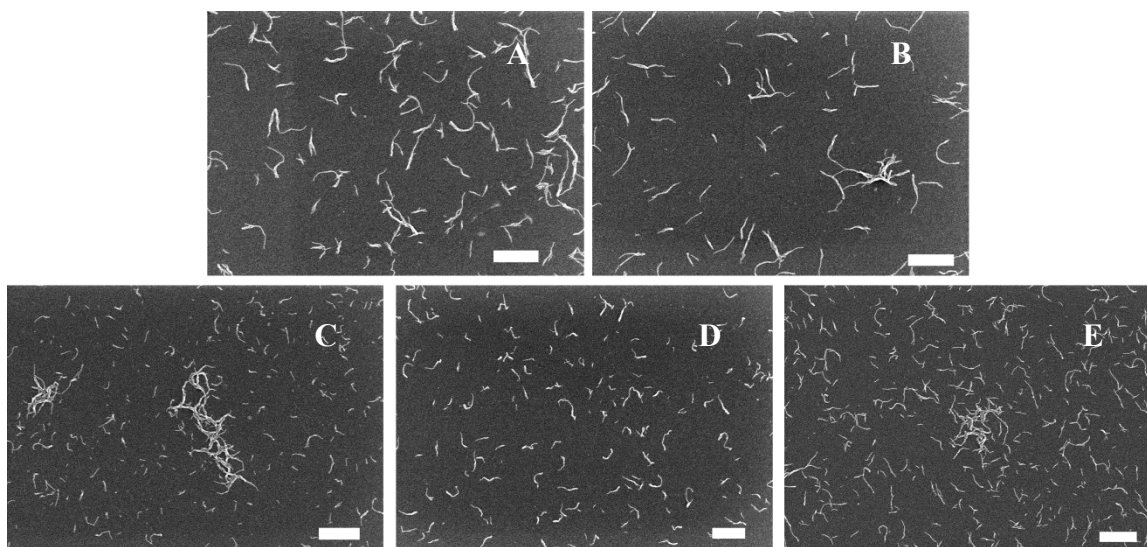


**Figure 2.11:** SEM images of **2.2a** (A), **2.2b** (B), **2.2c** (C), **2.2d** (D) and **2.2e** (E) in Methanol (0.01 mg/mL). Scale bar = 300 nm.

As revealed by the SEM images (Figure 2.11A–E), GAC bases **2.2a–e** readily self-assembled into short nanotubes in MeOH. But the shapes of nanotubes were not regular probably due to their poor solubility in MeOH. To address this problem, future work could be emphasized on modification of the GAC base with hydrophobic functional

groups containing alkyl chains of proper length to make it soluble in nonpolar solvents<sup>1e,12</sup> or hydrophilic groups (e.g. amino acid) to improve its solubility in water or MeOH.<sup>1</sup>

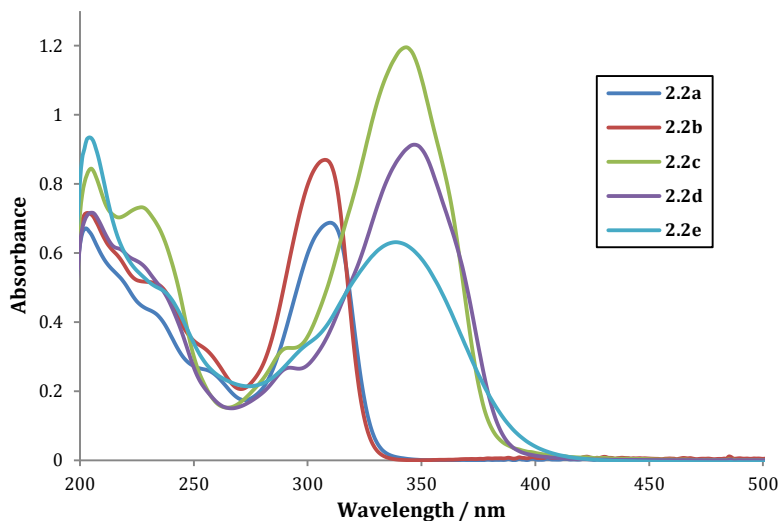


**Figure 2.12:** UV-vis spectra of **2.2a–e** in MeOH

The nanotubes formed by **2.2a–e** in MeOH were also characterized by UV-vis spectroscopy using aliquots of the same stock solutions used for the SEM studies. As shown in Figure 2.12, the nanotubes of **2.2a** in MeOH (0.01 mg/mL,  $1.88 \times 10^{-5}$  M) showed two maxima at 203 nm ( $\epsilon = 3.57 \times 10^4 \text{ M}^{-1} \text{ cm}^{-1}$ ) and 310 ( $\epsilon = 3.66 \times 10^4 \text{ M}^{-1} \text{ cm}^{-1}$ ). For the nanotubes of **2.2b** (0.01 mg/mL,  $2.59 \times 10^{-5}$  M), two maxima with similar wavelengths compared to **2.2a** were observed at 203 nm ( $\epsilon = 2.76 \times 10^4 \text{ M}^{-1} \text{ cm}^{-1}$ ) and 308 nm ( $\epsilon = 3.36 \times 10^4 \text{ M}^{-1} \text{ cm}^{-1}$ ). The nanotubes of **2.2c** (0.01 mg/mL,  $2.32 \times 10^{-5}$  M) gave three major maxima at 205 nm ( $\epsilon = 3.64 \times 10^4 \text{ M}^{-1} \text{ cm}^{-1}$ ), 227 nm ( $\epsilon = 3.16 \times 10^4 \text{ M}^{-1} \text{ cm}^{-1}$ ) and

343 nm ( $\epsilon = 5.15 \times 10^4 \text{ M}^{-1}\text{cm}^{-1}$ ) and one small shoulder at 292 nm ( $\epsilon = 1.40 \times 10^4 \text{ M}^{-1}\text{cm}^{-1}$ ). For the nanotubes of **2.2d** (0.01 mg/mL,  $2.14 \times 10^{-5} \text{ M}$ ), two major maxima were found at 205 nm ( $\epsilon = 3.35 \times 10^4 \text{ M}^{-1}\text{cm}^{-1}$ ) and 347 nm ( $\epsilon = 4.27 \times 10^4 \text{ M}^{-1}\text{cm}^{-1}$ ) and a small shoulder was found at 292 nm ( $\epsilon = 1.25 \times 10^4 \text{ M}^{-1}\text{cm}^{-1}$ ). The nanotubes formed by **2.2e** (0.01 mg/mL,  $2.15 \times 10^{-5} \text{ M}$ ) gave two maxima at 204 nm ( $\epsilon = 4.35 \times 10^4 \text{ M}^{-1}\text{cm}^{-1}$ ) and 339 nm ( $\epsilon = 2.94 \times 10^4 \text{ M}^{-1}\text{cm}^{-1}$ ). The results indicate that the absorption properties of the nanotubes are tunable with different functional groups attached to the G $\wedge$ C bases.

#### 2.4.2. Nanotube formation in other solvents



**Figure 2.13:** SEM images of **2.2a** in DMSO (0.01 mg/mL) at 0 h (A), 1 h (B) and 2 d (C).

Scale bar = 300 nm.

For the G $\wedge$ C base **2.2a**, the formation of RNTs was also investigated in DMSO that is a polar solvent with high dielectric constant and might dissolve this ionic compound better relative to other solvents. The stock solution of this compound and SEM samples were prepared as described above. Aliquots of the stock solution were taken at different time intervals (0 h, 1 h and 2 d) for imaging. SEM images (Figure 2.13) showed the formation

of RNTs at 0 h. At 1 h, longer RNTs were found. At 2 d, large aggregates of RNTs were observed.

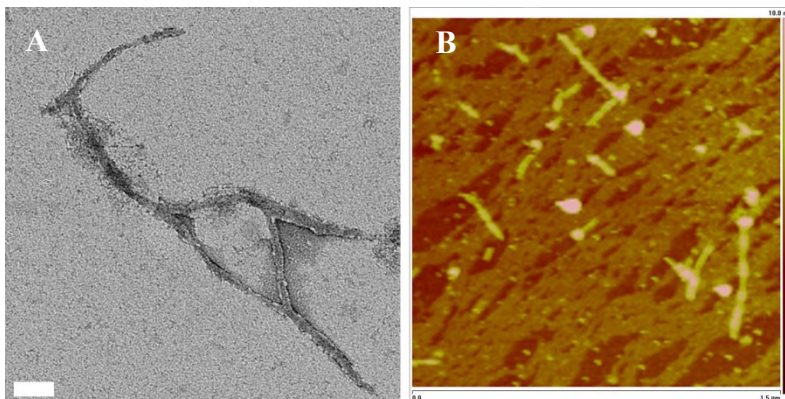


**Figure 2.14:** TEM (A, scale bar = 100 nm) and AFM (B) images of **2.2a** (0.01 mg/mL) in DMSO, aged for 1 h

The SEM sample at 1 h was chosen and stained with 0.2% uranyl acetate solution in MeCN for TEM visualization. The diameter of the RNT measured by TEM was  $5.5 \pm 1.0$  nm. This value is not accurate due to the poor quality of staining which resulted from using a method previously reported for other RNT systems. Thick fibers ( $> 20$  nm in diameter) were bundles instead of single tubes, thus they were not included in the measurements. To prepare AFM samples, the stock solution of **2.2a** was allowed to age for 1 h and one drop of this solution was deposited onto highly ordered pyrolytic graphite (HOPG). The images obtained in tapping mode (TM-AFM) showed 1D structures with an average height of  $4.18 \pm 0.3$  nm and thickness of the layer deposited around the tubes

was about 1.3 nm. The diameter measured by AFM was expected to be lower than the actual size, which could be attributed to the compression of the soft RNTs under the AFM tip.<sup>13</sup> Future work could be focused on optimizing sample preparation methods for TEM and AFM. For example, (a) looking for a better solvent for prepare the stock solutions, (b) developing a better staining method, (c) changing the concentration of the aliquots deposited on the substrates.<sup>14</sup>

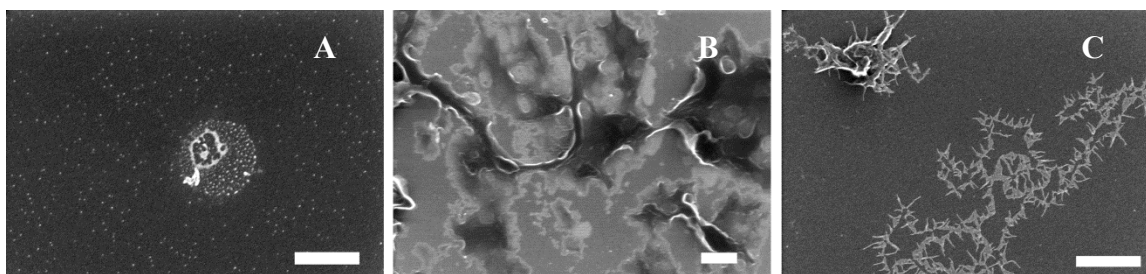


**Figure 2.15:** SEM images of **2.2d** in MeCN (A), DMF (B) and DMSO (C) at 0 h. Scale bar 300 nm.

For G<sup>AC</sup> base **2.2d**, the stock solutions were prepared in three different solvents, MeCN, DMF and DMSO as described previously and SEM samples were made from aliquots of the fresh stock solution. In MeCN, small dots were observed. Sheet-like structures and large aggregates formed in DMF. In DMSO, short dendritic structures were observed. They were not good solvents for RNT formation.

## 2.5. Conclusion

Protected G<sup>^</sup>C bases **2.1a–e** were successfully deprotected in 95% TFA/thioanisole or 4 M HCl/dioxane to give their respective bases **2.2a–e** that were then fully characterized by NMR in *d*-TFA:*d*<sub>6</sub>-DMSO (2:5) to confirm the structure and purity. Mass and combustion data were also obtained for them. In MeOH, all of the G<sup>^</sup>C bases **2.2a–e** could self-assemble into nanotubes that were visualized by SEM. The two main goals of this project proposed in Section 2.1 (i.e. characterization of the G<sup>^</sup>C bases by NMR and providing direct evidence for the formation of RNTs) were accomplished, which indicates that Beingsner and Deng's method involving a Suzuki-Miyaura coupling is capable of developing aromatic functionalized RNTs. However, the nanotubes formed by the G<sup>^</sup>C bases **2.2a–e** in MeOH were thick and their shape was poorly defined, which might be attributed to their poor solubility. Moreover, the measured diameter for the nanotubes formed by **2.2a** in DMSO with TEM and AFM was not accurate. Thus, future work should focus on introducing other functional groups to improve the solubility of the G<sup>^</sup>C bases, such that single RNT formation can be visualized. In the future, NMR and combustion data will also be obtained for Compounds **2.2f–i** which were currently characterized by high-resolution mass spectroscopy only.

## **2.6. Experimental Section**

### **2.6.1. General procedures**

#### **2.6.1.1. Self-assembly**

Stock solutions of G<sup>+</sup>C bases were prepared at 0.01 mg/ml or as indicated in the results section by adding G<sup>+</sup>C bases to either HPLC grade DMSO or methanol with 2 min sonication. They were then allowed to age at room temperature. Aliquots from these RNT stock solutions were used directly for imaging by SEM, AFM, and TEM as well as UV-vis spectroscopy.

#### **2.6.1.2. SEM imaging**

The SEM samples were prepared by depositing one droplet (10  $\mu$ L) of the stock solution on a carbon-coated 400-mesh copper grid (Electron Microscopy Sciences) and the droplet was allowed to sit on the grid for 10 s. Then the grid was blotted using filter paper. The samples were then air-dried and heated on a hotplate (100  $^{\circ}$ C) for 5 min before imaging to remove any residual solvents. All SEM images were obtained without negative staining, at 30 kV accelerating voltage and a working distance of 8.0 mm on a high resolution Hitachi S-4800 cold field emission SEM.

### **2.6.1.3. TEM imaging**

TEM investigation was carried out on JEOL 2200 FS TEM – 200kV Schottky field emission instrument equipped with an in-column omega filter. Bright field TEM images are acquired using energy filtered zero loss beams (slit width 10 eV) under low-dose method. Stock solutions were prepared as described in the self-assembly section. TEM samples were prepared by depositing a droplet of stock solution on a carbon-coated 400-mesh copper grid (Electron Microscopy Sciences). The droplet was allowed to sit on the grid for 10s and then blotted by filter paper. The staining of samples was performed by depositing one droplet of 0.2% uranyl acetate (in MeCN) for 120 s. The grid was then blotted, dried in air and the hotplate. Uranyl acetate solutions were prepared by dissolving uranyl acetate crystals in MeCN by 5 min sonication and proper heat.

### **2.6.1.4. AFM imaging**

For AFM measurement, clean HOPG (highly ordered pyrolytic graphite) and mica substrates ( $1 \times 1 \text{ cm}^2$ ) were prepared and aliquots of the stock solution were deposited by spin-coating at 2500 rpm for 30 s to remove the excessive precipitation from the surface of the sample. All samples were air-dried prior to imaging. Sample surface was observed using a Digital Instruments/Veeco Instruments MultiMode Nanoscope IV AFM equipped with an E scanner. For optimal height profile (minimizing compressibility), silicon

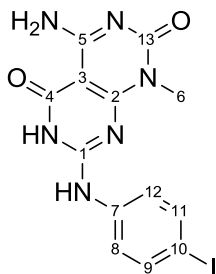
cantilevers (MikroMasch USA, Inc.) with extra-low spring constants of 0.45 N/m were used in tapping mode (TM-AFM). To obtain a clear image from surface, low scan rate (0.5-1 Hz) and amplitude setpoint (1 V) were chosen during measurement.

#### **2.6.1.5. General methods of synthesis and NMR characterization**

Unless otherwise noted, all reactions were performed under an atmosphere of N<sub>2</sub> using oven-dried glassware equipped with a magnetic stirrer and rubber septum. Reagent grade solvent Et<sub>2</sub>O was purified on an MBraun solvent purification system prior to use. All other commercial reagents were used without purification unless otherwise stated. <sup>1</sup>H and <sup>13</sup>C NMR spectra were recorded in the specified deuterated solvent on 600 MHz NMR spectrometers with the solvent as internal reference at 298 K unless otherwise stated. The NMR data is presented as follows: chemical shift, peak assignment, multiplicity, coupling constant, and integration. Residual <sup>1</sup>H shifts in *d*-TFA (11.5 ppm) and *d*<sub>6</sub>-DMSO (2.5 ppm) were used as the internal reference where stated for <sup>1</sup>H NMR. The following abbreviations were used to denote the multiplicities: s = singlet, d = doublet, t = triplet, m = multiplet, bs = broad singlet. *d*-TFA (116.6 and 164.2 ppm), *d*<sub>6</sub>-DMSO (39.5 ppm) were used as the internal references for <sup>13</sup>C NMR as stated.

## 2.6.2. Synthesis and characterization data of target molecules

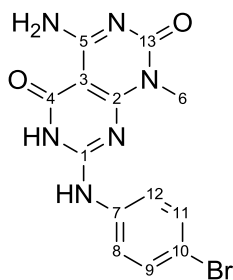
### 4-amino-7-((4-iodophenyl)amino)-1-methylpyrimido[4,5-*d*]pyrimidine-2,5(1*H*,6*H*)-dione (2.2a)



Compound **2.1a** (20 mg, 0.033 mmol) was dissolved in 95% TFA in thioanisole (2 mL) and the solution was stirred for 48 h. Et<sub>2</sub>O (8 mL) was then added and the precipitate formed was centrifuged down. The residual solid was suspended in Et<sub>2</sub>O (10 mL), sonicated for 10 min and centrifuged. This process was repeated five times before the solid was dried *in vacuo* for 48 h to give 16 mg of **2.2a** (C<sub>15.4</sub>H<sub>13</sub>F<sub>3</sub>IN<sub>6</sub>O<sub>4.1</sub>, 92%) as a white solid. <sup>1</sup>H NMR (600 MHz, *d*-TFA) δ (ppm): 7.99 (C<sub>9,11</sub>H, d, <sup>3</sup>*J* = 5.9 Hz, 2H, minor tautomer), (Due to the possible tautomerization as discussed in Section 2.3, this compound displays two sets of peaks for all of the protons with ratio of 2:1) 7.87 (C<sub>9,11</sub>H, d, <sup>3</sup>*J* = 7.6 Hz, 2H), 7.34 (C<sub>8,12</sub>H, d, <sup>3</sup>*J* = 8.2 Hz, 2H, 7.14 (C<sub>8,12</sub>H, d, <sup>3</sup>*J* = 5.9 Hz, 2H, minor tautomer), 3.75 (C<sub>6</sub>H, s, 3H, minor tautomer), 3.67 (C<sub>6</sub>H, s, 3H). <sup>13</sup>C NMR (150 MHz, *d*-TFA) δ (ppm): 166.1 (C<sub>4</sub>), (C<sub>2</sub> is covered by the solvent peak.), 158.2, 155.6, 152.1 (C<sub>1</sub>, C<sub>5</sub>, C<sub>13</sub>), 143.0 (C<sub>9,11</sub>, minor tautomer), 141.0 (C<sub>9,11</sub>), 136.1, 133.0 (C<sub>10</sub>), 130.2 (C<sub>8,12</sub>, minor tautomer), 127.2 (C<sub>8,12</sub>), 98.0, 93.9 (C<sub>7</sub>), 86.2, 85.5 (C<sub>3</sub>), 31.9 (C<sub>6</sub>), 31.7 (C<sub>6</sub>,

minor tautomer).  $^1\text{H}$  NMR (600 MHz, *d*-TFA:*d*<sub>6</sub>-DMSO (2:5))  $\delta$  (ppm): 7.75 (C<sub>9,11</sub>H, d,  $^3J = 8.8$  Hz, 2H), 7.39 (C<sub>8,12</sub>H, d,  $^3J = 8.2$  Hz, 2H), 3.35 (C<sub>6</sub>H, s, 3H).  $^{13}\text{C}$  NMR (150 MHz, *d*-TFA:*d*<sub>6</sub>-DMSO (2:5))  $\delta$  (ppm): 161.4 (C<sub>4</sub>), 161.0 (C<sub>2</sub>), 156.0, 153.8 (C<sub>1</sub>, C<sub>5</sub>), 148.3 (C<sub>13</sub>), 138.1 (C<sub>9,11</sub>), 136.5 (C<sub>10</sub>), 124.8 (C<sub>8,12</sub>), 90.1 (C<sub>7</sub>), 84.1 (C<sub>3</sub>), 29.6 (C<sub>6</sub>). (Assigned with COSY, HSQC and HMBC). Anal. calcd for C<sub>15</sub>H<sub>12</sub>F<sub>3</sub>IN<sub>6</sub>O<sub>4</sub> (M + TFA + 0.1Et<sub>2</sub>O): C, 34.79; H, 2.47; N, 15.81. Found: C, 34.69; H, 2.43; N, 15.59. Positive ESI-MS: calcd for [M + H<sup>+</sup>]/z, 411.0, found 411.3 ([M + H<sup>+</sup>]/z), 821.3 ([2M + H<sup>+</sup>]/z). High-resolution ESI-MS: calcd mass 411.0061, actual mass 411.0055.

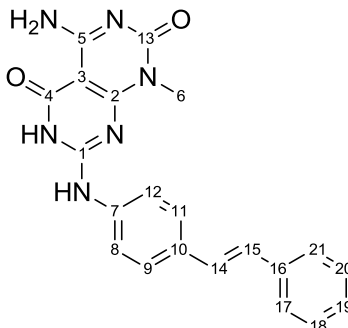
**4-amino-7-((4-bromophenyl)amino)-1-methylpyrimido[4,5-*d*]pyrimidine-2,5(1*H*,6*H*)-dione (2.2b)**



Compound **2.1b** (25 mg, 0.044 mmol) was dissolved in 95% TFA in thioanisole (2 mL) and the solution was stirred for 48 h. Et<sub>2</sub>O (8 mL) was then added and the precipitate formed was centrifuged down. The residual solid was suspended in Et<sub>2</sub>O (10 mL), sonicated and centrifuged down. This process was repeated five times before the solid was dried under vacuo for 48 h to give 18 mg of **2.2b** (C<sub>13.4</sub>H<sub>11.2</sub>F<sub>3</sub>BrN<sub>6</sub>O<sub>2.4</sub>, 67%) as a

white solid.  $^1\text{H}$  NMR (600 MHz, *d*-TFA, 298 K)  $\delta$  (ppm): 7.65 ( $\text{C}_{9,11}\text{H}$ , bs, 2H, minor tautomer), (Due to the possible tautomerization as discussed in Section 2.3, this compound displays two sets of peaks for all of the protons with ratio of 2:1) 7.55 ( $\text{C}_{9,11}\text{H}$ , d,  $^3J = 8.2$  Hz, 2H), 7.35 ( $\text{C}_{8,12}\text{H}$ , d,  $^3J = 8.2$ , 2H), 7.17 ( $\text{C}_{8,12}\text{H}$ , bs, 2H, minor tautomer), 3.64 ( $\text{C}_6\text{H}$ , s, 3H, minor isomer), 3.55 ( $\text{C}_6\text{H}$ , s, 3H).  $^1\text{H}$  NMR (600 MHz, *d*-TFA, 323 K)  $\delta$  (ppm): 7.86 ( $\text{C}_{9,11}\text{H}$ , bs, 2H), 7.62 ( $\text{C}_{8,12}\text{H}$ , bs, 2H), 7.49 ( $\text{C}_{8,12}\text{H}$ , bs, 2H, minor tautomer), 3.84 ( $\text{C}_6\text{H}$ , s, 3H).  $^1\text{H}$  NMR (600 MHz, *d*-TFA, 333 K)  $\delta$  (ppm): 8.08 ( $\text{C}_{9,11}\text{H}$ , bs, 2H), 7.76 ( $\text{C}_{8,12}\text{H}$ , bs, 2H), 4.05 ( $\text{C}_6\text{H}$ , s, 3H).  $^{13}\text{C}$  NMR (150 MHz, *d*-TFA)  $\delta$  (ppm): 165.7 ( $\text{C}_4$ ), 158.1, 155.6, 152.0 ( $\text{C}_1$ ,  $\text{C}_5$ ,  $\text{C}_{13}$ ), 136.7, 134.7 ( $\text{C}_{9,11}$ ), 135.3 ( $\text{C}_{10}$ ), 130.3, 127.2 ( $\text{C}_{8,12}$ ), 123.8 ( $\text{C}_7$ ), 86.0 ( $\text{C}_3$ ), 31.9 ( $\text{C}_6$ ).  $^1\text{H}$  NMR (600 MHz, *d*-TFA:*d* $_6$ -DMSO (2:5))  $\delta$  (ppm): 7.56 ( $\text{C}_{9,11}\text{H}$ , d,  $^3J = 8.8$  Hz, 2H), 7.52 ( $\text{C}_{8,12}\text{H}$ , d,  $^3J = 8.8$  Hz, 2H), 3.34 ( $\text{C}_6\text{H}$ , s, 3H).  $^{13}\text{C}$  NMR (150 MHz, *d*-TFA:*d* $_6$ -DMSO (2:5))  $\delta$  (ppm): 161.6 ( $\text{C}_4$ ), 161.2 ( $\text{C}_2$ ), 156.3, 154.1 ( $\text{C}_1$ ,  $\text{C}_5$ ), 148.5 ( $\text{C}_{13}$ ), 136.2 ( $\text{C}_{10}$ ), 132.4 ( $\text{C}_{9,11}$ ), 124.9 ( $\text{C}_{8,12}$ ), 84.2 ( $\text{C}_3$ ), 29.7 ( $\text{C}_6$ ). (Assigned with COSY, HSQC and HMBC). Anal. calcd for  $\text{C}_{13.4}\text{H}_{11.2}\text{F}_3\text{BrN}_6\text{O}_{2.4}$  ( $\text{M} + 0.2\text{TFA}$ ): C, 41.66; H, 2.98; N, 21.79. Found: C, 41.92; H, 2.46; N, 22.28. Positive ESI-MS: calcd for  $[\text{M} + \text{H}^+]/z$ , 365.0/363.0, found 365.4/363.3 ( $[\text{M} + \text{H}^+]/z$ , 97%/100%), 727.3 ( $[2\text{M} + \text{H}^+]/z$ ). High-resolution ESI-MS: calcd mass 363.0200, actual mass 363.0192.

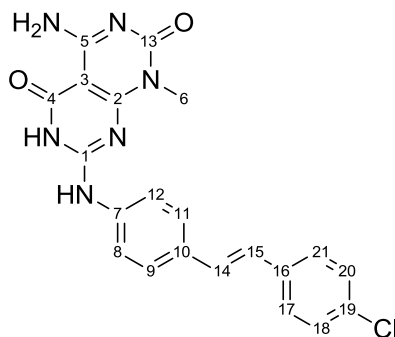
**(E)-4-amino-1-methyl-7-((4-styrylphenyl)amino)pyrimido[4,5-*d*]pyrimidine-2,5(1*H*,6*H*)-dione (2.2c)**



Compound **2.1c** (30 mg, 0.039 mmol) was dissolved in 4 M HCl/dioxane (3 mL) and heated to reflux for 2 h. Et<sub>2</sub>O (10 mL) was then added and the precipitate formed was centrifuged down. The residual solid was suspended in Et<sub>2</sub>O (5 mL), sonicated and centrifuged down. This process was repeated three times before the solid was dried under vacuo for 48 h to give 9 mg of **2.2c** (C<sub>21.4</sub>H<sub>19.5</sub>Cl<sub>1.1</sub>N<sub>6</sub>O<sub>2.2</sub>, 52%) as a pale yellow solid. <sup>1</sup>H NMR (600 MHz, *d*-TFA) δ (ppm): 7.65 – 7.07 ppm (C<sub>9, 11</sub>H, C<sub>8, 12</sub>H, C<sub>14</sub>H, C<sub>15</sub>H, C<sub>17, 21</sub>H, C<sub>18, 20</sub>H, C<sub>19</sub>H, m, 11H), 3.65 (C<sub>6</sub>H, s, 3H, minor isomer), (Due to the possible tautomerization as discussed in Section 2.3, this compound displays two sets of peaks for all of the protons with ratio of 2:1) 3.58 (C<sub>6</sub>H, s, 3H, major isomer). <sup>1</sup>H NMR (600 MHz, *d*-TFA:*d*<sub>6</sub>-DMSO (2:5)) δ (ppm): 7.62 (C<sub>9, 11</sub>H, d, <sup>3</sup>*J* = 8.8 Hz, 2H), 7.58 (C<sub>8, 12</sub>H, d, <sup>3</sup>*J* = 8.2 Hz, 2H), 7.55 (C<sub>17, 21</sub>H, d, <sup>3</sup>*J* = 7.6 Hz, 2H), 7.32 (C<sub>18, 20</sub>H, dd, <sup>3</sup>*J* = 7.6 Hz, 2H), 7.22 (C<sub>19</sub>H, m, 1H), 7.20 (C<sub>14</sub>H, C<sub>15</sub>H, s, 2H), 3.38 (C<sub>6</sub>H, s, 3H). <sup>13</sup>C NMR (150 MHz, *d*-TFA:*d*<sub>6</sub>-DMSO (2:5)) δ (ppm): 161.5 (C<sub>4</sub>), 161.2 (C<sub>2</sub>), 156.2, 153.8 (C<sub>1</sub>, C<sub>5</sub>), 148.5

(C<sub>13</sub>), 137.6, 136.0, 134.9 (C<sub>7</sub>, C<sub>10</sub>, C<sub>16</sub>), 129.2, 129.0, 128.2, 128.1, 127.5, 127.0 (C<sub>9</sub>, <sub>11</sub>H, C<sub>14</sub>, C<sub>15</sub>, C<sub>17, 21</sub>, C<sub>18, 20</sub>, C<sub>19</sub>), 122.9 (C<sub>8, 12</sub>), 84.1 (C<sub>3</sub>), 29.7 (C<sub>6</sub>). (Assigned with COSY and HSQC). Anal. calcd for C<sub>21.4</sub>H<sub>19.5</sub>Cl<sub>1.1</sub>N<sub>6</sub>O<sub>2.2</sub> (M + 0.1dioxane + 1.1HCl): C, 59.05; H, 4.61; N, 19.31. Found: C, 58.99; H, 4.56; N, 19.02. Positive ESI-MS: calcd for [M + H<sup>+</sup>]/z, 387.2, found 387.4 ([M + H<sup>+</sup>]/z), 773.5 ([2M + H<sup>+</sup>]/z). High-resolution ESI-MS: calcd mass 387.1569, actual mass 387.1562.

**(E)-4-amino-7-((4-(4-chlorostyryl)phenyl)amino)-1-methylpyrimido[4,5-*d*]pyrimidin-2,5(1*H*,6*H*)-dione (2.2d)**

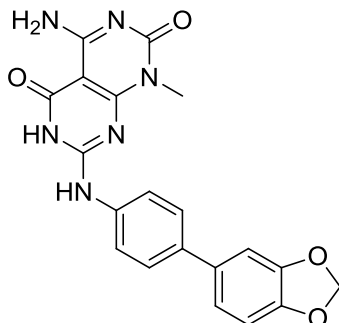


Compound **2.1d** (60 mg, 0.074 mmol) was dissolved in 4 M HCl/dioxane (6 mL) and heated to reflux for 2h. Et<sub>2</sub>O (10 mL) was then added and the precipitate formed was centrifuged down. The residual solid was suspended in Et<sub>2</sub>O (5 mL), sonicated and centrifuged down. This process was repeated three times before the solid was dried under vacuo for 48 h to give 27 mg of **2.2d** (C<sub>21</sub>H<sub>18.3</sub>Cl<sub>2.3</sub>N<sub>6</sub>O<sub>2</sub>, 78%) as a yellow solid. <sup>1</sup>H NMR (600 MHz, *d*-TFA:*d*<sub>6</sub>-DMSO (2:5)) δ (ppm): 7.63 (C<sub>9, 11</sub>H, d, <sup>3</sup>*J* = 8.2 Hz, 2H), 7.61



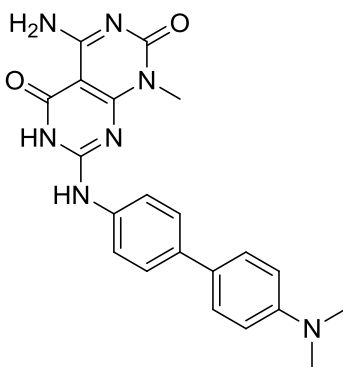
centrifuged down. This process was repeated three times before the solid was dried under vacuo for 48 h to give 14 mg of **2.2e** (C<sub>20.8</sub>H<sub>19.2</sub>Cl<sub>1.6</sub>N<sub>6</sub>O<sub>3.4</sub>, 80%) as an orange solid. <sup>1</sup>H NMR (600 MHz, *d*-TFA:*d*<sub>6</sub>-DMSO (2:5)) δ (ppm): 10.0 (C<sub>20</sub>H, s, 1H), 7.96 (C<sub>16,18</sub>H, d, <sup>3</sup>*J* = 8.8 Hz, 2H), 7.89 (C<sub>15,19</sub>H, d, <sup>3</sup>*J* = 8.2 Hz, 2H), 7.83 (C<sub>9,11</sub>H, d, <sup>3</sup>*J* = 8.8 Hz, 2H), 7.73 (C<sub>8,12</sub>H, d, <sup>3</sup>*J* = 8.2 Hz, 2H), 3.40 (C<sub>6</sub>H, s, 3H). <sup>13</sup>C NMR (150 MHz, *d*-TFA:*d*<sub>6</sub>-DMSO (2:5)) δ (ppm): 192.8 (C<sub>20</sub>), 161.3 (C<sub>4</sub>), 161.0 (C<sub>2</sub>), 156.1, 153.8 (C<sub>1</sub>, C<sub>5</sub>), 148.3 (C<sub>13</sub>), 145.4 (C<sub>17</sub>), 137.1, 136.0, 135.5 (C<sub>7</sub>, C<sub>10</sub>, C<sub>14</sub>), 130.6 (C<sub>16,18</sub>), 128.1 (C<sub>15,19</sub>), 127.4 (C<sub>9,11</sub>), 122.8 (C<sub>8,12</sub>), 84.1 (C<sub>3</sub>), 29.7 (C<sub>6</sub>). (Assigned with COSY, HSQC and HMBC). Anal. calcd for C<sub>20.8</sub>H<sub>19.2</sub>Cl<sub>1.6</sub>N<sub>6</sub>O<sub>3.4</sub> (M + 0.2dioxane + 1.6HCl): C, 53.81; H, 4.17; N, 18.10. Found: C, 54.17; H, 4.09; N, 17.77. Positive ESI-MS: calcd for [M + H<sup>+</sup>]/z, 389.1, found 389.3 ([M + H<sup>+</sup>]/z), 777.5 ([2M + H<sup>+</sup>]/z). High-resolution ESI-MS: calcd mass 389.1357, actual mass 389.1354.

**4-amino-7-((4-(benzo[d][1,3]dioxol-5-yl)phenyl)amino)-1-methylpyrimido[4,5-*d*]pyrimidine-2,5(1*H*,6*H*)-dione (2.2f)**



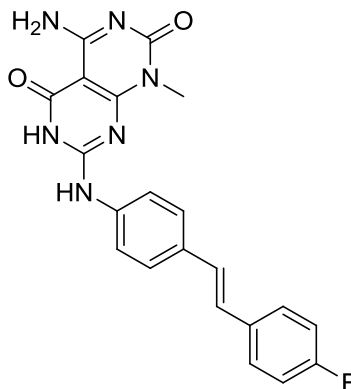
Compound **2.1f** (50 mg) was deprotected using the same method as described above to give 20 mg of **2.2f**. Positive ESI-MS: calcd for  $[M + H^+]/z$ , 405.1, found 405.2 ( $[M + H^+]/z$ ). High-resolution ESI-MS: calcd mass 405.1306, actual mass 405.1309.

**4-amino-7-((4'-(dimethylamino)-[1,1'-biphenyl]-4-yl)amino)-1-methylpyrimido[4,5-*d*]pyrimidine-2,5(1*H*,6*H*)-dione (2.2g)**



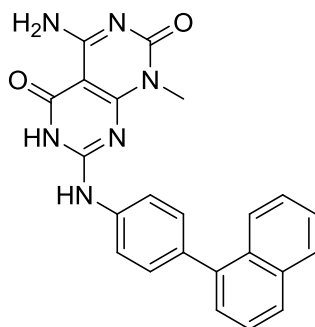
Compound **2.1g** (45 mg) was deprotected using the same method as described above to give 27 mg of **2.2g**. Positive ESI-MS: calcd for  $[M + H^+]/z$ , 404.2, found 404.3 ( $[M + H^+]/z$ ). High-resolution ESI-MS: calcd mass 404.1829, actual mass 404.1828.

**(E)-4-amino-7-((4-(4-fluorostyryl)phenyl)amino)-1-methylpyrimido[4,5-d]pyrimidin  
e-2,5(1H,6H)-dione (2.2h)**



Compound **2.1h** (58 mg) was deprotected using the same method as described above to give 24 mg of **2.2h**. Positive ESI-MS: calcd for  $[M + H^+]/z$ , 405.2, found 405.2 ( $[M + H^+]/z$ ). High-resolution ESI-MS: calcd mass 405.1470, actual mass 405.1464.

**4-amino-1-methyl-7-((4-(naphthalen-1-yl)phenyl)amino)pyrimido[4,5-d]pyrimidine-  
2,5(1H,6H)-dione (2.2i)**



Compound **2.1i** (13 mg) was deprotected using the same method as described above to give 4 mg of **2.2i**. Positive ESI-MS: calcd for  $[M + H^+]/z$ , 411.2, found 411.3 ( $[M + H^+]/z$ ).

$H^+]/z$ ). High-resolution ESI-MS: calcd mass 411.1564, actual mass 411.1560.

## 2.7. References

1. (a) Fenniri, H.; Mathivanan, P.; Vidale, K. L.; Sherman, D. M.; Hallenga, K.; Wood, K. V.; Stowell, J. G. *J. Am. Chem. Soc.* **2001**, *123*, 3854-3855. (b) Fenniri, H.; Deng, B. L.; Ribbe, A. E.; Hallenga, K.; Jacob, J.; Thiyagarajan, P. *Proc. Natl. Acad. Sci. U.S.A.* **2002**, *99*, 6487-6492. (c) Moralez, J. G.; Raez, J.; Yamazaki, T.; Motkuri, R. K.; Kovalenko, A.; Fenniri, H. *J. Am. Chem. Soc.* **2005**, *127*, 8307-8309. (d) Johnson, R. S.; Yamazaki, T.; Kovalenko, A.; Fenniri, H. *J. Am. Chem. Soc.* **2007**, *129*, 5735-5743. (e) Tikhomirov, G.; Oderinde, M.; Makeiff, D.; Mansoui, A.; Lu, W.; Heirtzler, F.; Kwok, D. Y.; Fenniri, H. *J. Org. Chem.* **2008**, *73*, 4248-4251. (f) Borzsonyi, G.; Beingessner, R. L.; Yamazaki, T.; Cho, J. Y.; Myles, A. J.; Malac, M.; Egerton, R.; Kawasaki, M.; Ishizuka, K.; Kovalenko, A.; Fenniri, H. *J. Am. Chem. Soc.* **2010**, *132*, 15136-15139. (g) Deng, B. L.; Beingessner, R. L.; Johnson, R. S.; Girdhar, N. K.; Danumah, C.; Yamazaki, T.; Fenniri, H. *Macromolecules* **2012**, *45*, 7157-7162.
2. (a) Chen, Y.; Bilgen, B.; Pareta, R. A.; Myles, A. J.; Fenniri, H.; Ciombor, D. M.; Aaron, R. K.; Webster, T. J. *Tissue Eng.* **2010**, *16*, 1233-1243. (b) Le, M. H. A.; Suri, S. S.; Rakotondradany, F.; Fenniri, H.; Singh, B. *Vet. Res.* **2010**, *41*, 75-86. (c) Zhang, L.; Hemeraz, U. D.; Fenniri, H.; Webster, T. J. *J. Biomed. Mater. Res. A* **2010**, *95A*, 550-563. (d) Meng, X.; Stout, D. A.; Sun, L.; Beingessner, R. L.; Fenniri,

- H.; Webster, T. J. *J. Biomed. Mater. Res. A* **2010**, *101A*, 1095-1102. (e) Song, S.; Chen, Y.; Yan, Z.; Fenniri, H.; Webster, T. J. *Int. J. Nanomed.* **2011**, *6*, 101-107. (f) Chen, Y.; Song, S.; Yan, Z.; Fenniri, H.; Webster, T. J. *Int. J. Nanomed.* **2011**, *6*, 1035-1044. (g) Suri, S. S.; Mills, S.; Aulakh, G. K.; Rakotondradany, F.; Fenniri, H.; Singh, B. *Int. J. Nanomed.* **2011**, *6*, 3113-3123.
3. Beingessner, R. L.; Deng, B. L.; Fanwick, P. E.; Fenniri, H. *J. Org. Chem.* **2008**, *73*, 931-939.
4. For reviews see: (a) Suzuki, A. *J. Organomet. Chem.* **1999**, *576*, 147-168. (b) Bellina, F.; Carpita, A.; Rossi, R. *Synthesis* **2004**, *15*, 2419-2440. (c) Miyaura, N.; Suzuki, A. *Chem. Rev.* **1995**, *95*, 2457-2483. (d) Suzuki, A. *Metal-Catalyzed Cross-Coupling Reactions*; Diederich, F., Stang, P. J., Eds.; Wiley-VCH: New York, 1998; Chapter 2.
5. (a) Starks, C. M.; Liotta, C. L.; Halpern, M. *Phase-Transfer Catalysis: Fundamentals, Applications, and Industrial Perspectives*; Chapman and Hall: New York, 1994. (b) Dehmlow, E. V.; Dehmlow, S. S. *Phase-Transfer Catalysis*, 3rd ed.; VCH: Weinheim, Germany, 1993. (c) Shioiri, T. Chiral Phase-Transfer Catalysis. In *Handbook of Phase-Transfer Catalysis*; Sasson, Y., Neumann, R., Eds.; Blackie: London, UK, 1997, Chapter 14.

6. Silverstein, R. M.; Webster, F. X.; Kiemle, D. J. *Spectrometric Identification of Organic Compounds*, 7th Ed.; John Wiley & Sons, Inc.: USA, 2005, Chapter 3-5.
7. (a) Martin-Palma, R. J.; Lakhtakia, A. *Nanotechnology: a crash course*; SPIE Publications: Washington, USA, 2010, Chapter 5. (b) Bhushan, B.; Marti, O. *Scanning Probe Microscopy – Principle of Operation, Instrumentation, and Probes*. In *Springer Handbook of Nanotechnology*; Bhushan, B., Eds.; Springer: New York, USA, 2004, Chapter 11.
8. Borzsonyi, G.; Alsbaiee, A.; Beingessner, R. L.; Fenniri, H. *J. Org. Chem.* **2010**, *75*, 7233-7239.
9. Laursen, J. S.; Engel-Andreasen, J.; Fristrup, P.; Harris, P.; Olsen, C. A. *J. Am. Chem. Soc.* **2013**, *135*, 2835-2844.
10. (a) Habibi-Khorassani, S. M.; Maghsoudlou, M. T.; Ebrahimi, A.; Sameh-Salari, S.; Vasheghani-Farahani, F.; Kazemian, M. A. *Concepts in Magnetic Resonance, Part A: Bridging Education and Research* **2013**, *42*, 101-107. (b) Torbeev, V. Y.; Fumi, E.; Ebert, M. O.; Schweizer, W. B.; Hilvert, D. *Helvetica Chimica Acta* **2012**, *95*, 2411-2420.
11. Fenniri, H.; Deng, B. L.; Ribbe, A. E. *J. Am. Chem. Soc.* **2002**, *124*, 11064-11072.
12. (a) Tikhomirov, G.; Yamazaki, T.; Kovalenko, A.; Fenniri, H. *Langmuir* **2008**, *24*, 4447-4450. (b) Durmus, A.; Gunbas, G.; Farmer, S. C.; Olmstead, M. M.; Mascal,

- M.; Legese, B.; Cho, J. Y.; Beingessner, R. L.; Yamazaki, T.; Fenniri, H. *J. Org. Chem.* **2013**, *78*, 11421-11426.
13. (a) Muir, T.; Morales, E.; Root, J.; Kumar, I.; Garcia, B.; Vellandi, C.; Jenigian, D.; Marsh, T.; Henderson, E.; Vesenska, J. *J. Vac. Sci. Technol. A* **1998**, *16*, 1172-1177. (b) DeRose, J. A.; Revel, J. P. *Thin Solid Films* **1998**, *331*, 194-202. (c) Kasumov, A. Y.; Klinov, D. V.; Roche, P. E.; Gueron, S.; Bouchiat, H. *Appl. Phys. Lett.* **2004**, *84*, 1007-1009.
14. (a) Hansma, H. G.; Revenko, I.; Kim, K.; Laney, D. E. *Nucleic Acids Research* **1996**, *24*, 713-720. (b) Adrian, M.; Dubochet, J.; Fuller, S. D.; Harris, J. R. *Micron* **1998**, *29*, 145-160. (c) Jackson, C. L.; Chanzy, H. D.; Booy, F. P.; Drake, B. J.; Tomalia, D. A.; Bauer, B. J.; Amis, E. J. *Macromolecules* **1998**, *32*, 6259-6265. (d) Wang, Y.; Song, R.; Li, Y.; Shen, J. *Surface Science* **2003**, *530*, 136-148.

## Chapter 3

### Synthesis and self-assembly of oligothiophene–G<sup>Λ</sup>C base hybrids

#### 3.1. Introduction

In recent decades,  $\pi$ -conjugated oligo- and polythiophenes with (semi) conducting and electroluminescent properties have been intensively studied for their potential applications in organic light emitting diodes (OLEDs),<sup>1</sup> organic field-effect transistors (OFETs),<sup>2</sup> and organic photovoltaic cells (OPVs).<sup>3</sup> The performance of these organic semiconductors strongly depends on ordering effects because an ordered matrix provides strong intermolecular  $\pi$ - $\pi$  interaction between chromophores which is critical for charge transport or exciton delocalization.<sup>4</sup> Self-assembly is a powerful tool in nanotechnology for constructing ordered nanostructures.<sup>5</sup> Recently, a new method has been employed based on biomolecules with self-assembling behavior to organize  $\pi$ -conjugated oligomers.<sup>6</sup> In this method, the hybrids of oligothiophenes with nucleotides,<sup>7</sup> peptides,<sup>8</sup> and sugars<sup>9</sup> are synthesized. Through the self-assembly of hybrids assisted by bio-moieties, oligothiophenes are efficiently arranged in highly ordered manners. However, this method is just emerging and the number of cases that have been studied is limited.

In my work, a novel approach to control the organization of oligothiophenes is established by utilizing self-assembled rosette nanotubes (RNTs) as a scaffold. To be specific, G^C bases, the self-assembling units of RNTs, are combined with  $\pi$ -conjugated ter- and sexithiophene molecules through Suzuki-Miyaura coupling reactions, producing hybrid compounds that readily form well-defined RNTs in solution with high reproducibility. The rational design of the oligothiophene–G^C base hybrids towards RNTs is briefly explained as follows. First, alkyl substituents were added to the oligothiophene backbones as G^C bases bearing alkyl chains were soluble and could readily self-assemble into RNTs in organic solvents.<sup>10</sup> Second, the alkyl side chains were arranged in a regioregular fashion because this arrangement could lead to efficient  $\pi$ - $\pi$  stacking of the conjugated oligothiophene backbones and consequently benefit the performance of the material.<sup>11</sup> Moreover, as the steric interactions between the alkyl chains could hinder a planar backbone and disrupt the conjugation, unsubstituted thiophene-2,5-diyil units were incorporated between the alkyl-substituted units to relieve the repulsion.<sup>12</sup>

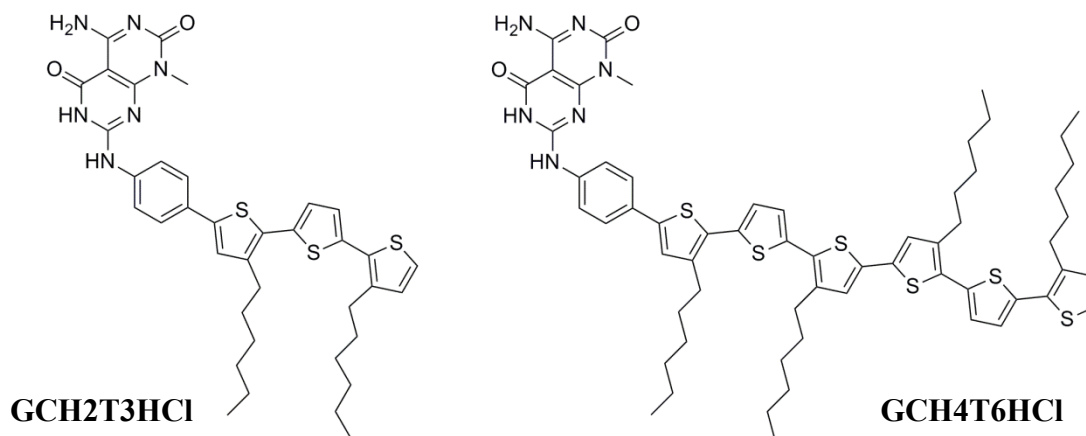


**Figure 3.1:** Oligothiophene-GAC base hybrids

In the following sections, I will first describe the synthesis of the ter- and sexithiophene functionalized GAC base hybrids (Figure 3.1, GCH2T3HCl and GCH4T6HCl). Then I will discuss the self-assembly of these hybrids into nanotubes under different external conditions (*e.g.* type of solvent, temperature variation *etc.*) and my use of SEM and UV-vis spectroscopy in investigating this process. Also I will present the accurate measurements of the nanostructures obtained by TEM and AFM.

### 3.2. Synthesis of oligothiophene functionalized GAC bases

The main precursor for both ter- and sexithiophene-GAC base hybrids, GAC iodide (19.2 g) abbreviated as GAC-I (**9**), was obtained from 2,4,6-trichloropyrimidine-5-carbaldehyde (**1**, 24.8 g) in 8 steps with an overall yield of 20% (Figure 3.2). It is to be used as the halide coupling partner in the Suzuki-Miyaura coupling reaction with thiophenylboronic esters. The previously reported procedure developed by Beingsner and Deng.<sup>13</sup> was

followed consistently for this large-scale synthesis of G<sup>Λ</sup>C-I. The purity and structure of each intermediate was confirmed by comparing its <sup>1</sup>H NMR spectrum to the results reported by Deng and co-workers<sup>13</sup> before it was carried on to the next step.

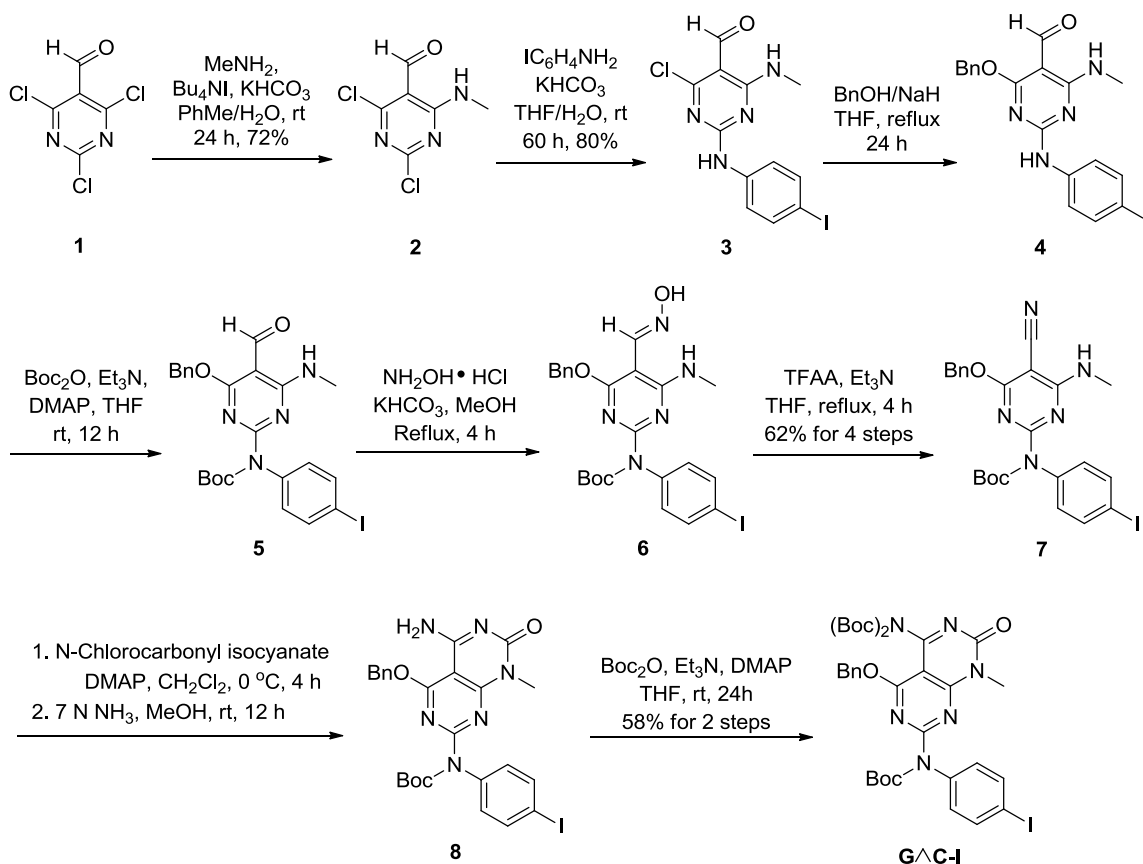


**Figure 3.2:** Synthesis of G<sup>Λ</sup>C iodide

As shown in Figure 3.2, 2,4,6-trichloropyrimidine-5-carbaldehyde (**1**) was first substituted with methylamine at position 6 via a highly regioselective S<sub>N</sub>Ar reaction under phase-transfer catalysis (PTC) conditions to give compound **2** in 72% yield. Second, aromatic substitution reaction at position 2 using 4-iodophenylamine was

conducted under another PTC procedure to convert compound **2** to **3** in 80% yield. Compound **3** was then converted to **7** in 62% yield over 4 steps including a more traditional  $S_NAr$  reaction substituting chloride with benzyloxide (**3**  $\rightarrow$  **4**), selective Boc protection of the 4-iodophenylamine fragment (**4**  $\rightarrow$  **5**), oxime generation and dehydration (**5**  $\rightarrow$  **6**  $\rightarrow$  **7**). The crude intermediates obtained within these 4 steps were carried on to the next step without further purification and the theoretical yield was used to calculate the stoichiometry of the next step. Their structures and purities were confirmed by  $^1H$  NMR. Compound **7** was purified by column chromatography and the one-pot reaction of **7** with *N*-chlorocarbonyl isocyanate followed by cyclization in a methanolic solution of ammonia afforded compound **8**. The primary amine of **8** was then protected by Boc groups to give G $\wedge$ C-I in 58% over the two steps. The identity and purity of G $\wedge$ C-I were proved by  $^1H$  NMR, LC-MS and TLC.

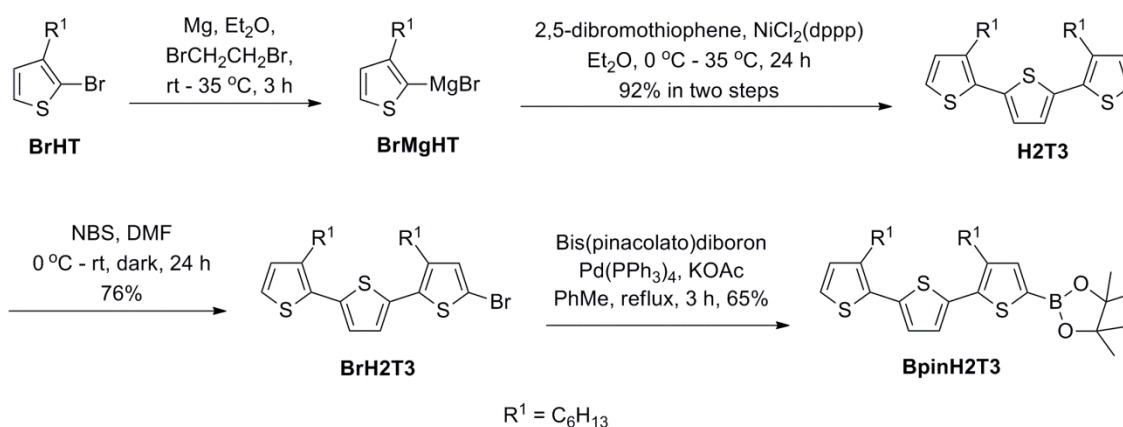
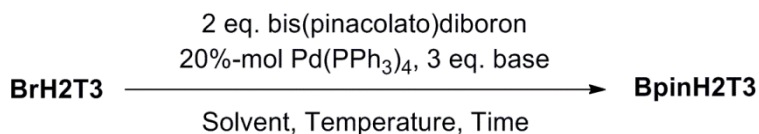


**Figure 3.3:** Synthesis of terthiophenylboronic ester BpinH2T3

The synthetic route of the terthiophenylboronic ester, abbreviated as BpinH2T3, is showed in Figure 3.3. It was designed as a coupling partner to react with G<sup>^</sup>C-I to give terthiophene-G<sup>^</sup>C base hybrid (GCH2T3HCl). Compound H2T3 was first prepared in 92% yield by a nickel-catalyzed Kumada coupling reaction of 2,5-dibromothiophene with 2.5 equivalents of Grignard reagent (BrMgHT) derived from 3-hexyl-2-thienyl bromide (BrHT) in-situ.<sup>14</sup> Then H2T3 was brominated with 1.1 equivalent of N-bromosuccinimide (NBS) in DMF to give BrH2T3 in 76% yield, according to the previously reported procedure.<sup>15</sup> BrH2T3 was only characterized by H NMR and TLC to prove its identity and purity.



entry	Base	Solvent	Temp (°C)	Time (h)	Products
1	K <sub>2</sub> CO <sub>3</sub>	PhMe	90	2	BrH2T3 (100%)*
2	K <sub>2</sub> CO <sub>3</sub>	PhMe	100	48	H4T6 (100%)
3	K <sub>2</sub> CO <sub>3</sub>	Dioxane	90	2	H2T3 (100%)
4	K <sub>2</sub> CO <sub>3</sub>	DMF	90	2	H4T6 (100%)
5	KOAc	PhMe	110	2	BpinH2T3/BrH2T3/H2T3 (43%/30%/26%)
6	KOAc	PhMe	80	4	BpinH2T3/H2T3 (67%/33%)
7	KOAc	PhMe	110	3	BpinH2T3/H2T3 (83%/17%)

\*The percentage numbers were estimated by the integration of the corresponding resonances in <sup>1</sup>H NMR spectra.

**Table 3.1:** Borylation attempts of BrH2T3 to generate BpinH2T3

With the use of BrH2T3, the Miyaura borylation reaction to generate the terthiophenylboronic ester, BpinH2T3, was explored as illustrated in Table 3.1. During optimization of the reaction conditions, BrH2T3 was treated with 20%-mol Pd(PPh<sub>3</sub>)<sub>4</sub>, 3 equivalents of base, and 2 equivalents of bis(pinacolato)diboron. The use of catalyst was reduced to 5%-mol when the reaction was scaled up. In entries 1–4, when K<sub>2</sub>CO<sub>3</sub> was chosen as the base, the desired product was not obtained. In entry 1, the reaction did not proceed in toluene at 90 °C after 2 h. As the temperature was increased to 100 °C, BrH2T3 was converted to the homocoupling byproduct H4T6 after 48 h (entry 2). In

dioxane, the starting material BrH<sub>2</sub>T<sub>3</sub> was debrominated to generate H<sub>2</sub>T<sub>3</sub> after 2 h at 90 °C (entry 3). In DMF (entry 4), the homocoupling byproduct H<sub>4</sub>T<sub>6</sub> was generated faster. The reaction completed in 2 h at 90 °C. These results might indicate that the boronic ester BpinH<sub>2</sub>T<sub>3</sub> generated in-situ was strongly activated by K<sub>2</sub>CO<sub>3</sub> and that further reaction of it with BrH<sub>2</sub>T<sub>3</sub> was accelerated.<sup>16</sup> Thus, in following entries 5–7, a weaker base, KOAc, was used instead. In entry 5, 43% of the starting BrH<sub>2</sub>T<sub>3</sub> was converted to the desired boronic ester BpinH<sub>2</sub>T<sub>3</sub>, 30% remained unreacted, and 26% of the starting material was converted to the byproduct H<sub>2</sub>T<sub>3</sub> after 2 h in toluene at 110 °C. As the reaction temperature decreased to 80 °C, BpinH<sub>2</sub>T<sub>3</sub> and H<sub>2</sub>T<sub>3</sub> were found in a ratio of 2:1 after 4 h. It showed that a decreased temperature would not reduce the generation of the debrominated byproduct. In entry 7, a similar condition to entry 5 was applied and after 3 h the major product was BpinH<sub>2</sub>T<sub>3</sub>. However, this boronic ester BpinH<sub>2</sub>T<sub>3</sub> was not entirely stable on silica and the highest yield achieved was 65% after the chromatographic purification.

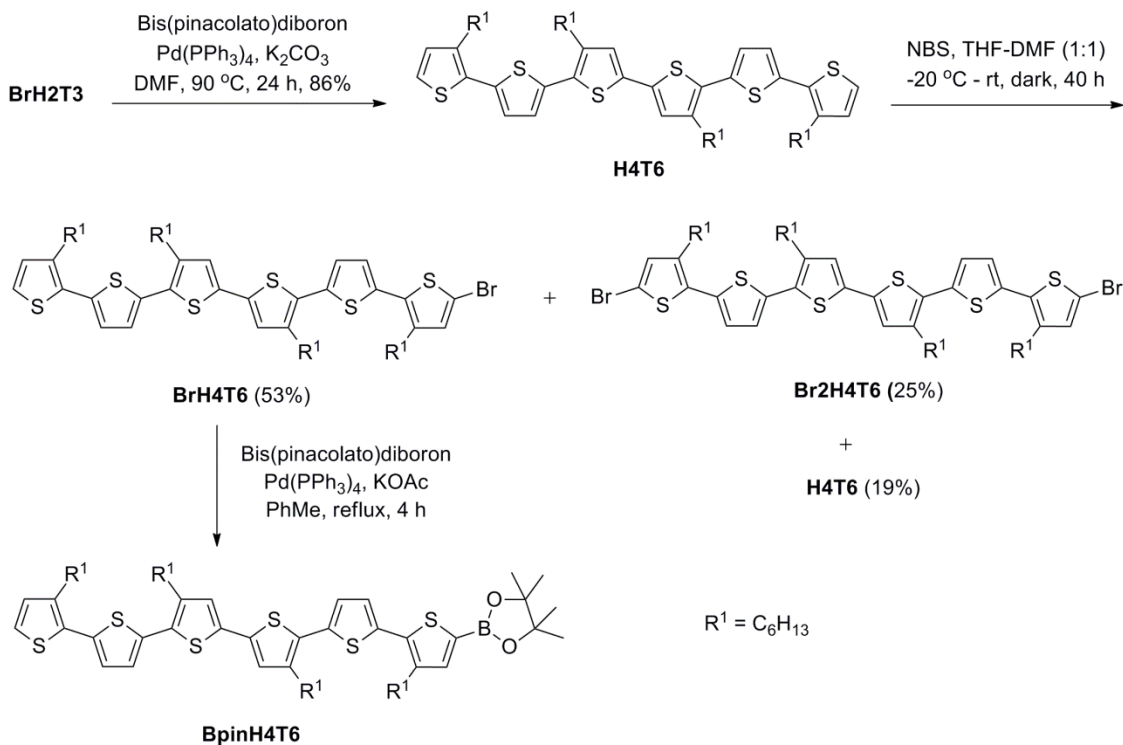


**Figure 3.4:** Synthesis of sexithiophenylboronic ester BpinH4T6

The synthetic pathway of sexithiophenylboronic ester, abbreviated as BpinH4T6, is showed in Figure 3.4. It was designed for sexithiophene-G<sup>^</sup>C base hybrid (GCH4T6HC1). Mono-brominated terthiophene BrH2T3 was first treated with 1.1 equivalents of bis(pinacolato)diboron, 5%-mol Pd(PPh<sub>3</sub>)<sub>4</sub>, 3 equivalents of K<sub>2</sub>CO<sub>3</sub> at 90 °C in DMF to give the sexithiophene H4T6 in 86% yield. This reaction was accidentally found during the exploration of the Miyaura borylation reaction for the terthiophenylboronic ester BpinH2T3 (Figure 3.4, entry 4). As discussed above, BpinH2T3 generated in-situ was further reacted with BrH2T3 because BpinH2T3 was activated by the strong base K<sub>2</sub>CO<sub>3</sub>.<sup>16</sup> Then H4T6 was brominated with 1.1 equivalents of NBS at -20 °C in

THF/DMF (1:1).<sup>17</sup> The choice of solvent was based on two factors: H4T6 was soluble in THF but not in DMF; the bromination reaction proceeded in DMF but not THF. After 40 h in the dark, the bromination reaction gave the desired mono-brominated product BrH4T6 (53%) and the dibromo-byproduct Br2H4T6 (25%). A proportion of 19% of H4T6 was also recovered. Following the isolation of BrH4T6, a Miyaura borylation reaction was attempted using the same borylation condition in the BpinH2T3 synthesis. The crude product isolated was carried on to the next step without further purification.

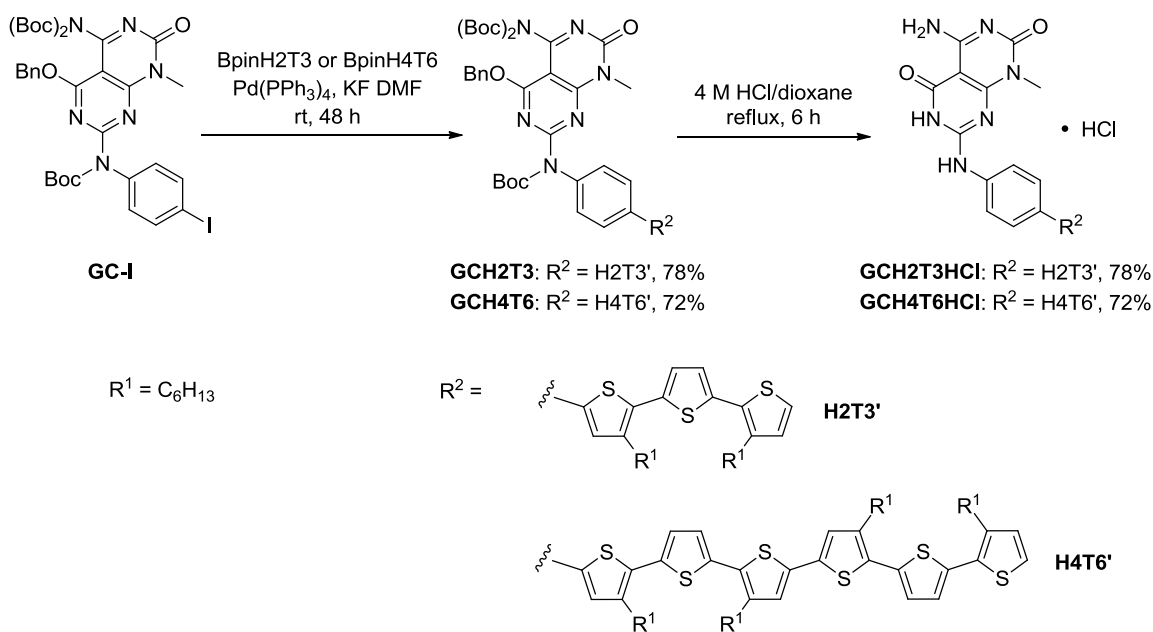


**Figure 3.5:** Suzuki-Miyaura coupling and deprotection reaction

As shown in Figure 3.5, protected oligothiophene functionalized GAC bases, GCH2T3 (78%) and GCH4T6 (72%), were prepared through a palladium-catalyzed coupling reaction of GAC-I with BpinH2T3 and BpinH4T6 respectively in the presence of 5%-mol

Pd(PPh<sub>3</sub>)<sub>4</sub> and 3 equivalents of KF at room temperature. Then GCH2T3 and GCH4T6 were deprotected to provide GCH2T3HCl (81%) and GCH4T6HCl (98%) as HCl salts, respectively.

The intermediates and the final compounds shown in Figure 3.3, 3.4 and 3.5 were characterized by <sup>1</sup>H NMR, <sup>13</sup>C NMR, and high-resolution mass spectroscopy. 2D NMR spectra were obtained for H2T3, BrH2T3, BpinH2T3, H4T6, BrH4T6, Br2H4T6, GCH2T3, and GCH4T6 to assist NMR peak assignments. Combustion data were obtained for final products GCH2T3HCl and GCH4T6HCl to calculate the actual molecular weights of those organic salts with HCl molecules incorporated. Melting points were determined for the solids, H4T6, BrH4T6, and Br2H4T6. All the characterization data were listed in Section 3.5.2.

### **3.3. Self-assembly**

#### **3.3.1. Effect of solvent and aging**

To explore the impact of solvent and aging might have on the self-assembly of the oligothiophene-G<sup>Λ</sup>C base hybrids, their stock solutions, prepared in different solvents (DCM, CB, and 1,2-DCE) were monitored over time (up to 30 d) by SEM, which is the quickest method to visualize nanostructures.

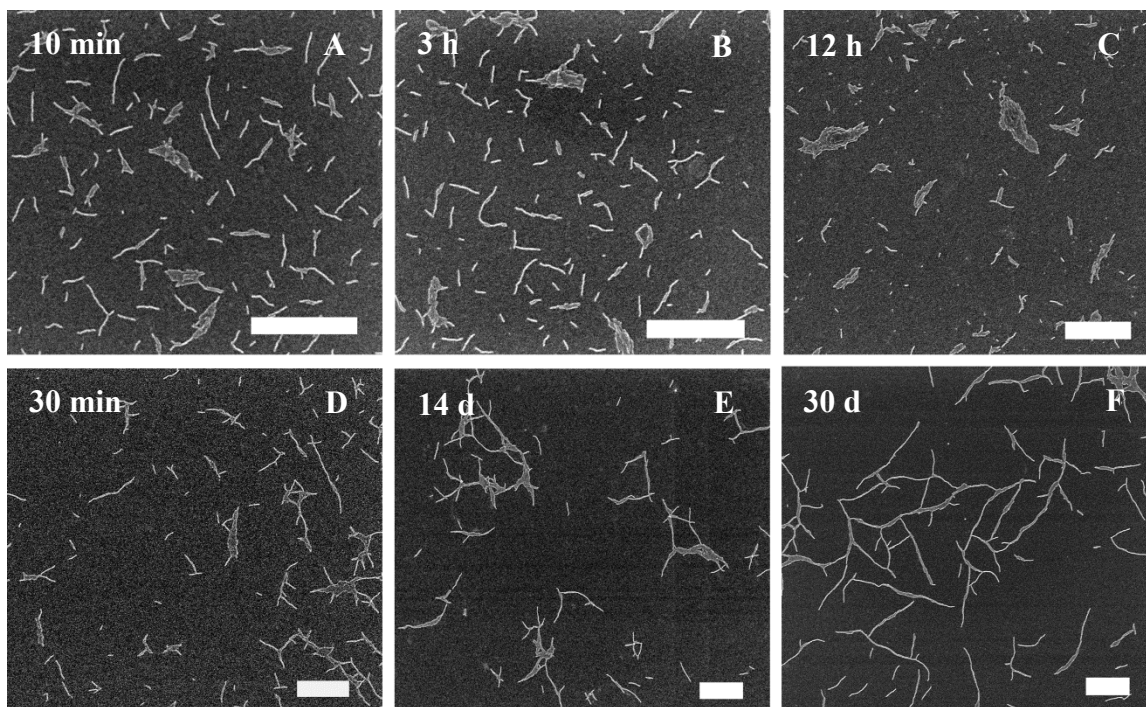


**Figure 3.6:** Time-dependent SEM images of GCH2T3HCl in DCM (A–C) and CB (D–F) at 0.01 mg/mL. Scale bar = 300 nm.

For GCH2T3HCl, the stock solutions were prepared at a concentration of 1.0 mg/mL ( $1.4 \times 10^{-3}$  M) by dissolving the compound in DCM or CB with the help of 1 min of sonication time followed by 10 s heating at reflux. At different time intervals, the aliquots of the stock solutions were taken and diluted to 0.01 mg/mL ( $1.4 \times 10^{-5}$  M) with the respective solvents. SEM samples were prepared by depositing small aliquots (10  $\mu$ L) of the diluted solutions on carbon coated TEM grids and allowing the aliquots to sit on the grids for 15 s before the excess was removed by blotting with filter paper at the edge of the grid. Then the samples were dried in high vacuum for 24 h prior to imaging. The

SEM images (Figure 3.6A–C) showed that the self-assembly of the G<sup>A</sup>C bases in DCM was rapid, which was indicated by the nanotubes found at 10 min. The SEM image of nanotubes at 3 h was identical to that at 10 min. At 12 h, fewer nanotubes were found probably due to their aggregations. In CB (Figure 3.6D–F), the formation of nanotubes was also fast. Short nanotubes were found at 30 min. Longer nanotubes were found at 14 d and 30 d. CB is a better solution for the self-assembly, which might be attributed to the increased solvation of the G<sup>A</sup>C bases in CB.

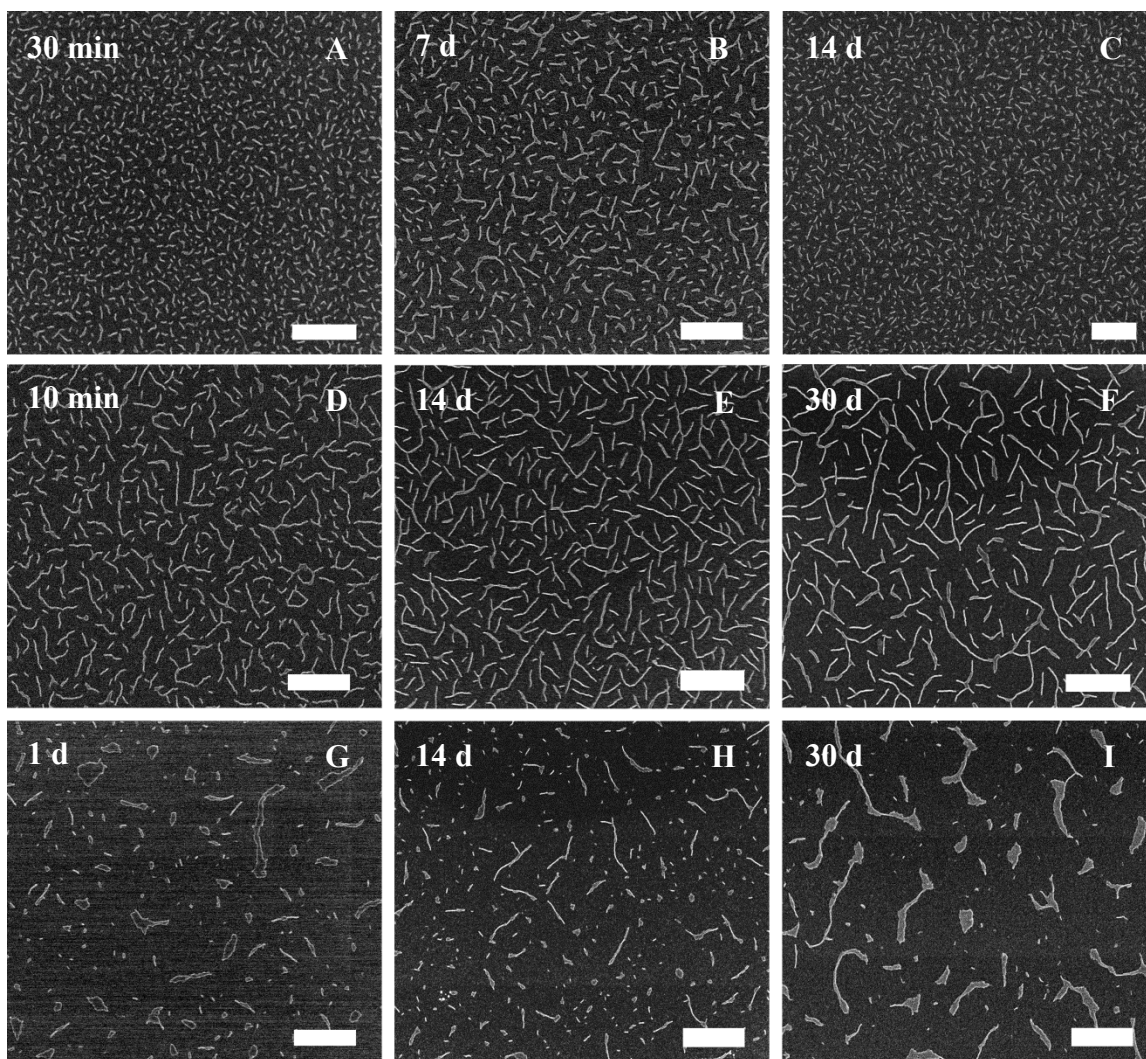


**Figure 3.7:** Time-dependent SEM images of GCH4T6HCl in DCM (A–C), 1,2-DCE (D–F), and CB (G–I) at 0.01 mg/mL. Scale bar = 300 nm.

For GCH4T6HCl, a similar experimental procedure as described above was used to investigate the self-assembly of the G<sup>+</sup>C bases in three solvents, DCM, 1,2-DCE, and CB. The stock solutions in DCM and 1,2-DCE were prepared at 0.1 mg/mL ( $8.8 \times 10^{-5}$  M) with 1 min sonication followed by 10 s heating at reflux. The stock solution in CB was made at a higher concentration of 1.0 mg/mL ( $8.8 \times 10^{-4}$  M) and heated to reflux for 30 min to

promote the RNT formation because initial attempts with 10 s of heating did not give nanotubes. The self-assembly of the G<sup>^</sup>C bases was then monitored by SEM using the aliquots (0.01 mg/mL,  $8.8 \times 10^{-6}$  M) diluted from the stock solutions at different time intervals. In DCM (Figure 3.7A–C), short nanotubes and small fragments were found at 30 min, and no obvious change was observed for 7 d and 14 d samples. In 1,2-DCE (Figure 3.7D–F), longer nanotubes than those in DCM were found at 10 min and there were less small fragments. Longer nanotubes were found at 14 d and 30 d. In CB (Figure 3.7G–I) where higher concentration and more heating were applied, amorphous fragments and short nanotubes were found at 1 d. At 14 d, longer nanotubes were found. At 30 d, only amorphous fragments were found. CB is not a good solvent for the self-assembly.

### **3.3.2. Effect of temperature variation**

To investigate the impacts of temperature might have on the absorption and morphology of the nanotubes in solutions, variable temperature UV-vis spectroscopy was performed and the SEM images of the nanotubes at the corresponding temperature gradients were taken. For GCH<sub>2</sub>T<sub>3</sub>HCl, the stock solution was first prepared in CB (1.0 mg/mL,  $1.4 \times 10^{-3}$  M) through the same method described above with 7 days' aging at room temperature. An aliquot of the stock solution was then taken and diluted to 0.01 mg/mL

( $1.4 \times 10^{-5}$  M) in CB. The diluted solution was heated up only to 368 K because the heating limitation of the UV-vis spectrometer used was 373 K. At each temperature gradient, this solution was allowed to sit for 5 min prior to UV-vis measurements and SEM sample preparation. The UV-vis measurements were carried out in a quartz cell of 1 cm path length using the diluted solution. The SEM samples were prepared by depositing one droplet (10  $\mu$ L) of the same solution on TEM grids at each temperature gradient. For GCH4T6HCl, an aliquot of the stock solution (0.1 mg/mL,  $8.8 \times 10^{-5}$  M in 1,2-DCE) aged for 7 days at room temperature was diluted to 0.01 mg/mL ( $8.8 \times 10^{-6}$  M) in the same solvent and the UV-vis measurements were taken in a quartz cell of 1 cm path length between 298 K and 348 K below the boiling point of 1,2-DCE (257 K). The SEM samples were prepared in the same way as described above for GCH2T3HCl.

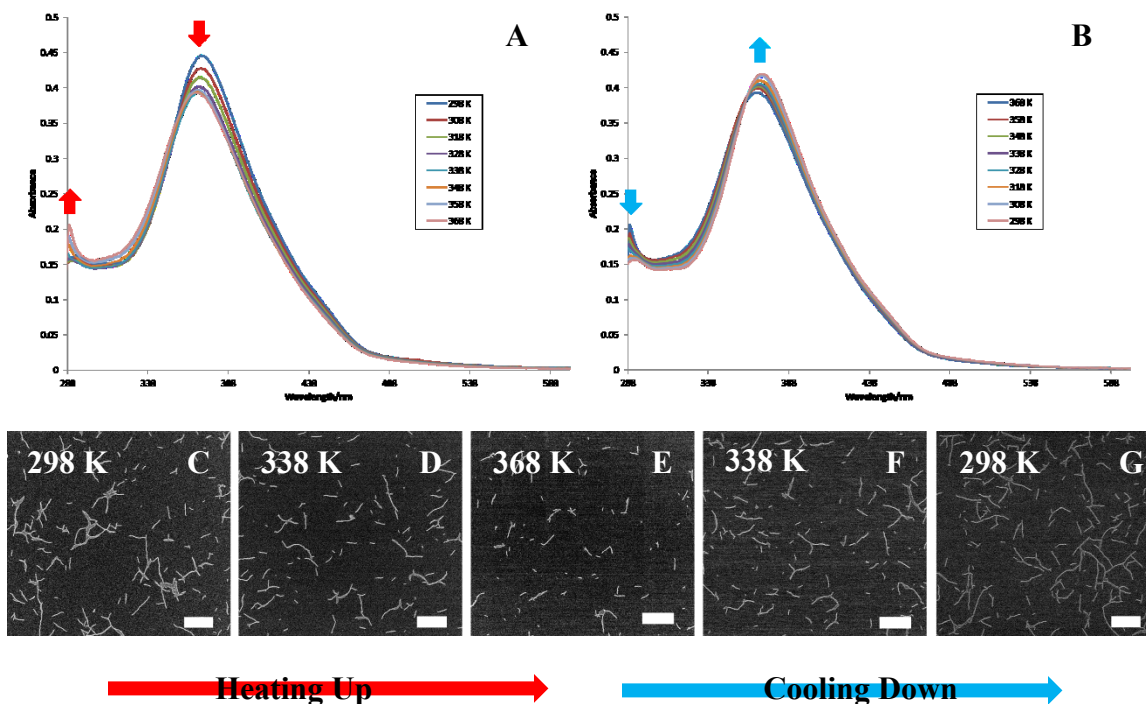


**Figure 3.8:** Variable temperature UV-vis spectra with increasing temperature (A) and decreasing temperature (B) and the corresponding SEM images of GCH2T3HCl (C–G) in CB (0.01 mg/mL,  $1.4 \times 10^{-5}$  M). Scale bar = 300 nm.

The initial UV-vis spectra of GCH2T3HCl recorded at 298 K (Figure 3.8A) showed two maxima, one at 294 nm corresponding to the bicyclic G<sup>^</sup>C cores<sup>18</sup> and the other at 371 nm originated from the terthiophene groups.<sup>12,14b,16,19</sup> As the temperature was raised to 368 K, they underwent two opposite shifts, 26.8% hyperchromism (increase in absorption) and 11.8% hypochromism (decrease in absorption), respectively. Hypsochromic (blue) shifts were observed for both of them, with the 368 K spectrum displaying maxima at 289 nm and 369 nm, representing 5 nm and 2 nm shifts, respectively. As the temperature was decreased from 368 K to 298 K (Figure 3.8B), the maximum at 289 nm underwent 23.7%

hypochromism and bathochromic (red) shift of 2 nm resulting in a maxima of lower absorption at 291 nm. Meanwhile, the maximum at 369 nm underwent 6.7% hyperchromism and 2 nm bathochromic shifts leading to a maximum of higher absorption at 371 nm. The SEM images (Figure 3.8C–G) displayed a partial breaking down of the nanotubes as the temperature increased to 368 K and a growth of the nanotubes as the temperature fell back to 298 K. The correlations between the absorptions and structures can be interpreted by the classic theories developed by Tinoco<sup>20</sup> and Rhodes.<sup>21</sup> When chromophores are closely arranged in a parallel fashion, the dipole-dipole coupling between light-excited chromophores and their neighbouring chromophores at ground state can lead to a decrease in absorption, while a co-linear arrangement of chromophores leads to an increase in absorption. In our group, these theories have been used to explain the decreased absorption observed in the self-assembly of RNTs, which indicates the vertical stacking of the G $\wedge$ C bases and the growth of RNTs.<sup>10c,22</sup> In particular, the shifts of the maxima at 294 nm (the G $\wedge$ C cores)<sup>18</sup> can be attributed to the degradation and growth of the nanotubes based on these theories. The shifts of the maximum at 371 nm of the terthiophene group might indicate the temperature-dependent intermolecular  $\pi$ -interactions between the terthiophenes.<sup>23</sup> When the temperature was increased, the  $\pi$ -interactions were disrupted which led to a decrease in absorption and a blue shift. When the temperature was decreased, the  $\pi$ -interactions became stronger which resulted

in an increase in absorption and a red shift.

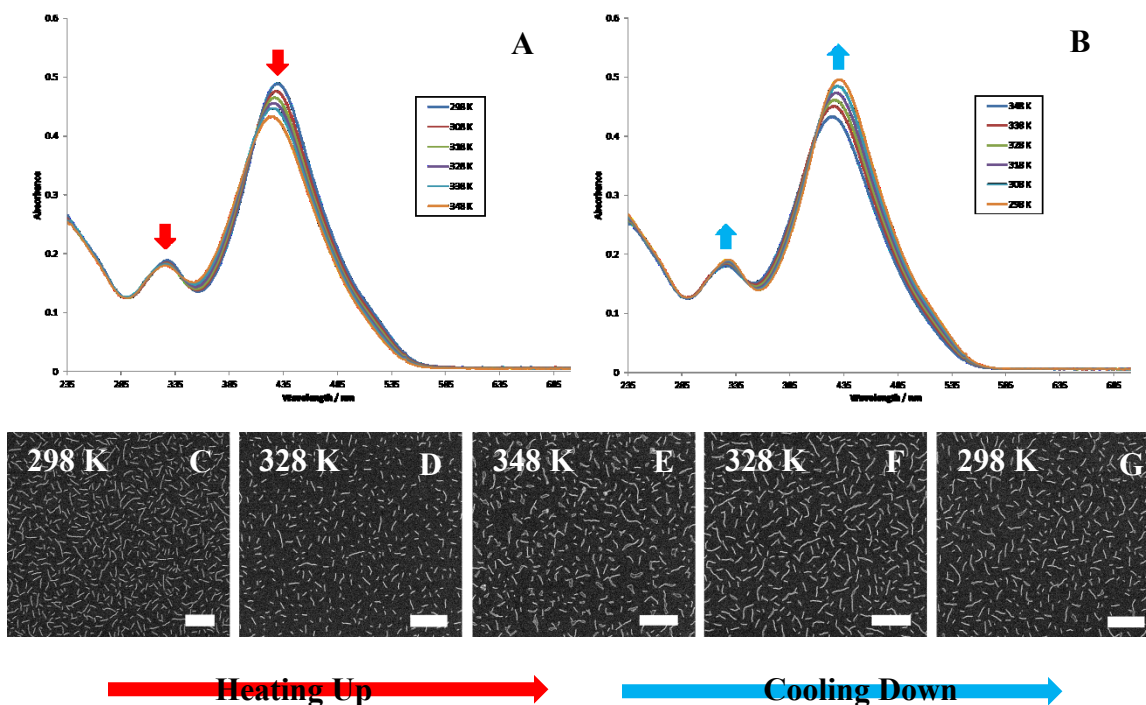


**Figure 3.9:** Variable temperature UV-vis spectra with increasing temperature (A) and decreasing temperature (B) and the corresponding SEM images of GCH4T6HCl (C–G) in 1,2-DCE (0.01 mg/mL,  $8.8 \times 10^{-6}$  M). Scale bar = 300 nm.

For GCH4T6HCl, the UV-vis spectra recorded at 298 K (Figure 3.9A) displayed two maxima at 328 nm and 430 nm. When the temperature rose to 348 K, hypsochromic and hypochromic shifts were observed for both of them. The maximum at 328 nm (298 K) shifted to 326 nm (348 K) with a 4.3% decrease in absorption and the maxima at 430 nm (298 K) shifted to 424 nm (348 K) with an 11.4% decrease in absorption. As the temperature fell back to 298 K (Figure 3.9B), the maxima underwent reverse shifts ( $\lambda_{\max}$

= 326 nm at 348 K  $\rightarrow$   $\lambda_{\text{max}} = 328$  nm at 298 K with a 5.5% increase in absorption;  $\lambda_{\text{max}} = 424$  nm at 348 K  $\rightarrow$   $\lambda_{\text{max}} = 431$  nm 298 K with a 14.5% increase in absorption). The SEM images (Figure 3.9C–E) did not display obvious changes of the nanotubes when the temperature varied between 298 K and 348 K. The nanotubes were stable upon heating up to 348 K.

The maxima at 430 nm corresponds to the sexithiophene groups.<sup>12,15,19,24</sup> and its shifts can be explained by the same hypothesis proposed for GCH2T3HCl previously. Furthermore, because the formation of oligothiophene functionalized RNTs is reversible and their properties are stimuli-responsive, the RNTs might be used for self-healing or smart materials.<sup>25</sup>

### 3.3.3. Diameter measurements

For GCH2T3HCl, the SEM sample made from its fresh stock solution at 0.1 mg/mL in DCM was stained with 0.25% uranyl acetate solution in MeCN/acetone (1:1) for TEM visualization. The diameter of the single nanotubes found by TEM was measured as  $4.05 \pm 0.16$  nm (Figure 3.10A). For preparing AFM samples, one drop of the stock solution of GCH2T3HCl at 0.1 mg/mL in CB with 7 d's aging was deposited onto Highly Ordered Pyrolytic Graphite (HOPG). The images obtained in tapping mode (TM-AFM) showed

1D tubular structures with an average height of  $3.86 \pm 0.13$  nm (Figure 3.10B). The diameter measured by AFM was close to but slightly lower the value measured by TEM, which could be attributed to the compression of the soft RNTs under the AFM tip.<sup>26</sup>

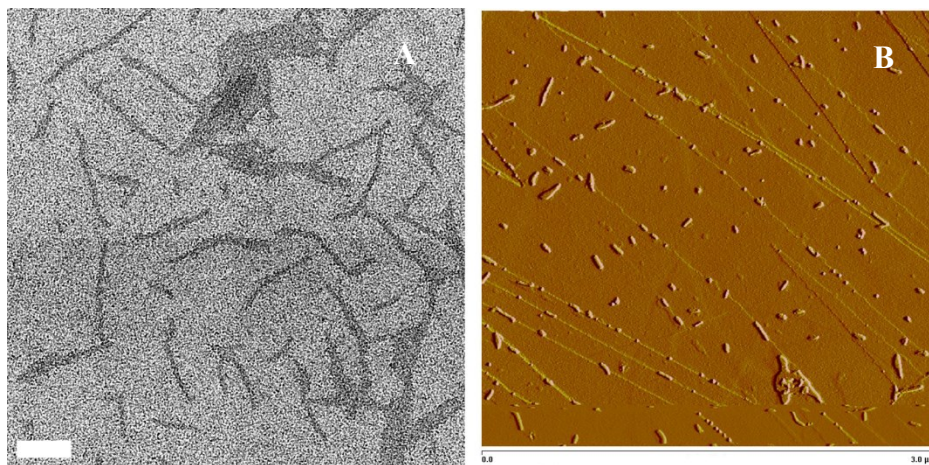


**Figure 3.10:** TEM (A, scale bar = 50 nm) and AFM (B) images of GCH2T3HCl

For GCH4T6HCl, aliquots of its stock solution in 1,2-DCE at 0.1 mg/mL with 7 d's aging was first taken and diluted to 0.01 mg/mL with the same solvent. The SEM sample was then prepared using one droplet of this diluted solution. After the SEM sample was dried under high vacuum for 24 h, it was stained with 0.25% uranyl acetate solution in MeCN/Acetone (1:1) for TEM visualization. The diameter of the single nanotubes found by TEM was measured as  $8.03 \pm 0.91$  nm (Figure 3.11A). This value was not accurate and might be higher than the actual size, which probably resulted from the poor quality of staining. For the AFM samples, one drop of the stock solution of GCH4T6HCl in 1,2-DCE at 0.1 mg/mL with 7 d's aging was deposited onto Highly Ordered Pyrolytic

Graphite (HOPG). The images obtained in tapping mode (TM-AFM) showed 1D tubular structures with an average height of  $5.58 \pm 0.33$  nm (Figure 3.11B). The diameter measured by AFM was  $\sim 2.5$  nm lower than the value obtained from TEM, which could be attributed to the compression of the soft RNTs under the AFM tip<sup>26</sup> and the thick stain layer coated on the nanotubes.

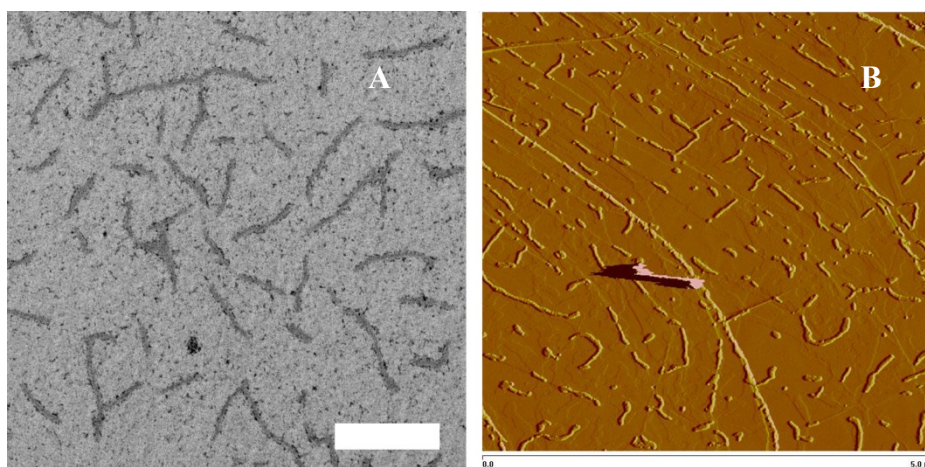


**Figure 3.11:** TEM (A, scale bar = 150 nm) and AFM (B) images of GCH4T6HCl

### 3.4. Conclusion

In this chapter, I presented the successful synthesis of a new class of hybrid compounds combining oligothiophenes and GAC bases, and their self-assembly into highly order 1D nanostructures RNTs. Particularly, protected GAC bases were functionalized with ter- and sexithiophenes through palladium-catalyzed coupling reactions. The flexibility of this method demonstrates great potential for being adapted to the synthesis of other oligomer-

GAC base hybrids in future research. SEM and UV-vis investigation into the self-assembly of the oligothiophene-GAC base hybrids under different conditions revealed that the formation of well-defined RNTs was rapid by GCH<sub>2</sub>T<sub>3</sub>HCl in CB and by GCH<sub>4</sub>T<sub>6</sub>HCl in 1,2-DCE, and that their structural and electronic properties were tunable by changing the external conditions (solvents, aging, and temperature). The variable temperature SEM and UV-vis investigation also suggested the self-organization of the oligothiophene groups and the self-healing behaviour of the RNTs. The diameters of ~4 nm were obtained for the terthiophene functionalized RNTs by TEM and AFM. For the sexithiophene functionalized RNTs, TEM measurements gave a diameter of ~8 nm and AFM measurements gave ~5.6 nm.

My work showed the potential of this RNT-based self-assembly method to construct highly ordered nanostructures of organic electronic materials. In the future, more electronic properties of these RNT materials such as conductivity and energy levels will be measured. Moreover, molecular modeling will be planned for the oligothiophene functionalized RNTs to investigate the orientation and packing of the hybrid compounds at molecular level.

## **3.5. Experimental Section**

### **3.5.1. General procedures**

#### **3.5.1.1. Self-assembly**

Stock solutions of thiophene functionalized G<sup>A</sup>C bases were prepared at either 1.0 mg/ml or 0.1 mg/mL by adding the compounds to the HPLC grade solvents with 1 min sonication followed by 10 s heating at reflux or as indicated in the results. DCM and CB were used for GCH<sub>2</sub>T<sub>3</sub>HCl while DCM, 1,2-DCE, and CB were used for GCH<sub>4</sub>T<sub>6</sub>HCl. The stock solutions were then allowed to age at room temperature. Aliquots from these RNT stock solutions were used directly for imaging by SEM, AFM, and TEM as well as UV-vis spectroscopy.

#### **3.5.1.2. SEM imaging**

The SEM samples were prepared by depositing one droplet (10 μL) of the stock solution on a carbon-coated 400-mesh copper grid (Electron Microscopy Sciences) and the droplet was allowed to sit on the grid for 15 s. Then the grid was blotted using filter paper. The samples were then dried under high vacuum for 24 h and heated on a hotplate (100 °C) for 5 min before imaging to remove any residual solvents. All SEM images were obtained without negative staining, at 30 kV accelerating voltage and a working distance of 8.0 mm on a high resolution Hitachi S-4800 cold field emission SEM.

### **3.5.1.3. TEM imaging**

For GCH2T3HCl, TEM investigation was carried out on JEOL 2200 FS TEM – 200kV Schottky field emission instrument equipped with an in-column omega filter. Bright field TEM images are acquired using energy filtered zero loss beams (slit width 10 eV) under low-dose method. Stock solutions were prepared as described in the self-assembly section. TEM samples were prepared by depositing a droplet of stock solution on a carbon-coated 400-mesh copper grid (Electron Microscopy Sciences). The droplet was allowed to sit on the grid for 15 s and then blotted by filter paper. The staining of samples was performed by dipping the samples in 0.25% uranyl acetate solution in MeCN/acetone (1:1) for 30 s. The grid was then blotted, dried under high vacuum for 24 h, and on the hotplate. Uranyl acetate solutions were prepared by dissolving uranyl acetate crystals in MeCN/Acetone (1:1) by 5 min sonication and proper heat. For GCH4T6HCl, TEM investigation was carried out under TE-mode of a high resolution Hitachi S-5500 cold field emission SEM. The sample preparation and staining were the same to GCH2T3HCl.

### **3.5.1.4. AFM imaging**

For AFM measurement, clean HOPG (highly ordered pyrolytic graphite) and mica substrates ( $1 \times 1 \text{ cm}^2$ ) were prepared and aliquots of the stock solution were deposited by spin-coating at 2500 rpm for 30 s to remove the excessive precipitation from the surface

of the sample. All samples were dried under high vacuum for 24 h prior to imaging. Sample surface was observed using a Digital Instruments/Veeco Instruments MultiMode Nanoscope IV AFM equipped with an E scanner. For optimal height profile in this investigation (minimizing compressibility), silicon cantilevers (MikroMasch USA, Inc.) with extra-low spring constants of 0.45 N/m were used in tapping mode (TM-AFM). To obtain a clear image from surface, low scan rate (0.5-1 Hz) and amplitude setpoint (1 V) were chosen.

#### **3.5.1.5. UV-vis spectroscopy**

UV-vis spectra were recorded on Perkin Elmer Lambda 1050 UV-vis-nir spectrophotometer coupled with PTP-1+1 Peltier system and PCB 1500 water Peltier system. The diluted aliquots of the stock solutions were placed in a quartz cell of 1 cm pathlength for UV measurements.

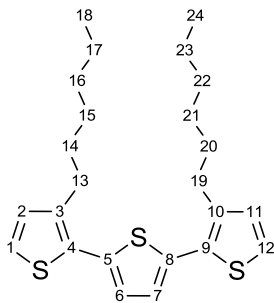
#### **3.5.1.6. General methods of synthesis and NMR characterization**

Unless otherwise noted, all reactions were performed under an atmosphere of N<sub>2</sub> using oven-dried glassware equipped with a magnetic stirrer and rubber septum. Reagent grade Et<sub>2</sub>O was distilled under inert atmosphere (N<sub>2</sub>) over CaH<sub>2</sub> before use. All other commercial reagents were used without purification unless otherwise stated. Melting

points were recorded on a Büchi B-545 melting point apparatus.  $^1\text{H}$  and  $^{13}\text{C}$  NMR spectra were recorded in the specified deuterated solvent on 600 MHz NMR spectrometers with the solvent as internal reference. The NMR data is presented as follows: chemical shift, peak assignment, multiplicity, coupling constant, integration. Residual  $^1\text{H}$  shifts in  $\text{CDCl}_3$  (7.26 ppm),  $\text{CD}_2\text{Cl}_2$  (5.32 ppm) and  $d_6$ -DMSO (2.5 ppm),  $d_6$ -DMF (8.01 ppm, 2.91 ppm, 2.74 ppm) were used as the internal reference where stated for  $^1\text{H}$  NMR. The following abbreviations were used to explain the multiplicities: s = singlet, d = doublet, t = triplet, m = multiplet, bs = broad singlet.  $\text{CDCl}_3$  (77.16 ppm),  $\text{CD}_2\text{Cl}_2$  (53.84 ppm),  $d_6$ -DMSO (39.5 ppm),  $d_6$ -DMF (162.7 ppm, 35.2 ppm, 30.1 ppm) were used as the internal references for  $^{13}\text{C}$  NMR as stated.

### 3.5.2. Synthesis of target molecules

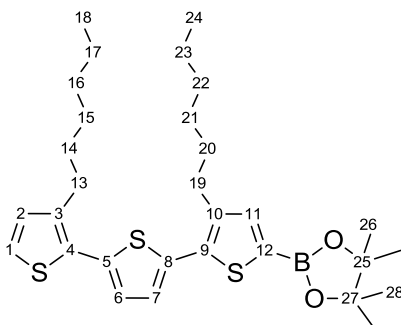
#### 3,3''-Dihexyl-2,2':5',2''-terthiophene (H2T3)



2-Bromo-3-hexylthiophene (4.52 g, 18.3 mmol) was slowly added to a suspension of magnesium turnings (532 mg, 21.9 mmol) in distilled  $\text{Et}_2\text{O}$  (25 mL) at room temperature and a few drops of 1,2-dibromoethane were added to initiate the reaction. Then the

mixture was heated to 35 °C for 3 h. The resulting Grignard reagent, 3-hexylthienyl magnesium chloride was added slowly via a cannula into a mixture of 2,5-dibromobithiophene (1.77 g, 7.3 mmol) and Ni(dppp)Cl<sub>2</sub> (60 mg, 0.11 mmol) in distilled Et<sub>2</sub>O (15 mL) while cooling on ice. The reaction mixture was then heated to reflux for 24 h and poured into ice/water (100 mL) containing 12 M HCl (20 mL). The product was extracted with Et<sub>2</sub>O (3 × 30 mL) and the combined organic layers were washed with water and brine, successively. The organic extracts were dried over anhydrous Na<sub>2</sub>SO<sub>4</sub>, filtered and evaporated. The residue was purified by column chromatography on silica gel (0-2% CH<sub>2</sub>Cl<sub>2</sub>/hexanes) to give H2T3 (2.81 g, 92%) as a light yellow oil. R<sub>f</sub> = 0.28 (SiO<sub>2</sub>, 2% CH<sub>2</sub>Cl<sub>2</sub>/hexanes). <sup>1</sup>H NMR (600 MHz, CDCl<sub>3</sub>) δ (ppm): 7.18 (C<sub>1</sub>H, C<sub>12</sub>H, d, <sup>3</sup>J = 5.3 Hz, 2H), 7.06 (C<sub>6</sub>H, C<sub>7</sub>H, s, 2H), 6.95 (C<sub>2</sub>H, C<sub>11</sub>H, d, <sup>3</sup>J = 5.3 Hz, 2H), 2.79 (C<sub>13</sub>H, C<sub>19</sub>H, t, <sup>3</sup>J = 7.9 Hz, 4H), 1.69 – 1.62 (C<sub>14</sub>H, C<sub>20</sub>H, tt, <sup>3</sup>J = 7.8 Hz, 4H), 1.40 – 1.36 (C<sub>15</sub>H, C<sub>21</sub>H, m, 4H), 1.34 – 1.28. (C<sub>16</sub>H, C<sub>17</sub>H, C<sub>22</sub>H, C<sub>23</sub>H, m, 8H), 0.91 – 0.87 (C<sub>18</sub>H, C<sub>24</sub>H, m, 6H). <sup>13</sup>C NMR (150 MHz, CDCl<sub>3</sub>) δ (ppm): 139.9 (C<sub>3</sub>, C<sub>10</sub>), 136.2 (C<sub>5</sub>, C<sub>8</sub>), 130.6 (C<sub>4</sub>, C<sub>9</sub>), 130.2 (C<sub>2</sub>, C<sub>11</sub>), 126.2 (C<sub>6</sub>, C<sub>7</sub>), 123.9 (C<sub>1</sub>, C<sub>12</sub>), 31.8, 22.8 (C<sub>16</sub>, C<sub>17</sub>, C<sub>22</sub>, C<sub>23</sub>), 30.9 (C<sub>14</sub>, C<sub>20</sub>), 29.4 (C<sub>13</sub>, C<sub>15</sub>, C<sub>19</sub>, C<sub>21</sub>), 14.2 (C<sub>18</sub>, C<sub>24</sub>). (Assigned with COSY, HSQC and HMBC). High-resolution ESI-MS: calcd mass 416.1666, actual mass 416.1666.

**2-(3,3''-Dihexyl-[2,2':5',2''-terthiophen]-5-yl)-4,4,5,5-tetramethyl-1,3,2-dioxaborolan  
e (BpinH2T3)**

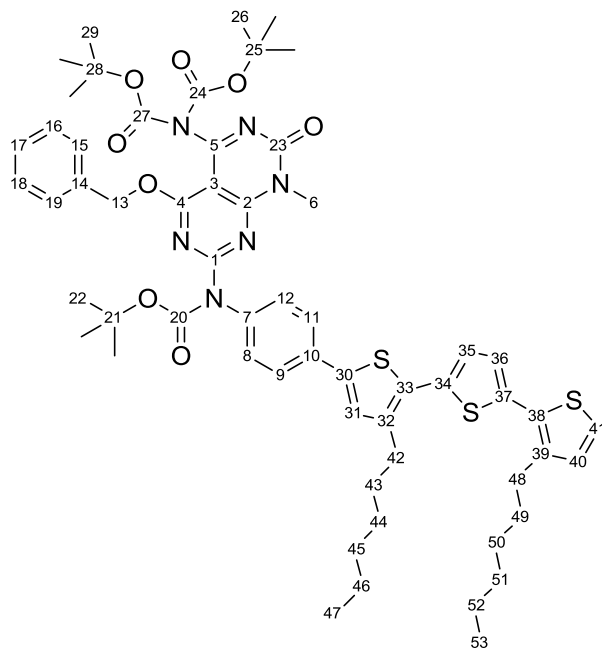


A mixture of BrH2T3 (0.76 g, 1.53 mmol), bis(pinacolato)diboron (0.78, 3.07 mmol), potassium acetate (452 mg, 4.60 mmol) and Pd(PPh<sub>3</sub>)<sub>4</sub> (5 mol%, 89 mg, 0.08 mmol) in toluene (30 mL) was bubbled with nitrogen gas for 30 min and heated to reflux for 3 h. The mixture was cooled to room temperature and diluted with Et<sub>2</sub>O (30 mL). The organic layer was filtered, washed with water and brine, dried over anhydrous Na<sub>2</sub>SO<sub>4</sub>, filtered and evaporated. The residue was purified by column chromatography on silica gel (10-30% CH<sub>2</sub>Cl<sub>2</sub>/hexanes) to give BpinH2T3 (0.54 g, 65%) as a light yellow oil. R<sub>f</sub> = 0.42 (SiO<sub>2</sub>, 50% CH<sub>2</sub>Cl<sub>2</sub>/hexanes). <sup>1</sup>H NMR (600 MHz, CDCl<sub>3</sub>) δ (ppm): 7.47 (C<sub>11</sub>H, s, 1H), 7.18 (C<sub>1</sub>H, d, <sup>3</sup>J = 5.3 Hz, 1H), 7.11 (C<sub>7</sub>H, d, <sup>3</sup>J = 3.5 Hz, 1H), 7.06 (C<sub>6</sub>H, d, <sup>3</sup>J = 4.1 Hz, 1H), 6.94 (C<sub>2</sub>H, d, <sup>3</sup>J = 5.3 Hz, 1H), 2.81 – 2.76 (C<sub>13</sub>H, C<sub>19</sub>H, m, 4H), 1.69 – 1.61 (C<sub>14</sub>H, C<sub>20</sub>H, m, 4H), 1.42 – 1.34 (C<sub>15</sub>H, C<sub>21</sub>H, C<sub>26</sub>H, C<sub>28</sub>H, m, 16H), 1.34 – 1.28 (C<sub>16</sub>H, C<sub>17</sub>H, C<sub>22</sub>H, C<sub>23</sub>H, m, 8H), 0.91 – 0.86 (C<sub>18</sub>H, C<sub>24</sub>H, m, 6H). <sup>13</sup>C NMR (150 MHz, CDCl<sub>3</sub>) δ (ppm): 141.0 (C<sub>12</sub>), 140.4 (C<sub>11</sub>), 140.0 (C<sub>3</sub>), 137.9 (C<sub>10</sub>), 136.7, 136.2 (C<sub>5</sub>, C<sub>8</sub>), 130.6 (C<sub>4</sub>), 130.3

(C<sub>2</sub>), 126.4 (C<sub>6</sub>, C<sub>7</sub>), 124.0 (C<sub>1</sub>), 84.4 (C<sub>25</sub>, C<sub>27</sub>), 31.9, 22.8 (C<sub>16</sub>, C<sub>17</sub>, C<sub>22</sub>, C<sub>23</sub>), 30.9, 30.8 (C<sub>14</sub>, C<sub>20</sub>), 29.5 (C<sub>13</sub>, C<sub>15</sub>, C<sub>19</sub>, C<sub>21</sub>), 25.0 (C<sub>26</sub>, C<sub>28</sub>), 14.3 (C<sub>18</sub>, C<sub>24</sub>). (Assigned with COSY, HSQC and HMBC). MALDI-TOF MS: calcd for [M<sup>+</sup>]/z, 542.3, found 542.2 ([M<sup>+</sup>]/z). High-resolution MALDI-FTICR MS: calcd mass 542.2513, actual mass 542.2513.

### ***tert*-Butyl**

**(4-(benzyloxy)-5-(bis(*tert*-butoxycarbonyl)amino)-8-methyl-7-oxo-7,8-dihydropyrimido[4,5-*d*]pyrimidin-2-yl)(4-(3,3''-dihexyl-[2,2':5',2''-terthiophen]-5-yl)phenyl)carbamate (GCH2T3)**

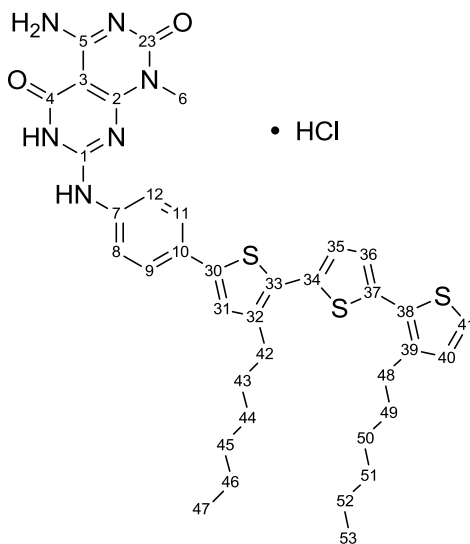


A mixture of BpinH2T3 (303 mg, 0.56 mmol), GC-I (298 mg, 0.37 mmol), potassium fluoride (65 mg, 1.12 mmol) and Pd(PPh<sub>3</sub>)<sub>4</sub> (10 mol%, 43 mg, 0.04 mmol) in anhydrous DMF (4 mL) was bubbled with nitrogen gas for 30 min and allowed to stir at room

temperature for 48 h. The mixture was diluted with Et<sub>2</sub>O (20 mL) and filtered. The organic layer was washed with water and brine, dried over anhydrous Na<sub>2</sub>SO<sub>4</sub>, filtered and evaporated. The residue was purified by column chromatography on silica gel (15-30% EtOAc/hexanes) to give GCH2T3 (315 mg, 78%) as a yellow oil. R<sub>f</sub> = 0.18 (SiO<sub>2</sub>, 30% EtOAc/hexanes). <sup>1</sup>H NMR (600 MHz, CD<sub>2</sub>Cl<sub>2</sub>) δ (ppm): 7.68 (C<sub>8</sub>H, C<sub>12</sub>H, d, <sup>3</sup>J = 8.8 Hz, 2H), 7.30 – 7.27 (C<sub>16</sub>H, C<sub>17</sub>H, C<sub>18</sub>H, C<sub>31</sub>H, m, 4H), 7.24 (C<sub>9</sub>H, C<sub>11</sub>H, d, <sup>3</sup>J = 8.2 Hz, 2H), 7.22 (C<sub>41</sub>H, d, <sup>3</sup>J = 5.3 Hz, 1H), 7.20 – 7.18 (C<sub>15</sub>H, C<sub>19</sub>H, m, 2H), 7.15 (C<sub>35</sub>H, d, <sup>3</sup>J = 3.5 Hz, 1H), 7.10 (C<sub>36</sub>H, d, <sup>3</sup>J = 4.1 Hz, 1H), 6.98 (C<sub>40</sub>H, d, <sup>3</sup>J = 4.7 Hz, 1H), 5.33 (C<sub>13</sub>H, s, 2H), 3.55 (C<sub>6</sub>H, s, 3H), 2.85 – 2.78 (C<sub>42</sub>H, C<sub>48</sub>H, m, 4H), 1.75 – 1.63 (C<sub>43</sub>H, C<sub>49</sub>H, m, 4H), 1.51 (C<sub>22</sub>H, s, 9H), 1.46 – 1.36 (C<sub>44</sub>H, C<sub>50</sub>H, 4H), 1.36 – 1.29 (C<sub>45</sub>H, C<sub>46</sub>H, C<sub>51</sub>H, C<sub>52</sub>H, C<sub>26</sub>H, C<sub>29</sub>H, m, 26H), 0.91 – 0.87 (C<sub>47</sub>H, C<sub>53</sub>H, m, 6H). <sup>13</sup>C NMR (150 MHz, CD<sub>2</sub>Cl<sub>2</sub>) δ (ppm): 166.2 (C<sub>4</sub>), 161.8 (C<sub>2</sub>), 161.5, 160.6 (C<sub>1</sub>, C<sub>5</sub>), 156.2 (C<sub>23</sub>), 152.4 (C<sub>20</sub>), 149.8 (C<sub>24</sub>, C<sub>27</sub>), 141.4 (C<sub>32</sub>), 141.2, 139.9 (C<sub>7</sub>, C<sub>10</sub>), 140.4 (C<sub>39</sub>), 136.7, 136.2 (C<sub>34</sub>, C<sub>37</sub>), 135.4 (C<sub>14</sub>), 133.7 (C<sub>30</sub>), 130.8 (C<sub>33</sub>), 130.6 (C<sub>40</sub>), 130.5 (C<sub>38</sub>), 129.1 (C<sub>9</sub>, C<sub>11</sub>), 128.9, 128.8 (C<sub>15</sub> – C<sub>19</sub>), 127.2 (C<sub>31</sub>), 126.6, 126.5 (C<sub>35</sub>, C<sub>36</sub>), 126.2 (C<sub>8</sub>, C<sub>12</sub>), 124.3 (C<sub>41</sub>), 93.7 (C<sub>3</sub>), 84.1, 83.8 (C<sub>21</sub>, C<sub>25</sub>, C<sub>28</sub>), 70.3 (C<sub>13</sub>), 32.1, 23.1 (C<sub>45</sub>, C<sub>46</sub>, C<sub>51</sub>, C<sub>52</sub>), 31.1, 31.0 (C<sub>43</sub>, C<sub>49</sub>), 30.4 (C<sub>6</sub>), 30.0, 29.7 (C<sub>42</sub>, C<sub>44</sub>, C<sub>48</sub>, C<sub>50</sub>), 28.1, 28.0 (C<sub>22</sub>, C<sub>26</sub>, C<sub>29</sub>), 14.3 (C<sub>47</sub>, C<sub>53</sub>). (Assigned with COSY, HSQC and HMBC). MALDI-TOF MS: calcd for [M<sup>•+</sup>]/z, 1088.5, found 1088.1 ([M<sup>•+</sup>]/z). High-resolution MALDI-FTICR MS: calcd mass 1088.4568,

actual mass 1088.4575.

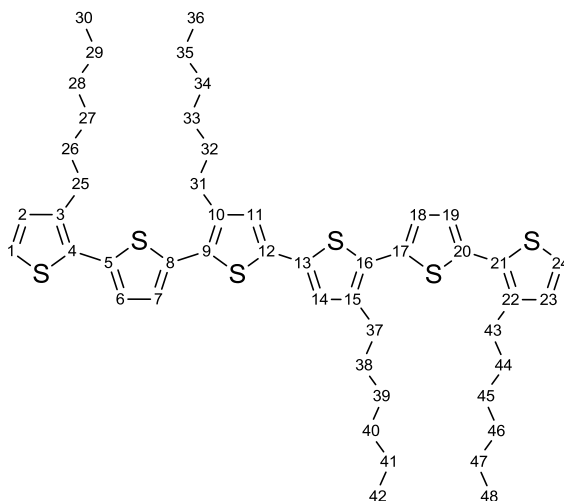
**4-amino-7-((4-(3,3''-dihexyl-[2,2':5',2''-terthiophen]-5-yl)phenyl)amino)-1-methylpyrimido[4,5-*d*]pyrimidine-2,5(1*H*,6*H*)-dione hydrochloride (GCH2T3HCl)**



GCH2T3 (83 mg, 0.076 mmol) was dissolved in 4 M HCl/dioxane (14 mL) and heated to reflux for 6 h. Et<sub>2</sub>O (10 mL) was then added and the precipitate formed was centrifuged down. The residual solid was suspended in Et<sub>2</sub>O (10 mL), sonicated and centrifuged down. This process was repeated three times before the solid was dried under vacuo for 48 h to give 44 mg of GCH2T3HCl (C<sub>37</sub>H<sub>42.5</sub>Cl<sub>0.5</sub>N<sub>6</sub>O<sub>2</sub>S<sub>3</sub>, 81%) as a yellow solid. <sup>1</sup>H NMR (600 MHz, *d*-TFA:*d*<sub>6</sub>-DMSO (2:5)) δ (ppm): 7.68 (C<sub>9</sub>H, C<sub>11</sub>H, d, <sup>3</sup>*J* = 8.8 Hz, 2H), 7.62 (C<sub>8</sub>H, C<sub>12</sub>H, d, <sup>3</sup>*J* = 8.2 Hz, 2H), 7.30 – 7.27 (C<sub>16</sub>H, C<sub>17</sub>H, C<sub>18</sub>H, C<sub>31</sub>H, m, 4H), 7.38 (C<sub>31</sub>H, s, 1H), C<sub>41</sub>H (deuterated by *d*-TFA), 7.15 (C<sub>35</sub>H, d, <sup>3</sup>*J* = 3.5 Hz, 1H), 7.12 (C<sub>36</sub>H, d, <sup>3</sup>*J* = 4.1 Hz, 1H), 6.97 (C<sub>40</sub>H, s, 1H), 3.39 (C<sub>6</sub>H, s, 3H), 2.77 – 2.70 (C<sub>42</sub>H, C<sub>48</sub>H, m, 4H),

1.66 – 1.55 (C<sub>43</sub>H, C<sub>49</sub>H, m, 4H), 1.37 – 1.20 (C<sub>44</sub>H, C<sub>45</sub>H, C<sub>46</sub>H, C<sub>50</sub>H, C<sub>51</sub>H, C<sub>52</sub>H, m, 12H), 0.83 – 0.78 (C<sub>47</sub>H, C<sub>53</sub>H, m, 6H). <sup>13</sup>C NMR (150 MHz, *d*-TFA:*d*<sub>6</sub>-DMSO (2:5)) δ (ppm): 161.6, 161.2, 156.3, 153.7, 148.5 (C<sub>1</sub>, C<sub>2</sub>, C<sub>4</sub>, C<sub>5</sub>, C<sub>23</sub>), 141.3, 141.0, 140.2, 136.1, 135.6, 130.9, 129.9, 129.7 (C<sub>7</sub>, C<sub>10</sub>, C<sub>30</sub>, C<sub>32</sub>, C<sub>33</sub>, C<sub>34</sub>, C<sub>37</sub>, C<sub>38</sub>, C<sub>39</sub>, C<sub>40</sub>, C<sub>41</sub>), 127.4, 126.8, 126.8, 126.2 (C<sub>9</sub>, C<sub>11</sub>, C<sub>31</sub>, C<sub>35</sub>, C<sub>36</sub>), 126.2 (C<sub>8</sub>, C<sub>12</sub>), 84.2 (C<sub>3</sub>), 31.6, 30.7, 30.5, 29.8, 29.6, 29.2 (C<sub>42</sub>, C<sub>43</sub>, C<sub>44</sub>, C<sub>45</sub>, C<sub>48</sub>, C<sub>49</sub>, C<sub>50</sub>, C<sub>51</sub>, C<sub>6</sub>), 22.6 (C<sub>46</sub>, C<sub>52</sub>), 14.1 (C<sub>47</sub>, C<sub>53</sub>). (Assigned with COSY and HSQC). Anal. calcd for C<sub>37</sub>H<sub>42.5</sub>Cl<sub>0.5</sub>N<sub>6</sub>O<sub>2</sub>S<sub>3</sub> (M + 0.5HCl): C, 61.96; H, 5.99; N, 11.72; S, 13.41. Found: C, 62.10; H, 5.87; N, 11.87; S, 13.36. Positive ESI-MS: calcd for [M + H<sup>+</sup>]/z, 699.3, found 699.3 ([M + H<sup>+</sup>]/z). High-resolution MALDI-FTICR MS: calcd mass 698.2526, actual mass 698.2527.

### 3,3'',3''',4'''-Tetrahexyl-2,2':5',2'':5'',2''':5''',2''':5''',2''''-sexithiophene (H4T6)

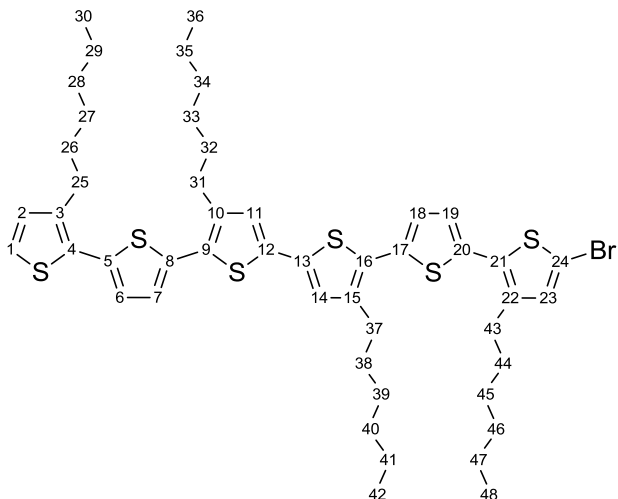


A mixture of BrH2T3 (0.50 g, 1.01 mmol), bis(pinacolato)diboron (282 mg, 1.11 mmol),

potassium carbonate (418 mg, 3.03 mmol) and Pd(PPh<sub>3</sub>)<sub>4</sub> (5 mol%, 58 mg, 0.05 mmol) in anhydrous DMF (10 mL) was bubbled with nitrogen gas for 30 min and heated at 90 °C for 24 h. The mixture was cooled to room temperature and diluted with Et<sub>2</sub>O (20 mL). The organic layer was washed with a plenty of water and brine, dried over anhydrous Na<sub>2</sub>SO<sub>4</sub>, filtered and evaporated. The residue was purified by column chromatography on silica gel (1-5% CH<sub>2</sub>Cl<sub>2</sub>/hexanes) to give H4T6 (0.36 g, 86%) as a red solid. R<sub>f</sub> = 0.10 (SiO<sub>2</sub>, 5% CH<sub>2</sub>Cl<sub>2</sub>/hexanes). M.p. = 69.5-70.5 °C. <sup>1</sup>H NMR (600 MHz, CDCl<sub>3</sub>) δ (ppm): 7.18 (C<sub>1</sub>H, C<sub>24</sub>H, d, <sup>3</sup>J = 5.3 Hz, 2H), 7.09 – 7.06 (C<sub>6</sub>H, C<sub>7</sub>H, C<sub>18</sub>H, C<sub>19</sub>H, m, 4H), 7.01 (C<sub>11</sub>H, C<sub>14</sub>H, s, 2H), 6.95 (C<sub>2</sub>H, C<sub>23</sub>H, d, <sup>3</sup>J = 5.3 Hz, 2H), 2.81 – 2.75 (C<sub>25</sub>H, C<sub>31</sub>H, C<sub>37</sub>H, C<sub>43</sub>H, m, 8H), 1.71 – 1.63 (C<sub>26</sub>H, C<sub>32</sub>H, C<sub>38</sub>H, C<sub>44</sub>H, m, 8H), 1.45 – 1.36 (C<sub>27</sub>H, C<sub>33</sub>H, C<sub>39</sub>H, C<sub>45</sub>H, m, 8H), 1.36 – 1.29 (C<sub>28</sub>H, C<sub>29</sub>H, C<sub>34</sub>H, C<sub>35</sub>H, C<sub>40</sub>H, C<sub>41</sub>H, C<sub>46</sub>H, C<sub>47</sub>H, m, 16H), 0.91 – 0.87 (C<sub>30</sub>H, C<sub>36</sub>H, C<sub>42</sub>H, C<sub>48</sub>H, m, 12H). <sup>13</sup>C NMR (150 MHz, CDCl<sub>3</sub>) δ (ppm): 140.6 (C<sub>10</sub>, C<sub>15</sub>), 140.0 (C<sub>3</sub>, C<sub>22</sub>), 136.3, 136.0 (C<sub>5</sub>, C<sub>8</sub>, C<sub>17</sub>, C<sub>20</sub>), 130.6 (C<sub>4</sub>, C<sub>21</sub>), 130.3 (C<sub>2</sub>, C<sub>23</sub>), 129.7 (C<sub>9</sub>, C<sub>16</sub>), 126.7 (C<sub>11</sub>, C<sub>14</sub>), 126.4, 126.1 (C<sub>6</sub>, C<sub>7</sub>, C<sub>18</sub>, C<sub>19</sub>), 124.0 (C<sub>1</sub>, C<sub>24</sub>), 31.9, 22.9 (C<sub>28</sub>, C<sub>29</sub>, C<sub>34</sub>, C<sub>35</sub>, C<sub>40</sub>, C<sub>41</sub>, C<sub>46</sub>, C<sub>47</sub>), 30.9, 30.7 (C<sub>26</sub>, C<sub>32</sub>, C<sub>38</sub>, C<sub>44</sub>), 29.8, 29.6, 29.5 (C<sub>25</sub>, C<sub>27</sub>, C<sub>31</sub>, C<sub>32</sub>, C<sub>37</sub>, C<sub>39</sub>, C<sub>43</sub>, C<sub>45</sub>), 14.3 (C<sub>30</sub>, C<sub>36</sub>, C<sub>42</sub>, C<sub>48</sub>). (Assigned with COSY, HSQC and HMBC). MALDI-TOF MS: calcd for [M•<sup>+</sup>]/z, 830.3, found 830.2 ([M•<sup>+</sup>]/z). High-resolution MALDI-FTICR MS: calcd mass 830.3170, actual mass 830.3169.

## 5-Bromo-3,3'',3''',4''-tetrahexyl-2,2':5',2'':5'',2''':5''',2''''-sexithiophene

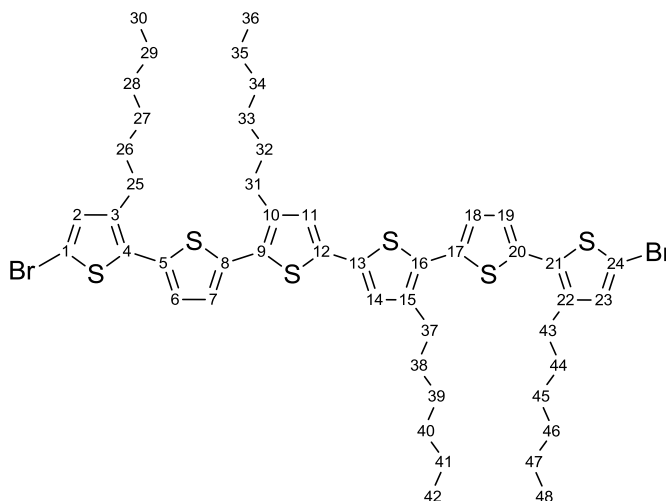
### (BrH4T6)



A solution of N-bromosuccinimide (0.73 g, 4.10 mmol) in THF/DMF (1:1, 20 mL) was added slowly to H4T6 (3.10 g, 3.73 mmol) in THF/DMF (1:1, 100 mL) at -20 °C over 1 h. The mixture was kept out of light and stirred for another 5 h at -20 °C. Then it was allowed to warm up to room temperature and the reaction was carried out for 40 h. Et<sub>2</sub>O (200 mL) was added and the organic layer was washed with a plenty of water and brine, dried over anhydrous Na<sub>2</sub>SO<sub>4</sub>, filtered and evaporated. The residue was purified by column chromatography on silica gel (0-3% CH<sub>2</sub>Cl<sub>2</sub>/hexanes) to give BrH4T6 (1.79 g, 53%) as an orange solid, Br<sub>2</sub>H4T6 (0.93 g, 25%), and H4T6 (0.58 g, 19%). R<sub>f</sub> = 0.41 (SiO<sub>2</sub>, 5% CH<sub>2</sub>Cl<sub>2</sub>/hexanes). M.p. = 67.5-68.5 °C. <sup>1</sup>H NMR (600 MHz, CDCl<sub>3</sub>) δ (ppm): 7.18 (C<sub>1</sub>H, d, <sup>3</sup>J = 5.3 Hz, 1H), 7.09 – 7.00 (C<sub>6</sub>H, C<sub>7</sub>H, C<sub>11</sub>H, C<sub>14</sub>H, C<sub>18</sub>H, C<sub>19</sub>H, m, 6H), 6.95 (C<sub>2</sub>H, d, <sup>3</sup>J = 5.3 Hz, 1H), 6.91 (C<sub>23</sub>H, s, 1H), 2.81 – 2.70 (C<sub>25</sub>H, C<sub>31</sub>H, C<sub>37</sub>H, C<sub>43</sub>H,

m, 8H), 1.72 – 1.59 (C<sub>26</sub>H, C<sub>32</sub>H, C<sub>38</sub>H, C<sub>44</sub>H, m, 8H), 1.45 – 1.36 (C<sub>27</sub>H, C<sub>33</sub>H, C<sub>39</sub>H, C<sub>45</sub>H, m, 8H), 1.36 – 1.28 (C<sub>28</sub>H, C<sub>29</sub>H, C<sub>34</sub>H, C<sub>35</sub>H, C<sub>40</sub>H, C<sub>41</sub>H, C<sub>46</sub>H, C<sub>47</sub>H, m, 16H), 0.91 – 0.87 (C<sub>30</sub>H, C<sub>36</sub>H, C<sub>42</sub>H, C<sub>48</sub>H, m, 12H). <sup>13</sup>C NMR (150 MHz, CDCl<sub>3</sub>) δ (ppm): 140.8, 140.6, 140.5 (C<sub>10</sub>, C<sub>15</sub>, C<sub>22</sub>), 140.0 (C<sub>3</sub>), 136.5, 136.3, 135.8, 135.2, 134.9, 134.8 (C<sub>5</sub>, C<sub>8</sub>, C<sub>12</sub>, C<sub>13</sub>, C<sub>17</sub>, C<sub>20</sub>), 132.9 (C<sub>23</sub>), 132.0, 130.5, 129.8, 129.3 (C<sub>4</sub>, C<sub>9</sub>, C<sub>16</sub>, C<sub>21</sub>), 130.3 (C<sub>2</sub>), 126.8, 126.7, 126.3, 126.0 (C<sub>6</sub>, C<sub>7</sub>, C<sub>11</sub>, C<sub>14</sub>, C<sub>18</sub>, C<sub>19</sub>), 124.0 (C<sub>1</sub>), 110.7 (C<sub>24</sub>), 31.8, 22.8 (C<sub>28</sub>, C<sub>29</sub>, C<sub>34</sub>, C<sub>35</sub>, C<sub>40</sub>, C<sub>41</sub>, C<sub>46</sub>, C<sub>47</sub>), 30.9, 30.7 (C<sub>26</sub>, C<sub>32</sub>, C<sub>38</sub>, C<sub>44</sub>), 29.9, 29.7, 29.5, 29.4, 29.3 (C<sub>25</sub>, C<sub>27</sub>, C<sub>31</sub>, C<sub>32</sub>, C<sub>37</sub>, C<sub>39</sub>, C<sub>43</sub>, C<sub>45</sub>), 14.2 (C<sub>30</sub>, C<sub>36</sub>, C<sub>42</sub>, C<sub>48</sub>). (Assigned with COSY, HSQC and HMBC). High-resolution MALDI-FTICR MS: calcd mass 908.2275, actual mass 908.2283.

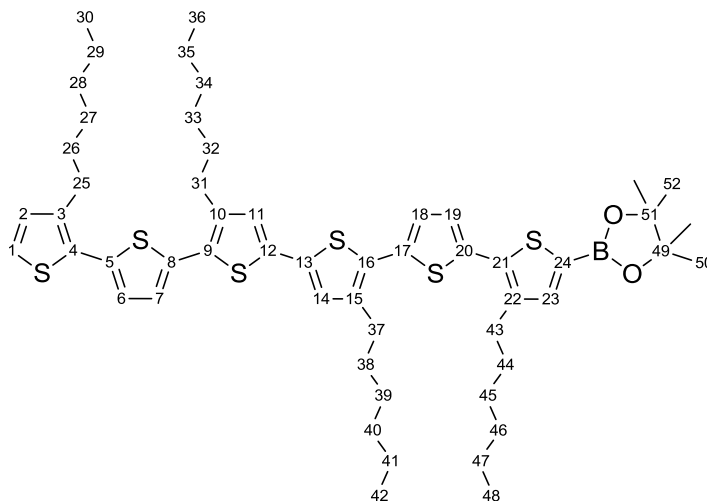
**5,5''''-dibromo-3,3''',3''''',4''''-tetrahexyl-2,2':5',2'':5'',2''':5''',2''''':5''''',2''''''-sexithio  
phene (Br2H4T6)**



Br2H4T6 (0.93 g, 25%) was isolated as an orange solid.  $R_f = 0.53$  (SiO<sub>2</sub>, 5% CH<sub>2</sub>Cl<sub>2</sub>/hexanes). M.p. = 98.0-99.5 °C. <sup>1</sup>H NMR (600 MHz, CDCl<sub>3</sub>)  $\delta$  (ppm): 7.06 (C<sub>6</sub>H, C<sub>19</sub>H, d, <sup>3</sup>J = 4.1 Hz, 2H), 7.02 – 6.99 (C<sub>7</sub>H, C<sub>11</sub>H, C<sub>14</sub>H, C<sub>18</sub>H, m, 4H), 6.91 (C<sub>2</sub>H, C<sub>23</sub>H, s, 2H), 2.77 – 2.70 (C<sub>25</sub>H, C<sub>31</sub>H, C<sub>37</sub>H, C<sub>43</sub>H, m, 8H), 1.71 – 1.59 (C<sub>26</sub>H, C<sub>32</sub>H, C<sub>38</sub>H, C<sub>44</sub>H, m, 8H), 1.44 – 1.34 (C<sub>27</sub>H, C<sub>33</sub>H, C<sub>39</sub>H, C<sub>45</sub>H, m, 8H), 1.34 – 1.28 (C<sub>28</sub>H, C<sub>29</sub>H, C<sub>34</sub>H, C<sub>35</sub>H, C<sub>40</sub>H, C<sub>41</sub>H, C<sub>46</sub>H, C<sub>47</sub>H, m, 16H), 0.91 – 0.87 (C<sub>30</sub>H, C<sub>36</sub>H, C<sub>42</sub>H, C<sub>48</sub>H, m, 12H). <sup>13</sup>C NMR (150 MHz, CDCl<sub>3</sub>)  $\delta$  (ppm): 140.8, 140.5 (C<sub>3</sub>, C<sub>10</sub>, C<sub>15</sub>, C<sub>22</sub>), 136.4, 135.1, 134.8 (C<sub>5</sub>, C<sub>8</sub>, C<sub>12</sub>, C<sub>13</sub>, C<sub>17</sub>, C<sub>20</sub>), 132.9 (C<sub>3</sub>, C<sub>23</sub>), 132.0, 129.4 (C<sub>4</sub>, C<sub>9</sub>, C<sub>16</sub>, C<sub>21</sub>), 126.8, 126.7, 126.0 (C<sub>6</sub>, C<sub>7</sub>, C<sub>11</sub>, C<sub>14</sub>, C<sub>18</sub>, C<sub>19</sub>), 110.7 (C<sub>1</sub>, C<sub>24</sub>), 31.8, 22.8 (C<sub>28</sub>, C<sub>29</sub>, C<sub>34</sub>, C<sub>35</sub>, C<sub>40</sub>, C<sub>41</sub>, C<sub>46</sub>, C<sub>47</sub>), 30.7 (C<sub>26</sub>, C<sub>32</sub>, C<sub>38</sub>, C<sub>44</sub>), 29.7, 29.4, 29.3 (C<sub>25</sub>, C<sub>27</sub>, C<sub>31</sub>, C<sub>32</sub>, C<sub>37</sub>, C<sub>39</sub>, C<sub>43</sub>, C<sub>45</sub>), 14.2 (C<sub>30</sub>, C<sub>36</sub>, C<sub>42</sub>, C<sub>48</sub>). (Assigned with COSY and HSQC).

High-resolution MALDI-FTICR MS: calcd mass 986.1381, actual mass 986.1386.

**4,4,5,5-Tetramethyl-2-(3,3'',3''',4''-tetrahexyl-[2,2':5',2'':5'',2''':5''',2''':5''',2''''-s  
exithiophen]-5-yl)-1,3,2-dioxaborolane (BpinH4T6)**



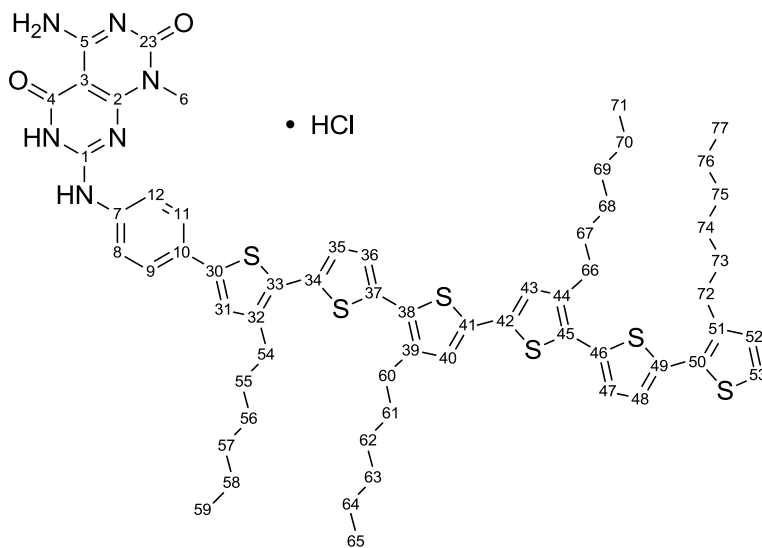
A mixture of BrH4T6 (1.79 g, 1.99 mmol), bis(pinacolato)diboron (1.01 mg, 3.98 mmol), potassium acetate (586 mg, 5.97 mmol) and Pd(PPh<sub>3</sub>)<sub>4</sub> (5 mol%, 115 mg, 0.10 mmol) in toluene (30 mL) was bubbled with nitrogen gas for 30 min and heated to reflux for 3.5 h. The mixture was cooled to room temperature and diluted with Et<sub>2</sub>O (100 mL). The organic layer was filtered, washed with water and brine, dried over anhydrous Na<sub>2</sub>SO<sub>4</sub>, filtered and evaporated to provide the crude BpinH4T6 (~1.99 mmol) as a red oil. This material was used in the next step without further purification. R<sub>f</sub> = 0.36 (SiO<sub>2</sub>, 30% CH<sub>2</sub>Cl<sub>2</sub>/hexanes). <sup>1</sup>H NMR (600 MHz, CDCl<sub>3</sub>) δ (ppm): 7.47 (C<sub>23</sub>H, s, 1H), 7.18 (C<sub>1</sub>H, d, <sup>3</sup>J = 4.7 Hz, 1H), 7.12 (C<sub>19</sub>H, d, <sup>3</sup>J = 3.5 Hz, 1H), 7.09 – 7.06 (C<sub>6</sub>H, C<sub>7</sub>H, C<sub>18</sub>H, m, 3H),



allowed to stir at room temperature for 48 h. The mixture was diluted with Et<sub>2</sub>O (50 mL) and filtered. The organic layer was washed with water and brine, dried over anhydrous Na<sub>2</sub>SO<sub>4</sub>, filtered and evaporated. The residue was purified by column chromatography on silica gel (10-20% THF/hexanes) to give GCH4T6 (1.06 mg, 72%) as a yellow oil. R<sub>f</sub> = 0.44 (SiO<sub>2</sub>, 30% THF/hexanes). <sup>1</sup>H NMR (600 MHz, CD<sub>2</sub>Cl<sub>2</sub>) δ (ppm): 7.69 (C<sub>8</sub>H, C<sub>12</sub>H, d, <sup>3</sup>J = 8.2 Hz, 2H), 7.31 – 7.27 (C<sub>16</sub>H, C<sub>17</sub>H, C<sub>18</sub>H, C<sub>31</sub>H, m, 4H), 7.24 (C<sub>9</sub>H, C<sub>11</sub>H, d, <sup>3</sup>J = 8.2 Hz, 2H), 7.22 – 7.18 (C<sub>15</sub>H, C<sub>19</sub>H, C<sub>53</sub>H, m, 3H), 7.16 (C<sub>35</sub>H, d, <sup>3</sup>J = 3.5 Hz, 1H), 7.14 (C<sub>36</sub>H, d, <sup>3</sup>J = 3.5 Hz, 1H), 7.11 (C<sub>47</sub>H, d, <sup>3</sup>J = 4.1 Hz, 1H), 7.09 (C<sub>48</sub>H, d, <sup>3</sup>J = 4.1 Hz, 1H), 7.06 (C<sub>40</sub>H, C<sub>43</sub>H, s, 2H), 6.97 (C<sub>52</sub>H, d, <sup>3</sup>J = 4.7 Hz, 1H), 5.33 (C<sub>13</sub>H, s, 2H), 3.55 (C<sub>6</sub>H, s, 3H), 2.87 – 2.77 (C<sub>54</sub>H, C<sub>60</sub>H, C<sub>66</sub>H, C<sub>72</sub>H, m, 8H), 1.76 – 1.62 (C<sub>55</sub>H, C<sub>61</sub>H, C<sub>67</sub>H, C<sub>73</sub>H, m, 8H), 1.52 (C<sub>22</sub>H, s, 9H), 1.48 – 1.29 (C<sub>26</sub>H, C<sub>29</sub>H, C<sub>56</sub>H, C<sub>57</sub>H, C<sub>58</sub>H, C<sub>62</sub>H, C<sub>63</sub>H, C<sub>64</sub>H, C<sub>68</sub>H, C<sub>69</sub>H, C<sub>70</sub>H, C<sub>74</sub>H, C<sub>75</sub>H, C<sub>76</sub>H, m, 42H), 0.93 – 0.87 (C<sub>59</sub>H, C<sub>65</sub>H, C<sub>71</sub>H, C<sub>77</sub>H, m, 12H). <sup>13</sup>C NMR (150 MHz, CD<sub>2</sub>Cl<sub>2</sub>) δ (ppm): 166.2 (C<sub>4</sub>), 161.8 (C<sub>2</sub>), 161.5, 160.6 (C<sub>1</sub>, C<sub>5</sub>), 156.2 (C<sub>23</sub>), 152.4 (C<sub>20</sub>), 149.8 (C<sub>24</sub>, C<sub>27</sub>), 141.5 (C<sub>32</sub>), 141.2 (C<sub>10</sub>), 141.2, 141.1 (C<sub>39</sub>, C<sub>44</sub>), 140.4 (C<sub>51</sub>), 140.0 (C<sub>7</sub>), 136.6, 136.3, 136.2, 136.0 (C<sub>34</sub>, C<sub>37</sub>, C<sub>46</sub>, C<sub>49</sub>), 135.4 (C<sub>14</sub>), 135.2, 135.1 (C<sub>41</sub>, C<sub>42</sub>), 133.7 (C<sub>30</sub>), 130.8 (C<sub>33</sub>), 130.7 (C<sub>52</sub>), 130.6 (C<sub>50</sub>), 129.9, 129.8 (C<sub>38</sub>, C<sub>45</sub>), 129.1 (C<sub>9</sub>, C<sub>11</sub>), 128.9, 128.8 (C<sub>15</sub> – C<sub>19</sub>), 127.3 (C<sub>31</sub>), 127.1 (C<sub>40</sub>, C<sub>43</sub>), 126.6, 126.5, 126.4 (C<sub>35</sub>, C<sub>36</sub>, C<sub>47</sub>, C<sub>48</sub>), 126.3 (C<sub>8</sub>, C<sub>12</sub>), 124.3 (C<sub>53</sub>), 93.7 (C<sub>3</sub>), 84.1, 83.8 (C<sub>21</sub>, C<sub>25</sub>, C<sub>28</sub>), 70.3 (C<sub>13</sub>), 32.1, 23.1 (C<sub>57</sub>, C<sub>58</sub>, C<sub>63</sub>, C<sub>64</sub>, C<sub>69</sub>, C<sub>70</sub>, C<sub>75</sub>, C<sub>76</sub>),

31.1, 31.0, 30.9 (C<sub>55</sub>, C<sub>61</sub>, C<sub>67</sub>, C<sub>73</sub>), 30.4 (C<sub>6</sub>), 30.0, 29.9, 29.7 (C<sub>54</sub>, C<sub>56</sub>, C<sub>60</sub>, C<sub>62</sub>, C<sub>66</sub>, C<sub>68</sub>, C<sub>72</sub>, C<sub>74</sub>), 28.1, 28.0 (C<sub>22</sub>, C<sub>26</sub>, C<sub>29</sub>), 14.3 (C<sub>59</sub>, C<sub>65</sub>, C<sub>71</sub>, C<sub>77</sub>). (Assigned with COSY, HSQC and HMBC). MALDI-TOF MS: calcd for [M<sup>•+</sup>]/z, 1502.6, found 1503.2 ([M<sup>•+</sup>]/z). High-resolution MALDI-FTICR MS: calcd mass 1502.6078, actual mass 1502.6058.

**4-amino-1-methyl-7-((4-(3,3'',3''',4''-tetrahexyl-[2,2':5',2'':5'',2''':5''',2''':5''',2''''':5''''',2''''''-sexithiophen]-5-yl)phenyl)amino)pyrimido[4,5-*d*]pyrimidine-2,5(1*H*,6*H*)-dione hydrochloride (GCH4T6HCl)**



GCH4T6 (96 mg, 0.064 mmol) was dissolved in 4 M HCl/dioxane (12 mL) and heated to reflux for 6 h. Et<sub>2</sub>O (10 mL) was then added and the precipitate formed was centrifuged down. The residual solid was suspended in Et<sub>2</sub>O (10 mL), sonicated and centrifuged down. This process was repeated three times before the solid was dried under vacuo for

48 h to give 71 mg of GCH4T6HCl ( $C_{61}H_{72.5}Cl_{0.5}N_6O_2S_6$ , 98%) as a yellow solid.  $^1H$  NMR (600 MHz,  $d$ -TFA: $d_6$ -DMF (2:5))  $\delta$  (ppm): 7.79 ( $C_8H$ ,  $C_9H$ ,  $C_{11}H$ ,  $C_{12}H$ , bs, 4H), 7.51 ( $C_{31}H$ , s, 1H), 7.32 ( $C_{35}H$ ,  $C_{36}H$ , d,  $^3J = 2.9$  Hz, 2H), 7.29 ( $C_{40}H$ ,  $C_{43}H$ , bs, 2H), 7.26 ( $C_{47}H$ , d,  $^3J = 3.5$  Hz, 1H), 7.21 ( $C_{48}H$ , d,  $^3J = 4.1$  Hz, 1H),  $C_{53}H$  (deuterated by  $d$ -TFA), 7.06 ( $C_{52}H$ , s, 1H), 3.53 ( $C_6H$ , s, 3H), 2.88 – 2.80 ( $C_{54}H$ ,  $C_{60}H$ ,  $C_{66}H$ ,  $C_{72}H$ , m, 8H), 1.76 – 1.62 ( $C_{55}H$ ,  $C_{61}H$ ,  $C_{67}H$ ,  $C_{73}H$ , m, 8H), 1.46 – 1.24 ( $C_{56}H$ ,  $C_{57}H$ ,  $C_{58}H$ ,  $C_{62}H$ ,  $C_{63}H$ ,  $C_{64}H$ ,  $C_{68}H$ ,  $C_{69}H$ ,  $C_{70}H$ ,  $C_{74}H$ ,  $C_{75}H$ ,  $C_{76}H$ , m, 24H), 0.90 – 0.84 ( $C_{59}H$ ,  $C_{65}H$ ,  $C_{71}H$ ,  $C_{77}H$ , m, 12H). Due to the poor solubility, some carbons were not recorded and some were covered by the solvent peaks.  $^{13}C$  NMR (150 MHz,  $d$ -TFA/  $d_6$ -DMF (2:5))  $\delta$  (ppm): 161.4, 156.8, 148.5 ( $C_1$ ,  $C_2$ ,  $C_4$ ,  $C_5$ ,  $C_{23}$ ), 141.6, 141.4, 141.3, 141.2, 140.3 ( $C_7$ ,  $C_{10}$ ,  $C_{32}$ ,  $C_{39}$ ,  $C_{44}$ ,  $C_{51}$ ), 136.4, 136.1, 135.5, 135.4, 134.9, 134.8 ( $C_{30}$ ,  $C_{34}$ ,  $C_{37}$ ,  $C_{41}$ ,  $C_{42}$ ,  $C_{46}$ ,  $C_{49}$ ), 130.9, 130.0, 129.6, 127.7, 126.8, 126.1, 125.0 ( $C_8$ ,  $C_9$ ,  $C_{11}$ ,  $C_{12}$ ,  $C_{31}$ ,  $C_{33}$ ,  $C_{35}$ ,  $C_{36}$ ,  $C_{38}$ ,  $C_{40}$ ,  $C_{43}$ ,  $C_{45}$ ,  $C_{47}$ ,  $C_{48}$ ,  $C_{50}$ ,  $C_{52}$ ,  $C_{53}$ ), 31.8, 22.7 ( $C_{57}$ ,  $C_{58}$ ,  $C_{63}$ ,  $C_{64}$ ,  $C_{69}$ ,  $C_{70}$ ,  $C_{75}$ ,  $C_{76}$ ), 30.6, 30.4 ( $C_6$ ,  $C_{54}$ ,  $C_{55}$ ,  $C_{56}$ ,  $C_{60}$ ,  $C_{61}$ ,  $C_{62}$ ,  $C_{66}$ ,  $C_{67}$ ,  $C_{68}$ ,  $C_{72}$ ,  $C_{73}$ ,  $C_{74}$ ), 13.8 ( $C_{59}$ ,  $C_{65}$ ,  $C_{71}$ ,  $C_{77}$ ). Anal. calcd for  $C_{61}H_{72.5}Cl_{0.5}N_6O_2S_6$  ( $M + 0.5HCl$ ): C, 64.73; H, 6.47; N, 7.43; S, 16.99. Found: C, 64.43; H, 6.37; N, 7.20; S, 17.32. Positive ESI-MS: calcd for  $[M + H^+]/z$ , 1113.4, found 1113.5 ( $[M + H^+]/z$ ). High-resolution MALDI-FTICR MS: calcd mass 1112.4036, actual mass 1112.4042.

### 3.6. References

1. Mitschke, U.; Bäuerle, P. *J. Mater. Chem.* **2000**, *10*, 1471-1507.
2. Würthner, F. *Angew. Chem., Int. Ed.* **2001**, *40*, 1037-1039.
3. Hoppe, H.; Sariciftci, N. S. *J. Mater. Res.* **2004**, *19*, 1924-1945.
4. (a) Sirringhaus, H.; Brown, P. J.; Friend, R. H.; Nielsen, M. M.; Bechgaard, K.; Langeveld-Voss, B. M. W.; Spiering, A. J. H.; Janssen, R. A. J.; Meijer, E. W.; Herwig, P.; deLeeuw, D. M. *Nature* **1999**, *401*, 685-688. (b) Hoofman, R. J. O. M.; de Haas, M.; Siebbeles L. D. A.; Warmann, J. M. *Nature* **1998**, *392*, 54-56.
5. (a) Lehn, J. M. *Angew. Chem., Int. Ed.* **1988**, *27*, 89-112. (b) Lehn, J. M. *Angew. Chem., Int. Ed.* **1990**, *29*, 1304-1319. (c) Whitesides, G. M.; Mathias, J. P.; Seto, C. T. *Science* **1991**, *254*, 1312-1319. (d) Lehn, J. M. *Science* **2002**, *295*, 2400-2403. (e) Whitesides, G. M.; Grzybowski, B. *Science* **2002**, *295*, 2418-2421.
6. Jatsch, A.; Schillinger, E. K.; Schmid, S.; Bäuerle, P. *J. Mater. Chem.* **2010**, *20*, 3563-3578.
7. (a) Bäuerle, P.; Emge, A. *Adv. Mater.* **1998**, *10*, 324-330. (b) Jatsch, A.; Kopyshov, A.; Mena-Osteritz, E.; Bäuerle, P. *Org. Lett.* **2008**, *10*, 961-964.
8. (a) Diegelmann, S.; Gorham, J.; Tovar, J. *J. Am. Chem. Soc.* **2008**, *130*, 13840-13841. (b) Klok, H. A.; Rösler, A.; Götz, G.; Mena-Osteritz, E.; Bäuerle, P.

- Org. Biomol. Chem.* **2004**, *2*, 3541-3544. (c) Schillinger, E. K.; Mena-Osteritz, E.; Hentschel, J.; Börner, H.; Bäuerle, P. *Adv. Mater.* **2009**, *21*, 1562-1567.
9. Schmid, S.; Mena-Osteritz, E.; Kopyshev, A.; Bäuerle, P. *Org. Lett.* **2009**, *11*, 5098-5101.
10. (a) Tikhomirov, G.; Oderinde, M.; Makeiff, D.; Mansoui, A.; Lu, W.; Heirtzler, F.; Kwok, D. Y.; Fenniri, H. *J. Org. Chem.* **2008**, *73*, 4248-4251. (b) Tikhomirov, G.; Yamazaki, T.; Kovalenko, A.; Fenniri, H. *Langmuir* **2008**, *24*, 4447-4450. (c) Durmus, A.; Gunbas, G.; Farmer, S. C.; Olmstead, M. M.; Mascal, M.; Legese, B.; Cho, J. Y.; Beingsner, R. L.; Yamazaki, T.; Fenniri, H. *J. Org. Chem.* **2013**, *78*, 11421-11426.
11. Sirringhaus, H.; Tessler, N.; Friend, R. H. *Science* **1998**, *280*, 1741-1744.
12. Henderson, P. T.; Collard, D. M. *Chem. Mater.* **1996**, *7*, 1879-1889.
13. Beingsner, R. L.; Deng, B. L.; Fanwick, P. E.; Fenniri, H. *J. Org. Chem.* **2008**, *73*, 931-939.
14. (a) Kanato, H.; Takimiya, K.; Otsubo, T.; Aso, Y.; Nakamura, T.; Araki, Y.; Ito, O. *J. Org. Chem.* **2004**, *69*, 7183-7189. (b) Saravanan, C.; Liu, C. L.; Chang, Y. M.; Lu, J. D.; Hsieh, Y. J.; Rwei, S. P.; Wang, S. P. *ACS Appl. Mater. Interfaces* **2012**, *4*, 6133-6141.

15. Destri, S.; Ferro, D. R.; Khotina, I. A.; Porzio, W.; Farina, A. *macromol. Chem. Phys.* **1998**, *199*, 1973-1979.
16. Ishiyama, T.; Murata, M.; Miyaura, N. *J. Org. Chem.* **1995**, *60*, 7508-7510.
17. Koch, F. P. V.; Smith, P.; Heeney, M. *J. Am. Chem. Soc.* **2013**, *135*, 13695-13698.
18. (a) Fenniri, H.; Mathivanan, P.; Vidale, K. L.; Sherman, D. M.; Hallenga, K.; Wood, K. V.; Stowell, J. G. *J. Am. Chem. Soc.* **2001**, *123*, 3854-3855. (b) Moralez, J. G.; Ruez, J.; Yamazaki, T.; Motkuri, R. K.; Kovalenko, A.; Fenniri, H. *J. Am. Chem. Soc.* **2005**, *127*, 8307-8309. (c) Johnson, R. S.; Yamazaki, T.; Kovalenko, A.; Fenniri, H. *J. Am. Chem. Soc.* **2007**, *129*, 5735-5743.
19. Zotti, G.; Zecchin, S.; Vercelli, B. *Chem. Mater.* **2006**, *18*, 3151-3161.
20. Tinoco, I. J. *J. Am. Chem. Soc.* **1960**, *82*, 4875-4790.
21. Rhodes, W. *J. Am. Chem. Soc.* **1961**, *55*, 3609-3617.
22. Borzsonyi, G.; Beingessner, R. L.; Yamazaki, T.; Cho, J. Y.; Myles, A. J.; Malac, M.; Egerton, R.; Kawasaki, M.; Ishizuka, K.; Kovalenko, A.; Fenniri, H. *J. Am. Chem. Soc.* **2010**, *132*, 15136-15139.
23. (a) Tsai, W. W.; Tevis, I. D.; Tayi, A. S.; Cui, H.; Stupp, S. I. *J. Phys. Chem. B* **2010**, *114*, 14778-14786. (b) Kreyes, A.; Amirkhani, M.; Lieberwirth, I.; Mauer, R.; Laquai, F.; Landfester, K.; Ziener, U. *Chem. Mater.* **2010**, *22*, 6453-6458.

24. Kiriya, N.; Jähne, E.; Adler, H. J.; Schneider, M.; Kiriya, A.; Gorodyska, G.; Minko, S.; Jehnichen, D.; Simon, P.; Fokin, A. A.; Stamm, M. *Nano. Lett.* **2003**, *3*, 707-712.
25. Hager, M. D.; Greil, P.; Leyens, C.; van der Zwaag, S.; Schubert, U. S. *Adv. Mater.* **2010**, *22*, 5424-5430.
26. (a) Muir, T.; Morales, E.; Root, J.; Kumar, I.; Garcia, B.; Vellandi, C.; Jenigian, D.; Marsh, T.; Henderson, E.; Vesenska, J. *J. Vac. Sci. Technol. A* **1998**, *16*, 1172-1177.
- (b) DeRose, J. A.; Revel, J. P. *Thin Solid Films* **1998**, *331*, 194-202. (c) Kasumov, A. Y.; Klinov, D. V.; Roche, P. E.; Gueron, S.; Bouchiat, H. *Appl. Phys. Lett.* **2004**, *84*, 1007-1009.

## Chapter 4

### Summary of this thesis work and outlook

#### 4.1. Summary of this thesis work

Rosette nanotubes (RNTs) are a class of self-assembled organic materials with highly ordered nanostructures. The self-assembling unit of the RNTs is the G<sup>^</sup>C base and it can be readily functionalized through organic reactions. These properties of the RNTs make them an excellent candidate to construct an ordered matrix of organic electronic materials, which, as discussed previously, is essential for the performance of organic electronic devices. But the potential application of RNTs in this field is unexplored. My thesis demonstrates a new method to functionalize G<sup>^</sup>C bases with semiconducting and electroluminescent oligothiophenes, and explores their self-assembly into RNTs for organic electronic applications.

Organic electronic materials such as oligothiophenes are composed of  $\pi$ -conjugated aromatic moieties. As the initial attempts to utilize RNTs in electronic applications, a series of aromatic functionalized G<sup>^</sup>C bases were synthesized in order to prepare aromatic functionalized RNTs. To confirm the identity and purity of the newly synthesized G<sup>^</sup>C bases, NMR spectra had to be obtained. However, this proved to be

challenging as the G $\wedge$ C bases were not soluble in common NMR solvents such as *d*<sub>6</sub>-benzene, *d*-chloroform, *d*<sub>6</sub>-acetone, *d*<sub>4</sub>-methanol and *d*<sub>6</sub>-DMSO. They were soluble in *d*-TFA but underwent an acid-catalyzed keto-enol tautomerization, which complicated the NMR spectra and peak assignments. This problem was solved by adding *d*<sub>6</sub>-DMSO to prevent the tautomerization. Using a mixture of *d*-TFA:*d*<sub>6</sub>-DMSO (2:5), <sup>1</sup>H and <sup>13</sup>C NMR spectra with enhanced-resolution were obtained. High-resolution mass and combustion data were also obtained for the characterization. These results proved the identity and purity of these aromatic functionalized G $\wedge$ C bases. Then the self-assembly of these G $\wedge$ C bases were explored using SEM. They were found to readily self-assemble into nanotubes in methanol. However, the shape of the nanotubes was not regular probably due their poor solubility in MeOH. To address this problem, the G $\wedge$ C bases can be functionalized with hydrophilic groups *e.g.* amino acids. The G $\wedge$ C bases can also be functionalized with alkyl chains substituted with hydrophobic groups that will improve their solubility in nonpolar solvents such as hexane and chloroform.

Next, using Suzuki-Miyaura coupling reactions, G $\wedge$ C bases were functionalized with oligothiophenes, which have semiconducting and electroluminescent properties. Ter- and sexithiophenes were used in this thesis. The thiophene backbones were substituted with alkyl chains to promote the solubility of the resulting oligothiophene functionalized G $\wedge$ C

bases in nonpolar solvents. Nonpolar solvents such as DCM, 1,2-DCE, and CB have been widely used for the fabrication of organic electronic devices. In these solvents, GAC bases readily self-assembled into well-defined RNTs as visualized by SEM. TEM and AFM were also used to visualize and measure the RNTs. Furthermore these RNTs were stable in solution upon aging and heating. These results reveal the capability of RNT as a scaffold to control the organization of  $\pi$ -conjugated organic semiconductors such as oligothiophenes at the nanoscale level. These highly ordered oligothiophene nanomaterials have potential applications in organic electronic devices because the performance of those devices strongly depends on the ordering effects as discussed previously.

## **4.2. Outlook**

The future work will be focused on computer simulation studies of the oligothiophene functionalized RNTs and determining important electronic properties such as charge carrier mobility, conductivity, and energy levels of these materials. Sufficient protected ter- and sexithiophene functionalized GAC bases (> 2 g for each compound) have been synthesized for these future studies.

Molecular modeling will be carried out for the oligothiophene functionalized RNTs to

further understand the orientation and packing of oligothiophene groups on the surface of the RNTs. The diameter of the RNTs can be calculated by modeling. It will provide more evidence to prove the formation of RNTs if the calculated values are comparable to the experimental values measured by TEM and AFM. Modeling can also be used to calculate the intermolecular  $\pi$ - $\pi$  distance, which is an important parameter for electronic communication among the chromophores. Many researchers have used molecular modeling to simulate and compute self-assembled nanomaterials composed of semiconducting oligomers.<sup>1</sup> For example, Börner, Bäuerle, and Khokhlov Groups collaborated on computer simulation studies of self-assembled nanofibers of thiophene-peptide diblock oligomers using an all-atom molecular model.<sup>2</sup> They studied possible intermolecular arrangements and characteristic features of the nanofibers. Our group investigated the thermodynamically stable conformation of RNTs substituted with alkyl chains in nonpolar solvents such as hexane and chloroform, using Macromodel 8.5 with the OPLS-AA force field.<sup>3</sup> These literature examples of molecular modeling provide guidelines for the computer simulations study of the oligothiophene functionalized RNTs.

For organic semiconductor, charge carrier mobility characterizes how quickly charge carriers (*i.e.* electrons and holes) can move in the material. It is a key parameter that

impacts the performance of organic electronic devices. Charge carrier mobility in organic semiconductors can be measured using many different techniques.<sup>4</sup> For example Time of Flight (TOF) is a widely used method for organic semiconductors. In TOF measurements, a thin layer of charge carriers is generated in the sample by a short laser pulse incident. Driven by the applied uniform electric field, the charge carriers move across the sample. The transit time, the thickness of the sample and the applied voltage are measured to calculate the charge carrier mobility. In the Field-Effect Transistor (FET) method, a FET device is fabricated for charge carrier mobility measurements. The conductivity of the FET device is controlled by an applied electric field called the gate voltage. The charge carrier mobility is determined using  $I$ - $V$  curves of the FET device as a function of varying gate voltages. Details of the TOF and FET as well as many other methods can be found in ref. 4.

Conductivity is also an important parameter for organic electronic devices. It is approximately proportional to the charge carrier mobility. Accurate conductivity of the oligothiophene functionalized RNTs can be measured by Conducting Probe Atomic Force Microscopy (CPAFM).<sup>5</sup> In the measurements, a layer of the nanomaterial is probed by a conducting AFM tip. Under variable voltage, an  $I$ - $V$  curve is recorded. The conductivity can be determined using this curve.

HOMO and LUMO energy levels of the oligothiophene functionalized RNTs can be determined by cyclic voltammetry, which generates voltammograms. The voltammograms display oxidation potentials for calculating HOMO levels and reduction potential for calculating LUMO levels.<sup>6</sup>

Moreover, using the functionalization method demonstrated in this thesis, other oligomers such as oligo(*p*-phenylene vinylene) (OPV) can be combined with G<sup>+</sup>C bases to prepare OPV functionalized RNTs for potential organic LED and photovoltaic applications.<sup>7</sup> The OPV functionalized G<sup>+</sup>C bases can be characterized by NMR in the mixture of *d*-TFA:*d*<sub>6</sub>-DMSO (2:5), which in this thesis led to the successful NMR characterization of the aromatic functionalized G<sup>+</sup>C bases.

### 4.3. References

1. Jatsch, A.; Schillinger, E. K.; Schmid, S.; Bäuerle, P. *J. Mater. Chem.* **2010**, *20*, 3563–3578.
2. Shaytan, A. K.; Schillinger, E. K.; Khalatur, P. G.; Mena-Osteritz, E.; Hentschel, J.; Börner, H. G.; Bäuerle, P.; Khokhlov, A. R. *ACS Nano* **2011**, *5*, 6894-6909.
3. Tikhomirov, G.; Yamazaki, T.; Kovalenko, A.; Fenniri, H. *Langmuir* **2008**, *24*, 4447-4450. Behanna, H. A.; Donners, J. J. J. M.; Gordon, A. C.; Stupp, S. I. *J. Am. Chem. Soc.* **2005**, *127*, 1193-1200.
4. Kokil, A.; Yang, K.; Kumar, J. *J. Poly. Sci. Part B: Polymer Physics* **2012**, *50*, 1130-1144.
5. Loiacono, M. J.; Granstrom, E. L.; Frisbie, C. D. *J. Phys. Chem. B* **1998**, *102*, 1679-1688.
6. Tsai, W. W.; Tevis, I. D.; Tayi, A. S.; Cui, H.; Stupp, S. I. *J. Phys. Chem. B* **2010**, *114*, 14778-14786.
7. (a) Iwaura, R.; Hoeben, F. J. M.; Masuda, M.; Schenning, A. P. H. J.; Meijer E. W.; Shimizu, T. *J. Am. Chem. Soc.* **2006**, *128*, 13298-13304. (b) Janssen, P. G. A.; Vandenbergh, J.; van Dongen, J. L. J.; Meijer, E. W.; Schenning, A. P. H. J. *J. Am. Chem. Soc.* **2007**, *129*, 6078-6079. (c) Matmour, R.; De Cat, I.; George, S. J.; Adriaens, Wencke.; Leclere, P.; Bomans, P. H. H.; Sommerdijk, N. A. J. M.; Gielen,

J. C.; Christianen, P. C. M.; Heldens, J. T.; van Hest, J. C. M.; Lowik, D. W. P. M.;  
De Feyter, S.; Meijer, E. W.; Schenning, A. P. H. J. *J. Am. Chem. Soc.* **2008**, *130*,  
14576-14583.

## Bibliography

8. Adrian, M.; Dubochet, J.; Fuller, S. D.; Harris, J. R. *Micron* **1998**, *29*, 145-160.
9. Alemdaroglu, F.; Herrmann, A. *Org. Biomol. Chem.* **2007**, *5*, 1311-1320.
10. Bäuerle, P.; Emge, A. *Adv. Mater.* **1998**, *10*, 324-330.
11. Behanna, H. A.; Donners, J. J. J. M.; Gordon, A. C.; Stupp, S. I. *J. Am. Chem. Soc.* **2005**, *127*, 1193-1200.
12. Beingessner, R. L.; Deng, B. L.; Fanwick, P. E.; Fenniri, H. *J. Org. Chem.* **2008**, *73*, 931-939.
13. Bellina, F.; Carpita, A.; Rossi, R. *Synthesis* **2004**, *15*, 2419- 2440.
14. Berl, V.; Huc, I.; Khoury, R. G.; Krische, M. J.; Lehn, J. M. *Nature*, **2000**, *407*, 720-723.
15. Bhushan, B.; Marti, O. Scanning Probe Microscopy – Principle of Operation, Instrumentation, and Probes. In *Springer Handbook of Nanotechnology*; Bhushan, B., Eds.; Springer: New York, USA, 2004, Chapter 11.
16. Bong, D. T.; Clark, T. D.; Granja, J. R.; Ghadiri, M. R. *Angew. Chem. Int. Ed.* **2001**, *40*, 988-1011.
17. Bonifazi, D.; Maggini, L. *Chem. Soc. Rev.* **2012**, *41*, 211-241. Kim, H. S.; Parquette, J. R. *Nanoscale* **2012**, *4*, 6940-6947.

18. Borzsonyi, G.; Alsbaiee, A.; Beingessner, R. L.; Fenniri, H. *J. Org. Chem.* **2010**, *75*, 7233-7239.
19. Borzsonyi, G.; Beingessner, R. L.; Yamazaki, T.; Cho, J. Y.; Myles, A. J.; Malac, M.; Egerton, R.; Kawasaki, M.; Ishizuka, K.; Kovalenko, A.; Fenniri, H. *J. Am. Chem. Soc.* **2010**, *132*, 15136-15139.
20. Chen, J. H.; Seeman, N. C. *Nature*, **1991**, *350*, 631-633.
21. Chen, Y.; Bilgen, B.; Pareta, R. A.; Myles, A. J.; Fenniri, H.; Ciombor, D. M.; Aaron, R. K.; Webster, T. J. *Tissue Eng.* **2010**, *16*, 1233-1243.
22. Chen, Y.; Song, S.; Yan, Z.; Fenniri, H.; Webster, T. J. *Int. J. Nanomed.* **2011**, *6*, 1035-1044.
23. Chhabra, R.; Moralez, J. G.; Ruez, J.; Yamazaki, T.; Cho, J. Y.; Myles, A. J.; Kovalenko, A.; Fenniri, H. *J. Am. Chem. Soc.* **2010**, *132*, 32-33.
24. Childers, W. S.; Ni, R.; Mehta, A. K.; Lynn, D. G. *Curr. Opin. Chem. Biol.* **2009**, *13*, 652-659.
25. Cousins, B. G.; Das, A. K.; Sharma, R.; Li, Y.; McNamara, J. P.; Hillier, I. H.; Kinloch, I. A.; Ulijn, R. V. *Small*, **2009**, *5*, 587-590.
26. Cram, D. J. *Science* **1988**, *240*, 760-767.
27. Cram, D. J. *Nature* **1992**, *356*, 29-36.
28. Das, A. K.; Collins, R.; Ulijn, R. V. *Small* **2008**, *4*, 279-287.

29. Dehmlow, E. V.; Dehmlow, S. S. *Phase-Transfer Catalysis*, 3rd ed.; VCH: Weinheim, Germany, 1993.
30. Deng, B. L.; Beingessner, R. L.; Johnson, R. S.; Girdhar, N. K.; Danumah, C.; Yamazaki, T.; Fenniri, H. *Macromolecules* **2012**, *45*, 7157-7162.
31. DeRose, J. A.; Revel, J. P. *Thin Solid Films* **1998**, *331*, 194-202.
32. Destri, S.; Ferro, D. R.; Khotina, I. A.; Porzio, W.; Farina, A. *macromol. Chem. Phys.* **1998**, *199*, 1973-1979.
33. Diegelmann, S.; Gorham, J.; Tovar, J. *J. Am. Chem. Soc.* **2008**, *130*, 13840-13841.
34. Durmus, A.; Gunbas, G.; Farmer, S. C.; Olmstead, M. M.; Mascal, M.; Legese, B.; Cho, J. Y.; Beingessner, R. L.; Yamazaki, T.; Fenniri, H. *J. Org. Chem.* **2013**, *78*, 11421-11426.
35. Fenniri, H.; Deng, B. L.; Ribbe, A. E. *J. Am. Chem. Soc.* **2002**, *124*, 11064-11072.
36. Fenniri, H.; Deng, B. L.; Ribbe, A. E.; Hallenga, K.; Jacob, J.; Thiyagarajan, P. *Proc. Natl. Acad. Sci. U.S.A.* **2002**, *99*, 6487-6492.
37. Fenniri, H.; Mathivanan, P.; Vidale, K. L.; Sherman, D. M.; Hallenga, K.; Wood, K. V.; Stowell, J. G. *J. Am. Chem. Soc.* **2001**, *123*, 3854-3855.
38. Gazit, E. *Chem. Soc. Rev.* **2007**, *36*, 1263-1269.
39. Ghadiri, M. R.; Granja, J. R.; Milligan, R. A.; McRee, D. E.; Khazanovich, N. *Nature* **1993**, *366*, 324-327.

40. Grimsdale, A. C.; Müllen, K. *Angew. Chem., Int. Ed.* **2005**, *44*, 5592-5629.
41. Habibi-Khorassani, S. M.; Maghsoodlou, M. T.; Ebrahimi, A.; Sameh-Salari, S.; Vasheghani-Farahani, F.; Kazemian, M. A. *Concepts in Magnetic Resonance, Part A: Bridging Education and Research* **2013**, *42*, 101-107.
42. Hager, M. D.; Greil, P.; Leyens, C.; van der Zwaag, S.; Schubert, U. S. *Adv. Mater.* **2010**, *22*, 5424-5430.
43. Halperin, A.; Tirrell, M.; Lodge, T. *Adv. Polym. Sci.* **1992**, *100*, 31-71.
44. Hansma, H. G.; Revenko, I.; Kim, K.; Laney, D. E. *Nucleic Acids Research* **1996**, *24*, 713-720.
45. Hartgerink, J. D.; Beniash, E.; Stupp, S. I. *Science* **2001**, *294*, 1684-1688.
46. Hartgerink, J. D.; Granja, J. R.; Milligan, R. A.; Ghadiri, M. R. *J. Am. Chem. Soc.* **1996**, *118*, 43-50.
47. Henderson, P. T.; Collard, D. M. *Chem. Mater.* **1996**, *7*, 1879-1889.
48. Hill, J. P.; Jin, W.; Kosaka, A.; Fukushima, T.; Ichihara, H.; Shimomura, T.; Ito, K.; Hashizume, T.; Ishii, N.; Aida, T. *Science* **2004**, *304*, 1481-1483.
49. Hoeben, F. J. M.; Jonkheijm, P.; Meijer, E. W.; Schenning, A. P. H. J. *Chem. Rev.* **2005**, *105*, 1491-1546.
50. Hoofman, R. J. O. M.; de Haas, M.; Siebbeles L. D. A.; Warmann, J. M. *Nature* **1998**, *392*, 54-56.

51. Hoppe, H.; Sariciftci, N. S. *J. Mater. Res.* **2004**, *19*, 1924-1945.
52. [http://www.nobelprize.org/nobel\\_prizes/chemistry/laureates/1987/](http://www.nobelprize.org/nobel_prizes/chemistry/laureates/1987/) (access July 7, 2014).
53. Ikkala, O.; Brinke, G. *Chem. Commun.* **2004**, *19*, 2131-2137.
54. Ishiyama, T.; Murata, M.; Miyaura, N. *J. Org. Chem.* **1995**, *60*, 7508-7510.
55. Iwaura, R.; Hoeben, F. J. M.; Masuda, M.; Schenning, A. P. H. J.; Meijer E. W.; Shimizu, T. *J. Am. Chem. Soc.* **2006**, *128*, 13298-13304.
56. Jackson, C. L.; Chanzy, H. D.; Booy, F. P.; Drake, B. J.; Tomalia, D. A.; Bauer, B. J.; Amis, E. J. *Macromolecules* **1998**, *32*, 6259-6265.
57. Janssen, P. G. A.; Vandenbergh, J.; van Dongen, J. L. J.; Meijer, E. W.; Schenning, A. P. H. J. *J. Am. Chem. Soc.* **2007**, *129*, 6078-6079.
58. Jatsch, A.; Kopyshov, A.; Mena-Osteritz, E.; Bäuerle, P. *Org. Lett.* **2008**, *10*, 961-964.
59. Jatsch, A.; Schillinger, E. K.; Schmid, S.; Bäuerle, P. *J. Mater. Chem.* **2010**, *20*, 3563-3578.
60. Johnson, R. S.; Yamazaki, T.; Kovalenko, A.; Fenniri, H. *J. Am. Chem. Soc.* **2007**, *129*, 5735-5743.
61. Jun, H. W.; Paramonov, S. E.; Dong, H.; Forraz, N.; McGuckin, C.; Hartgerink, J. D. *J. Biomater. Sci. Polym. Ed.* **2008**, *19*, 665-676.

62. Kanato, H.; Takimiya, K.; Otsubo, T.; Aso, Y.; Nakamura, T.; Araki, Y.; Ito, O. *J. Org. Chem.* **2004**, *69*, 7183-7189.
63. Kasumov, A. Y.; Klinov, D. V.; Roche, P. E.; Gueron, S.; Bouchiat, H. *Appl. Phys. Lett.* **2004**, *84*, 1007-1009.
64. Khoe, U.; Yang, Y.; Zhang, S. *Langmuir* **2009**, *25*, 4111-4114.
65. Khoe, U.; Yang, Y.; Zhang, S. *Macromol. Biosci.* **2008**, *8*, 1060-1067.
66. Kim, F. S.; Ren, G.; Jenekhe, S. A. *Chem. Mater.* **2011**, *23*, 682-732.
67. Kiriy, N.; Jähne, E.; Adler, H. J.; Schneider, M.; Kiriy, A.; Gorodyska, G.; Minko, S.; Jehnichen, D.; Simon, P.; Fokin, A. A.; Stamm, M. *Nano. Lett.* **2003**, *3*, 707-712.
68. Klok, H. A.; Rösler, A.; Götz, G.; Mena-Osteritz, E.; Bäuerle, P. *Org. Biomol. Chem.* **2004**, *2*, 3541-3544.
69. Koch, F. P. V.; Smith, P.; Heeney, M. *J. Am. Chem. Soc.* **2013**, *135*, 13695-13698.
70. Kokil, A.; Yang, K.; Kumar, J. *J. Poly. Sci. Part B: Polymer Physics* **2012**, *50*, 1130-1144.
71. Kreyes, A.; Amirkhani, M.; Lieberwirth, I.; Mauer, R.; Laquai, F.; Landfester, K.; Ziener, U. *Chem. Mater.* **2010**, *22*, 6453-6458.
72. Kwak, M.; Herrmann, A. *Chem. Soc. Rev.* **2011**, *40*, 5745-5755.
73. Laromaine, A.; Koh, L.; Murugesan, M.; Ulijn, R. V.; Stevens, M. M. *J. Am. Chem. Soc.* **2007**, *129*, 4156-4157.

74. Laursen, J. S.; Engel-Andreasen, J.; Fristrup, P.; Harris, P.; Olsen, C. A. *J. Am. Chem. Soc.* **2013**, *135*, 2835-2844.
75. Le, M. H. A.; Suri, S. S.; Rakotondradany, F.; Fenniri, H.; Singh, B. *Vet. Res.* **2010**, *41*, 75-86.
76. Lehn, J. M. *Angew. Chem., Int. Ed.* **1988**, *27*, 89-112.
77. Lehn, J. M. *Angew. Chem., Int. Ed.* **1990**, *29*, 1304-1319.
78. Lehn, J. M. *Science* **2002**, *295*, 2400-2403.
79. Lehn, J. M. *Supramolecular Chemistry: Concepts and Perspectives*; John Wiley & Sons: Hoboken, NJ, 1995.
80. Loiacono, M. J.; Granstrom, E. L.; Frisbie, C. D. *J. Phys. Chem. B* **1998**, *102*, 1679-1688.
81. Lowik, D. W. P. M.; van Hest, J. C. M. *Chem. Soc. Rev.* **2004**, *33*, 234-245.
82. Martin-Palma, R. J.; Lakhtakia, A. *Nanotechnology: a crash course*; SPIE Publications: Washington, USA, 2010, Chapter 5.
83. Mathias, J. P.; Simanek, E. E.; Seto, C. T.; Whitesides, G. *Angew. Chem., Int. Ed.* **1993**, *32*, 1766-1769.
84. Matmour, R.; De Cat, I.; George, S. J.; Adriaens, Wencke.; Leclere, P.; Bomans, P. H. H.; Sommerdijk, N. A. J. M.; Gielen, J. C.; Christianen, P. C. M.; Heldens, J. T.;

- van Hest, J. C. M.; Lowik, D. W. P. M.; De Feyter, S.; Meijer, E. W.; Schenning, A. P. H. J. *J. Am. Chem. Soc.* **2008**, *130*, 14576-14583.
85. Meng, X.; Stout, D. A.; Sun, L.; Beingessner, R. L.; Fenniri, H.; Webster, T. J. *J. Biomed. Mater. Res. A* **2010**, *101A*, 1095-1102.
86. Mitschke, U.; Bäuerle, P. *J. Mater. Chem.* **2000**, *10*, 1471-1507.
87. Miyaura, N.; Suzuki, A. *Chem. Rev.* **1995**, *95*, 2457-2483.
88. Moralez, J. G.; Raez, J.; Yamazaki, T.; Motkuri, R. K.; Kovalenko, A.; Fenniri, H. *J. Am. Chem. Soc.* **2005**, *127*, 8307-8309.
89. Moulin, E.; Cid, J. J.; Giuseppone, N. *Adv. Mater.* **2013**, *25*, 477-487.
90. Muir, T.; Morales, E.; Root, J.; Kumar, I.; Garcia, B.; Vellandi, C.; Jenigian, D.; Marsh, T.; Henderson, E.; Vesenka, J. *J. Vac. Sci. Technol. A* **1998**, *16*, 1172-1177.
91. Muthukumar, M.; Ober, C. K.; Thomas, E. L. *Science* **1997**, *277*, 1225-1232.
92. Nilsson, K. P. R.; Rydberg, J.; Baltzer, L.; Inganäs, O. *Proc. Natl. Acad. Sci. U.S.A.* **2003**, *100*, 10170-10174.
93. Paramonov, S. E.; Jun, H. W.; Hartgerink, J. D. *J. Am. Chem. Soc.* **2006**, *128*, 7291-7298.
94. Pederson, C. J. *J. Am. Chem. Soc.* **1967**, *89*, 7017-7036.
95. Ramstrom, O.; Bunyapaiboonsri, T.; Lohmann, S.; Lehn, J. M. *Biochim. Biophys. Acta.* **2002**, *1572*, 178-186.

96. Ranganathan, D.; Lakshmi, C.; Karle, I. L. *J. Am. Chem. Soc.* **1999**, *121*, 6103-6107.
97. Rhodes, W. *J. Am. Chem. Soc.* **1961**, *55*, 3609-3617.
98. Rotomskis, R.; Augulis, R.; Snitka, V.; Valiokas, R.; Liedberg, B. *J. Phys. Chem. B* **2004**, *108*, 2833-2838.
99. Santoso, S.; Hwang, W.; Hartman, H.; Zhang, S. *Nano Lett.* **2002**, *2*, 687-691.
100. Saravanan, C.; Liu, C. L.; Chang, Y. M.; Lu, J. D.; Hsieh, Y. J.; Rwei, S. P.; Wang, S. P. *ACS Appl. Mater. Interfaces* **2012**, *4*, 6133-6141.
101. Schenning, A. P. H. J.; Meijer, E. W. *Chem. Commun.* **2005**, *26*, 3245-3258.
102. Schillinger, E. K.; Mena-Osteritz, E.; Hentschel, J.; Börner, H.; Bäuerle, P. *Adv. Mater.* **2009**, *21*, 1562-1567.
103. Schmid, S.; Mena-Osteritz, E.; Kopyshev, A.; Bäuerle, P. *Org. Lett.* **2009**, *11*, 5098-5101.
104. Schwab, A. D.; Smith, D. E.; Bond-Watts, B.; Johnston, D. E.; Hone, J.; Johnson, A. T.; de Paula, J. C.; Smith, W. F. *Nano Lett.* **2004**, *4*, 1261-1265.
105. Schwab, A. D.; Smith, D. E.; Rich, C. S.; Young, E. R.; Smith, W. F.; de Paula, J. C. *J. Phys. Chem. B* **2003**, *107*, 11339-11345.
106. Seeman, N. C. *Angew. Chem., Int. Ed.* **1998**, *37*, 3220-3238.
107. Seeman, N. C. *Nature*, **2003**, *421*, 427-431.
108. Seto, C. T.; Whitesides, G. M. *J. Am. Chem. Soc.* **1993**, *115*, 905-916.

109. Shaytan, A. K.; Schillinger, E. K.; Khalatur, P. G.; Mena-Osteritz, E.; Hentschel, J.; Börner, H. G.; Bäuerle, P.; Khokhlov, A. R. *ACS Nano* **2011**, *5*, 6894-6909.
110. Shioiri, T. Chiral Phase-Transfer Catalysis. In *Handbook of Phase-Transfer Catalysis*; Sasson, Y., Neumann, R., Eds.; Blackie: London, UK, 1997, Chapter 14.
111. Silva, G. A.; Czeisler, C.; Niece, K. L.; Beniash, E.; Harrington, D. A.; Kessler, J. A.; Stupp, S. I. *Science* **2004**, *303*, 1352-1355.
112. Silverstein, R. M.; Webster, F. X.; Kiemle, D. J. *Spectrometric Identification of Organic Compounds*, 7th Ed.; John Wiley & Sons, Inc.: USA, 2005, Chapter 3-5.
113. Siringhaus, H.; Brown, P. J.; Friend, R. H.; Nielsen, M. M.; Bechgaard, K.; Langeveld-Voss, B. M. W.; Spiering, A. J. H.; Janssen, R. A. J.; Meijer, E. W.; Herwig, P.; deLeeuw, D. M. *Nature* **1999**, *401*, 685-688.
114. Siringhaus, H.; Tessler, N.; Friend, R. H. *Science* **1998**, *280*, 1741-1744.
115. Song, S.; Chen, Y.; Yan, Z.; Fenniri, H.; Webster, T. J. *Int. J. Nanomed.* **2011**, *6*, 101-107.
116. Starks, C. M.; Liotta, C. L.; Halpern, M. *Phase-Transfer Catalysis: Fundamentals, Applications, and Industrial Perspectives*; Chapman and Hall: New York, 1994.
117. Stendahl, J. C.; Rao, M. S.; Guler, M. O.; Stupp, S. I. *Adv. Funct. Mater.* **2006**, *16*, 499-508.
118. Storhoff, J. J.; Mirkin, C. A. *Chem. Rev.* **1999**, *99*, 1849-1862.

119. Stupp, S. I.; Palmer, L. C. *Chem. Mater.* **2014**, *26*, 507-518.
120. Suri, S. S.; Mills, S.; Aulakh, G. K.; Rakotondradany, F.; Fenniri, H.; Singh, B. *Int. J. Nanomed.* **2011**, *6*, 3113-3123.
121. Suzuki, A. *J. Organomet. Chem.* **1999**, *576*, 147-168.
122. Suzuki, A. *Metal-Catalyzed Cross-Coupling Reactions*; Diederich, F., Stang, P. J., Eds.; Wiley-VCH: New York, 1998; Chapter 2.
123. Tikhomirov, G.; Oderinde, M; Makeiff, D.; Mansoui, A.; Lu, W.; Heirtzler, F.; Kwok, D. Y.; Fenniri, H. *J. Org. Chem.* **2008**, *73*, 4248-4251.
124. Tikhomirov, G.; Oderinde, M; Makeiff, D.; Mansoui, A.; Lu, W.; Heirtzler, F.; Kwok, D. Y.; Fenniri, H. *J. Org. Chem.* **2008**, *73*, 4248-4251.
125. Tikhomirov, G.; Yamazaki, T.; Kovalenko, A.; Fenniri, H. *Langmuir* **2008**, *24*, 4447-4450.
126. Tinoco, I. J. *J. Am. Chem. Soc.* **1960**, *82*, 4875-4790.
127. Toledano, S.; Williams, R. J.; Jayawarna, V.; Ulijn, R. V. *J. Am. Chem. Soc.* **2006**, *128*, 1070-1071.
128. Torbeev, V. Y.; Fumi, E.; Ebert, M. O.; Schweizer, W. B.; Hilvert, D. *Helvetica Chimica Acta* **2012**, *95*, 2411-2420.
129. Tsai, W. W.; Tevis, I. D.; Tayi, A. S.; Cui, H.; Stupp, S. I. *J. Phys. Chem. B* **2010**, *114*, 14778-14786.

130. Ulijn, R. V.; Smith, A. M. *Chem. Soc. Rev.* **2008**, *37*, 664-675.
131. von Maltzahn, G.; Vauthey, S.; Santoso, S.; Zhang, S. *Langmuir* **2003**, *19*, 4332-4337.
132. Wang, Y.; Song, R.; Li, Y.; Shen, J. *Surface Science* **2003**, *530*, 136-148.
133. Wang, Z.; Medforth, C. J.; Shelnutt, J. A. *J. Am. Chem. Soc.* **2004**, *126*, 15954-15955.
134. Whitesides, G. M.; Grzybowski, B. *Science* **2002**, *295*, 2418-2421.
135. Whitesides, G. M.; Mathias, J. P.; Seto, C. T. *Science* **1991**, *254*, 1312-1319.
136. Wu, J.; Pisula, W.; Müllen, K. *Chem. Rev.* **2007**, *107*, 718-747.
137. Würthner, F. *Angew. Chem., Int. Ed.* **2001**, *40*, 1037-1039.
138. Zhang, L.; Hemeraz, U. D.; Fenniri, H.; Webster, T. J. *J. Biomed. Mater. Res. A* **2010**, *95A*, 550-563.
139. Zhao, X.; Pan, F.; Xu, H.; Yaseen, M.; Shan, H.; Hauser, C. A. E.; Zhang, S.; Lu, J. *R. Chem. Soc. Rev.* **2010**, *39*, 3480-3498.
140. Zotti, G.; Zecchin, S.; Vercelli, B. *Chem. Mater.* **2006**, *18*, 3151-3161.